



Vol 4, No. 1 August 2010

DFI JOURNAL

The Journal of the Deep Foundations Institute

PAPERS:

- Drilled Displacement Piles – Current Practice and Design –
Prasenjit Basu, Monica Prezzi, Dipanjan Basu [3]**
- Analysis of a Deep Excavation In Calgary, Alberta –
Thomas Lardner, Matthew Janes, K.Y. Lo, Guangfeng Qu,
Silvana Micic [21]**
- Analyzing Drivability of Open Ended Piles in Very
Dense Sands – James A. Schneider, Ivy A. Harmon [32]**
- Support of Structures in Expansive Shale Using Recycled
Plastic Piles – Lance A. Roberts, Eric Brandner [45]**
- Peak and Post-Peak Shear Strength of Cement-Bentonite –
Paul J. Axtell, Timothy D. Stark, John C. Dillon [59]**

Deep Foundations Institute is the Industry Association of Individuals and Organizations Dedicated to Quality and Economy in the Design and Construction of Deep Foundations.

From the Editors and Publisher

While the success of the Journal is principally due to the contributing authors, the peer reviewers also make a substantial contribution. We wish to again compliment the reviewers of papers for their astute comments and suggestions.

The peer review process contributes substantially to the quality of the papers published. It has been our practice to seek out at least three reviewers for each paper. The search for knowledgeable reviewers is usually aided by utilizing DFI's technical committees to nominate reviewers from the applicable committee, but there have been instances where we have stepped outside of this source to find reviewers whose areas of expertise suit the subject of the paper. Ideally, after one or two rounds of review and resubmission of the paper, all the reviewers reach the point where they recommend acceptance of the paper "as is". There have been instances where this does not happen and one of the three reviewers remains dissatisfied, while the other two consider the paper acceptable without further change. When this happens, the paper in question is delayed while the Publisher and Editorial Board try to assess whether to accept the paper "as is" or mediate some changes to address the remarks of the dissenting reviewer. Such was the situation with two of the papers in this issue of the DFI Journal, causing later than scheduled publication. Please forgive us for considering quality of content more important than schedule.

To date we have not formally invited discussion on Journal papers. We do now wish to advise our readers that we are open to publishing valid discussions on paper published in past issues of the DFI Journal. This could serve as a useful outlet for any dissenting reviewers to make known their views.

The editors are pleased that the Journal will now be available for free on-line to DFI members, which will increase the widespread dissemination of published papers. We hope that authors will be even more encouraged to submit and maintain the tradition of high-quality practice-oriented geotechnical papers for publication. The journal will continue to focus on subjects that are directly relevant to deep foundations practice and thus will provide a bridge between academia doing applied research, practicing professionals, and the construction industry.

Comments, suggestions, and submissions are welcome and may be submitted via the DFI website at www.dfi.org



The Journal of the Deep Foundations Institute publishes practice-oriented, high quality papers related to the broad area of "Deep Foundations Engineering". Papers are welcome on topics of interest to the geo-professional community related to, all systems designed and constructed for the support of heavy structures and excavations, but not limited to, different piling systems, drilled shafts, ground modification geosystems, soil nailing and anchors. Authors are also encouraged to submit papers on new and emerging topics related to innovative construction technologies, marine foundations, innovative retaining systems, cutoff wall systems, and seismic retrofit. Case histories, state of the practice reviews, and innovative applications are particularly welcomed and encouraged.

Journal Publisher

Manuel A. Fine, B.A.Sc, P.Eng

Journal Editors

Ali Porbaha, Ph.D., P.E.
California State University
Sacramento, CA, USA

Dan A. Brown, Ph.D. *Dan Brown and Associates*, Sequatchie, TN, USA

Zia Zafir, Ph.D., P.E.
Kleinfelder Sacramento, CA, USA

Associate Editors

Lance A. Roberts, Ph.D., P.E.
South Dakota School of Mines and Technology
Rapid City, SD USA

Thomas Weaver, Ph.D., P.E.
Nuclear Regulatory Commission
Rockville, MD USA

Published By Deep Foundations Institute

Copyright © 2009 Deep Foundations Institute.
All rights reserved. Written permission must be obtained from DFI to reprint journal contents, in whole or in part.

Contact
DFI Headquarters
326 Lafayette Avenue
Hawthorne, NJ 07506
dfihq@dfi.org
www.dfi.org

DFI, its directors and officers, and journal editors assume no responsibility for the statements expressed by the journal's authors. International Standard Serial Number (ISSN): 1937-5247

2010 DFI Board of Trustees

President:

Rudolph P. Frizzi
Langan Engineering & Environmental Services
Elmwood Park, NJ USA

Vice-President:

James A. Morrison
Kiewit Construction Group Inc.
Omaha, NE USA

Secretary:

Robert B. Bittner
Bittner-Shen Consulting Engineers, Inc.
Portland, OR USA

Treasurer:

Patrick Bermingham
Bermingham Foundation Solutions
Hamilton, ON Canada

Immediate Past President:

Seth L. Pearlman
Menard
Bridgeville, PA USA

Other Trustees:

David Borger
Skyline Steel LLC
Parsippany, NJ USA

Maurice Bottiau
Franki Geotechnics B
Saintes, Belgium

Dan Brown
Dan Brown and Associates
Sequatchie, TN USA

Bernard H. Hertlein
AECOM USA, Inc.
Vernon Hills, IL USA

Matthew Janes
Isherwood Associates
Burnaby, BC, Canada

James O. Johnson
Condon-Johnson & Associates, Inc.
Oakland, CA USA

Douglas Keller
Richard Goettle, Inc.
Cincinnati, OH USA

Samuel J. Kosa
Monotube Pile Corporation
Canton, OH USA

Kirk A. McIntosh
MACTEC Engineering & Consulting, Inc.
Jacksonville, FL USA

Raymond J. Poletto
Mueser Rutledge Consulting Engineers
New York, NY USA

John Wolosick
Hayward Baker
Alpharetta, GA USA

Mike Wysocky
Thatcher Foundations, Inc.
Gary, IN USA

Drilled Displacement Piles – Current Practice and Design

Prasenjit Basu, Assistant Professor, Department of Civil and Environmental Engineering, Pennsylvania State University, University Park, PA 16802, USA, Ph: 1-863-814-4010, e-mail: pbasu@engr.psu.edu

Monica Prezzi, Associate Professor, School of Civil Engineering, Purdue University, West Lafayette, IN 47907, USA, Ph: 1-765-494-5034, Fax: 1-765-494-0395, e-mail: mprezzi@purdue.edu

Dipanjan Basu, Assistant Professor, Department of Civil Engineering, University of Connecticut, CT 06269-2037, USA, Ph: 1-860-486-5023, e-mail: dbasu@engr.uconn.edu

ABSTRACT

Drilled displacement piles are being increasingly used as foundation elements, particularly in projects requiring fast construction. Different types of drilled displacement (DD) piles are available in practice. DD piles are classified according to the drilling tool design and installation method. The capacity of a DD pile, depending on its type, is between the capacities of geometrically similar nondisplacement and full-displacement piles installed in the same soil profile. This paper provides an overview of the different types of DD piles and their installation techniques and describes three design methods used in practice. It also compares DD pile capacities obtained with these design methods for two different sites.

INTRODUCTION

A wide variety of pile types are currently available for use in geotechnical engineering practice. The response of these piles to loading varies greatly depending on the installation or construction methods employed. On one end of the pile behavior spectrum are the nondisplacement piles (e.g., bored piles or drilled shafts) and, on the other end, are the full-displacement piles (e.g., closed-ended pipe piles or precast reinforced concrete piles). Nondisplacement piles are constructed by removing a cylinder of soil from the ground and replacing the void created with concrete and reinforcement. Full-displacement piles, on the other hand, are driven or jacked into the ground. During the installation of full-displacement piles, significant changes in the void ratio and stress state of the *in situ* soil take place because the soil surrounding the pile shaft is displaced mainly in the lateral direction and the soil below the base of the pile is preloaded. These changes produce a stiffer load-displacement response for the displacement piles than that of the nondisplacement piles, particularly in the case of sandy soils which gain additional strength through densification.

There are other types of piles (e.g., open-ended pipe piles) that show behavior intermediate between nondisplacement and full-displacement piles. These piles are often called partial-

displacement piles. Many auger piles, which are installed by drilling a continuous-, segmented- or partial-flight auger into the ground, fall under this category. A variety of auger piling equipment is available in the market; each one is associated with a certain degree of soil displacement during installation. The commonly used terminologies used for auger piles in North America and Europe are presented in Fig. 1.

A special class of auger piles was created as a result of advances in auger piling technology; these are commonly known as “screw piles” in Europe, and “drilled displacement” or “augered displacement” piles in the USA (Brown and Drew 2000; Brown 2005; Prezzi and Basu 2005). These piles have been used in Europe over the last few decades and are becoming popular in the U.S. Drilled displacement (DD) piles are rotary displacement piles installed by inserting a specially designed helical auger segment into the ground with both a vertical force and a torque. Soil is displaced laterally within the ground (with minimal spoil generated), and the void created is filled with grout or concrete. The installation of DD piles produces greater soil displacement than that produced by continuous-flight-auger (CFA) or auger cast-in-place (ACIP) piles (these piles are generally associated with small soil displacement). The axial capacity of the different types of DD piles depends on the radial soil displacement

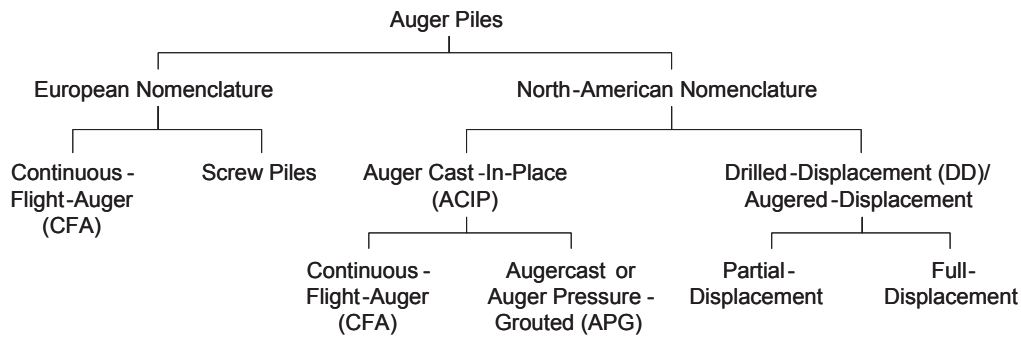


[FIG. 1] Nomenclature used for auger piles in Europe and the U.S. (modified after Prezzi and Basu 2005)

OVERVIEW OF DD PILING TECHNOLOGY

The development of DD piling technology evolved from the continuous-flight auger (CFA) piling technology. The remarkable progress in piling

caused by their installation (the radial soil displacement depends on the soil type and state, the design of the DD pile drilling tool, and the drilling rig technology).

From a design point of view, full-displacement piles are preferable because they are capable of carrying larger loads than partial- or nondisplacement piles of similar geometry. However, pile driving may cause excessive vibration to neighboring structures or create excessive noise that may be unacceptable under certain conditions. Additionally, in some soil profiles, the use of driven piles may not be advisable. DD piles often offer a viable alternative in cases where the installation of driven full-displacement piles is not advisable. The advantages of DD piles are (i) the ease and fast rate of construction with minimal vibration or noise, and minimal spoil (important for contaminated sites), (ii) the high load-carrying capacity due to partial or full displacement of the soil surrounding the pile, and (iii) the associated savings that result when they are installed in the right soil conditions.

This paper presents a review of the current DD pile practice, including DD pile installation methods, quality control procedures, and three design methods. The ultimate capacities of five different types of DD piles are calculated with the design methods used in practice and compared with those obtained from pile load test results reported in the literature. Additionally, in a separate design example, the capacities of a DD pile, a full-displacement pile and a nondisplacement pile in a residual soil profile are compared.

rig capabilities over the past few decades and the improvement of the auger pile drilling tools and installation techniques helped speed up the installation process and resulted in larger lateral soil displacement. The piles that ensued because of these developments were called DD piles. However, DD piles are not just limited to those that are variations of the CFA or ACIP piles. A variety of other piles that have significantly different installation (drilling) tools are also included in this broad pile classification: Atlas, De Waal, Fundex, Olivier, Omega, Pressure-Grouted Displacement (PGD), and SVV piles (see Fig. 2). In general, the drilling tool of a DD pile contains one or more of the following components: a) a soil displacement body (an enlarged-diameter section which facilitates lateral soil movement), b) a helical, partial-flight auger segment, and c) a specially designed sacrificial tip, which is attached to the bottom of the drilling tool. The shape of the displacement body varies from one pile type to another; broadly, it consists of a cylindrical body that, in some cases, also contains single or multiple helices (Fig. 2). A casing (mandrel) of diameter smaller than or equal to the diameter of the pile is connected to the drilling tool.

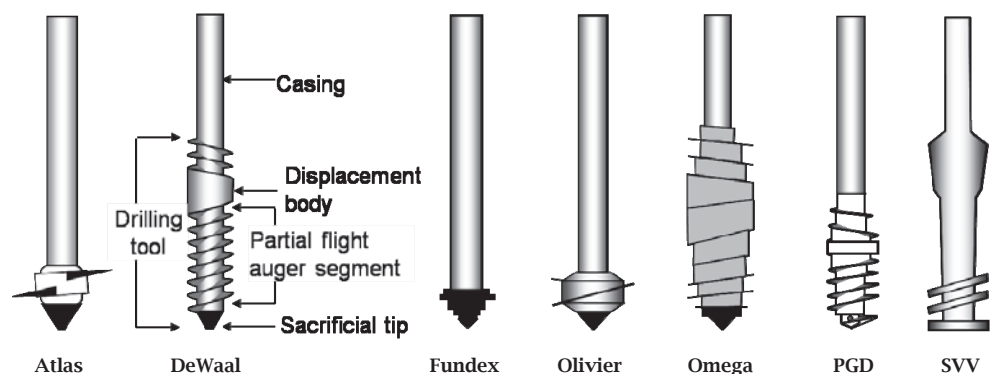


[FIG. 2] Drilling tools for installation of drilled displacement piles.

Piling rigs with high torque capacities (150 kN-m to 500 kN-m or more) (110 kip ft to 370 kip ft) that provide vertical thrust during the drilling process are required for installation of DD piles [drilling proceeds as a result of both the rotation of the drilling tool and the crowd (axial) force typically applied by hydraulic rams]. Once the drilling tool reaches the desired depth, the sacrificial tip (if used) is released from the casing or displacement body. Concrete or grout is then placed through the casing as the drilling tool and the casing are extracted from the ground. The reinforcement is inserted either before or after concrete placement. The drilling tool and casing can be withdrawn from the ground with or without rotation (the rotation may be clockwise or counter-clockwise). A nearly smooth pile shaft is obtained if the casing is withdrawn with alternating 180° clockwise and counter-clockwise rotations (as in the case of the Fundex pile). A nearly smooth shaft also results if the drilling tool is rotated clockwise as it is withdrawn from the ground (e.g., De Waal, PGD, and Omega piles). However, if the displacement body is rotated counter-clockwise (e.g., Atlas and Olivier piles) during withdrawal, then a screw-shaped shaft is obtained.

Proper knowledge of the subsurface profile is required for selecting the most efficient pile type for a given site. For a number of sites in the U.S., Siegel *et al.* (2007) reported an increase in cone penetration test (CPT) resistance q_c due to the installation of DD piles. The maximum increase in q_c was observed in the case of loose sand with normalized value of CPT resistance q_{c1} less than 50 [$q_{c1} = (q_c/p_a)(p_a/\sigma'_{v0})^{0.5}$; where p_a = atmospheric pressure = 100 kPa and σ'_{v0} = *in situ* vertical effective stress; Siegel *et al.* 2007]. However, according to Bustamante and Ganeselli (1998), the performance of DD piles may be compromised because of possible difficulties encountered during installation in very loose sandy soils or very soft clayey soils (characterized by SPT blow count $N < 5$ or $q_c < 1$ MPa or 145 psi). In the case of very dense sandy soils or thick alluvium layers, a drastic drop in the penetration rate may be observed and premature wear of the screw head (drilling tool) may result (Bustamante and Ganeselli 1998). According to NeSmith (2002), the installation of auger pressure-grouted displacement (APGD) piles (which can more generally be called PGD piles) becomes difficult in dense sand layers with $q_c > 14$ MPa (2,030 psi). In the case of

thick clay deposits, the excess pore pressure generated during installation of DD piles may cause bleeding of fresh concrete and loss of pile integrity (NeSmith 2002). However, an assessment of the potential problems that may occur during the installation of DD piles can only be made after full consideration of specific site conditions and equipment capabilities (piling rig and drilling tool).

INSTALLATION TECHNIQUES FOR DIFFERENT DD PILES

Atlas Pile

The Atlas pile is a drilled, dual-displacement, cast-in-place concrete pile (De Cock and Imbo 1994). Lateral displacement of soil occurs both during drilling and extraction of the auger (this is the reason why it is called a dual-displacement pile). The Atlas pile is installed using a purpose-built drilling rig with a base rotary drive (Bottiau 2006). The Atlas pile rig has two hydraulic rams that can work independently (one ram taking over from the other after its full stroke is achieved) to allow a continuous drilling operation. In the case of hard soils, the two hydraulic rams can be used simultaneously. The rig can be operated at dual rotational speeds. This helps control the drilling tool penetration rate in different soil types.

A sacrificial tip (a lost pile shoe) is attached to a displacement body, which, in turn, is attached to a steel casing or mandrel (Fig. 3). The displacement body consists of a cast-iron dismountable helical head with an enlarged helical flange. The joint between the displacement body and the sacrificial tip is made watertight. The combined action of the torque and the vertical thrust forces the casing down into the ground with a continuous, clockwise, helical penetrating movement. After the desired depth is reached, the steel shoe is detached from the casing by rotating the casing counter-clockwise (thereby opening the connection between the steel shoe and the casing). Subsequently, the steel reinforcing cage is inserted into the casing, and high-slump concrete is poured through a hopper placed on top of the casing to cast the pile shaft. As the casing and the displacement body are extracted by a vertical pulling force and counter-clockwise rotation, concrete completely fills the helical bore formed by the upward-moving displacement screw. This way, a screw-shaped shaft is formed. The flange thickness of the screw-shaped shaft varies

depending on the extraction procedure (i.e., the ratio of rotational to translational speeds during extraction) (De Cock and Imbo 1994; Geoforum 2008). After concrete placement is complete, it is possible to push a supplementary reinforcing cage into the concrete.

The diameter of the displacement body (which is the same as the minimum diameter of the pile shaft) typically ranges from 0.31 m to 0.56 m (1.00 ft to 1.84 ft), while that of the enlarged helical flange ranges from 0.45 m to 0.81 m (1.48 ft to 2.66 ft) (Bustamante and Gianceselli 1998; De Cock and Imbo 1994). The Atlas pile length can reach up to 22-25 m (72-82 ft). In highly compressible soils or in soils with large cavities or voids, a thin-walled casing is often attached to the screw head of the Atlas piles (Bustamante and Gianceselli 1998). The casing is left in the ground with the sacrificial tip.

De Waal Pile

The drilling tool used to install the De Waal pile consists of a sacrificial tip, a partial-flight auger and a displacement body (Fig. 4). The tool is attached to a casing. The partial-flight auger is closed at the bottom with the sacrificial tip. To install the De Waal pile, the drilling tool is rotated clockwise to the required depth with a torque and a vertical force. After reaching the desired depth, concrete is placed into the casing to a level above the ground level, the sacrificial tip is released, and the tool is extracted using clockwise rotation and a vertical force. Upward transport of soil during extraction is restricted due to the presence of reverse auger flights above the displacement body. The concrete level within the casing is maintained above the ground level during extraction. A reinforcement cage is typically installed after concrete placement. Unlike the Atlas pile, installation of the De Waal pile creates a nearly smooth shaft.

Fundex Pile

In the Fundex pile installation, a casing/tube with a conical auger tip attached to its end is rotated clockwise and pushed down into the soil (Fig. 5). The joint between the casing and the conical tip is made watertight. As the casing penetrates into the ground, soil is displaced laterally. In dense or hard layers, drilling can be combined with grout injection or water jetting through the conical tip. After the desired depth is reached, the sacrificial conical tip, which forms an enlarged pile base, is released. The reinforcement cage is then inserted into

the casing, and concrete is placed. As the concrete is placed, the casing is extracted in an oscillating upward and downward motion with alternate 180° clockwise and counter-clockwise rotations. The withdrawal of the casing with both clockwise and counter-clockwise rotations produces a nearly smooth shaft.

The diameter of the conical tip ranges from 0.45 m to 0.67 m (1.5 ft to 2.2 ft), while that of the casing ranges from 0.38 m to 0.52 m (15 in to 20 in) (American Pile Driving Inc. 2007; Geoforum 2008). The length of the Fundex pile can reach up to 25-35 m (82-115 ft).

Olivier Pile

The installation of the Olivier pile is similar to that of the Atlas pile (Fig. 6). However, the drilling rigs used to install the Olivier piles are different from those of the Atlas piles (the rotary drives are different; the Atlas pile rig has a bottom-type rotary drive with a fixed rate of penetration, while the Olivier pile rig uses a top-type rotary drive with variable rate of penetration). A lost tip is attached to a partial-flight auger which, in turn, is attached to a casing. The casing, which is rotated clockwise continuously, penetrates into the ground by the action of a torque and a vertical force. At the desired installation depth, the lost tip is released, and the reinforcing cage is inserted into the casing. Concrete is then placed inside the casing through a funnel. The casing and the partial-flight auger are extracted by counter-clockwise rotation. Similar to the Atlas pile, the shaft of the Olivier pile has the shape of a screw.

Omega Pile

In the case of the Omega pile, drilling is done by a displacement auger (with varying flange diameter), which is closed at the bottom with a sacrificial tip (Fig. 7). The flange diameter of the auger segments increases gradually from both ends and becomes equal to the diameter of the central displacement body. A casing is attached to the upper end of the displacement auger. After reaching the required depth, concrete is injected under pressure, and the sacrificial tip is released. The auger is slowly rotated clockwise and pulled up to produce a nearly smooth shaft. The reinforcement cage is then vibrated down into the fresh concrete. For some Omega piles, it is possible to place the reinforcement cage (or bar) into the drilling stem (casing) even before concrete is placed (Bottiau et al. 1998).

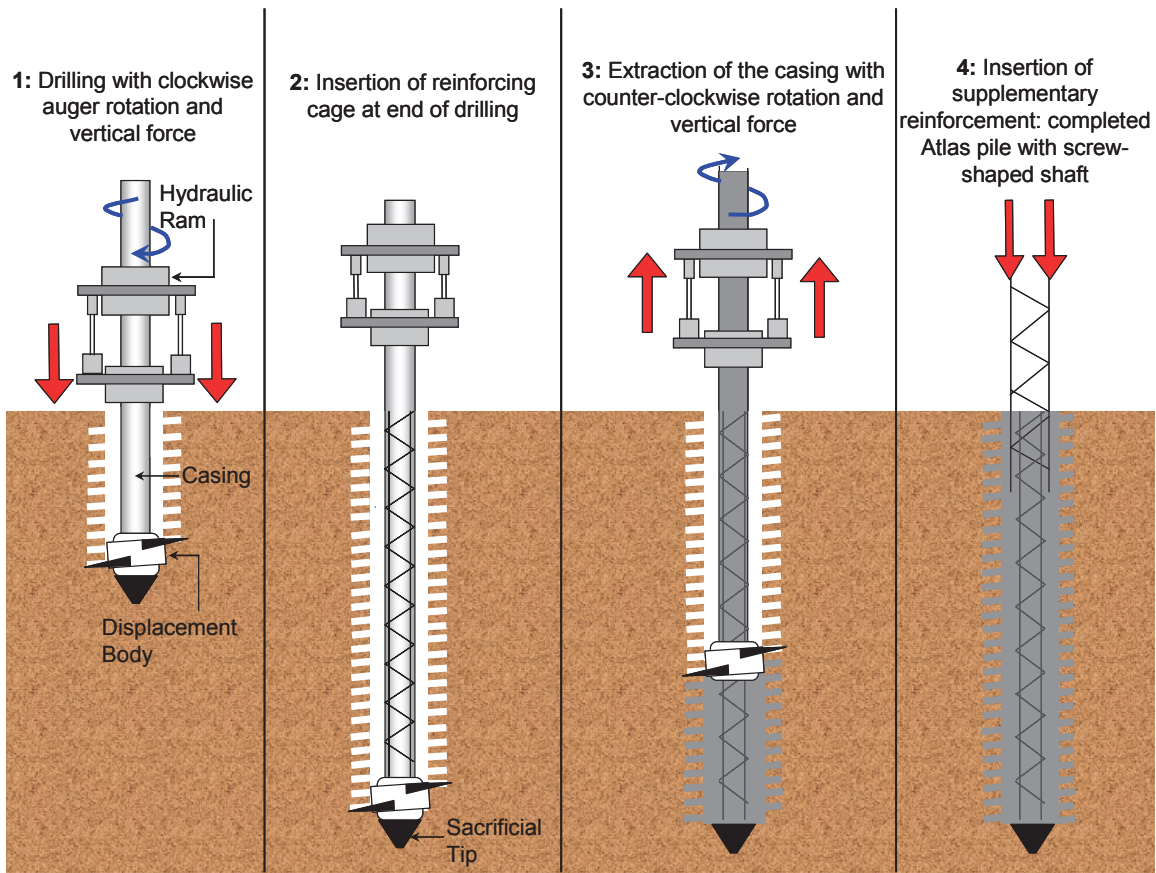


[FIG. 3] Installation stages for the Atlas pile.

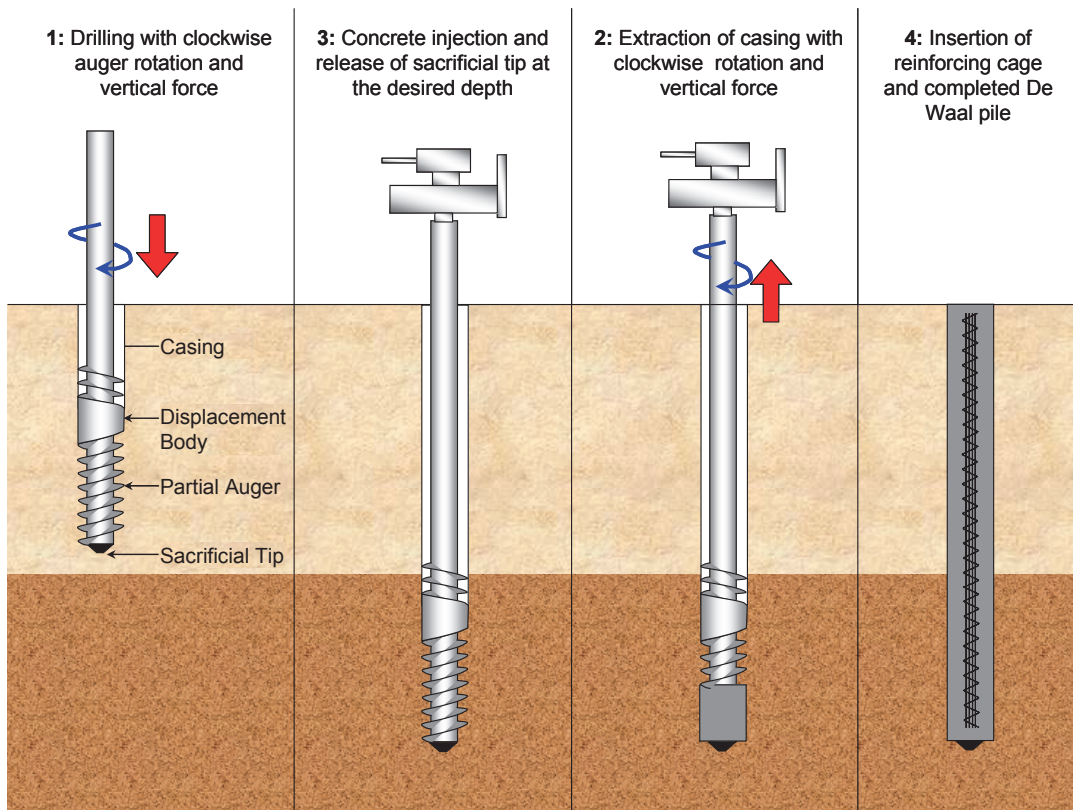


[FIG. 4] Installation stages for the DeWaal pile.

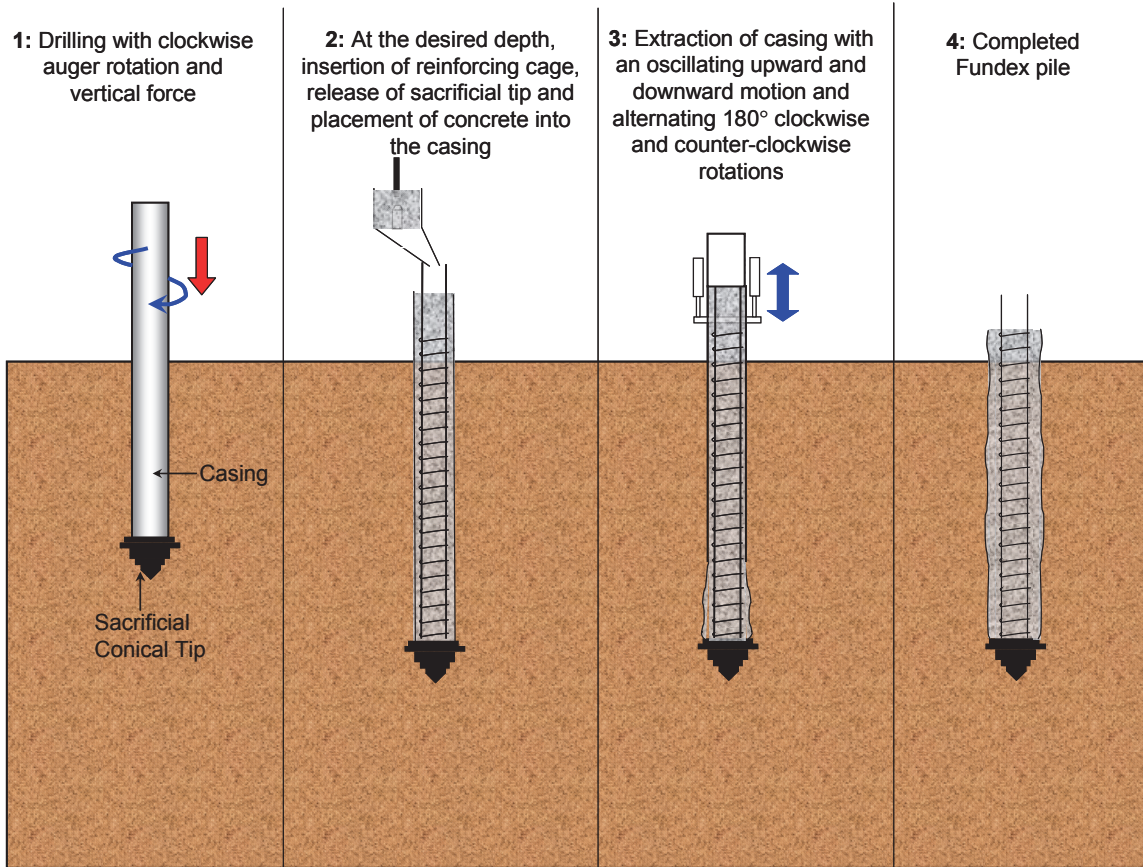


[FIG. 5] Installation stages for the Fundex pile.

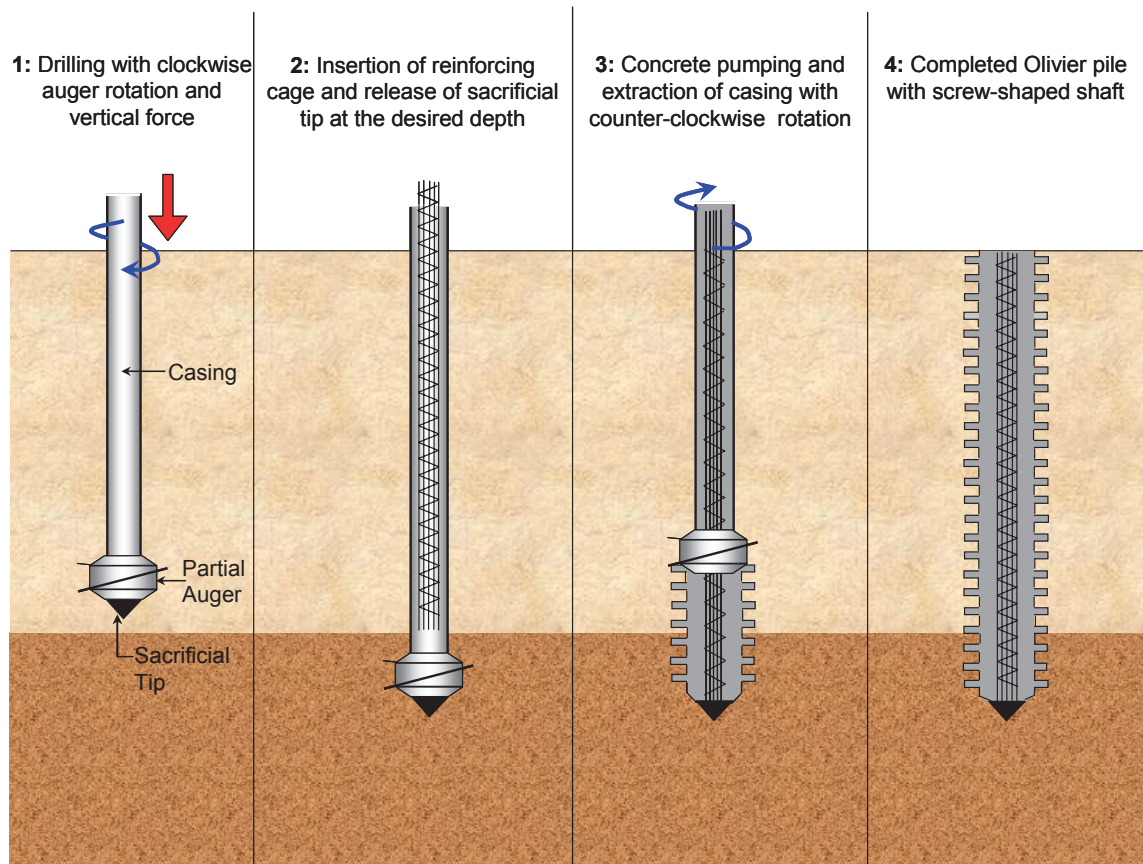


[FIG. 6] Installation stages for the Olivier pile.

PGD Pile

The PGD piling technology is a modification of the Auger Pressure-Grouted (APG) piling system (Brettmann and NeSmith 2005). The APG pile is a type of CFA pile which is constructed by pumping fluid grout under pressure during the withdrawal of the continuous-flight auger. During the installation of a PGD pile (Fig. 8), the surrounding soil is displaced laterally as the drilling tool is advanced into the ground. There are basically two types of PGD piles: 1) pressure-grouted with partial soil displacement and 2) pressure-grouted with full soil displacement. The PGD pile rigs are capable of producing both a torque and a downward crowd force, facilitating the drilling operations. Once the desired depth is reached, high-strength grout is pumped under pressure through the drill stem and the drilling tool is withdrawn as it rotates clockwise. The reinforcement cage is inserted into the grout column to complete the pile installation process. Note that the term *Auger Pressure-Grouted Displacement* (APGD) is also used in practice to refer to this type of DD pile (NeSmith 2002; Brettmann and NeSmith 2005).

The full-displacement PGD piles, which are typically installed in loose to medium dense sands (corresponding to SPT blow count $N < 25$), can be 0.3-0.45 m (12-18 in) in diameter and up to 24 m (79 ft) in length (NeSmith 2002; Brettmann and NeSmith 2005). The diameter of the partial-displacement PGD pile ranges from 0.3-0.5 m (12-20 in). These piles reach up to 17 m (79 ft) in length and are used in loose to dense sands with $N < 50$ (NeSmith 2002; Brettmann and NeSmith 2005).

SVV Pile

The SVV pile (STRABAG Vollverdrängungsbohrpfahl), developed by Jebens GmbH, is a large-displacement DD pile (Fig. 9). The pile is installed using a casing that has a segment with an enlarged diameter and a drill head. The SVV pile typically has a diameter of 0.44 m (18 in) and a length of up to 20 m (66 ft) (Geoforum 2008).

INSTALLATION MONITORING

Continuous monitoring during the installation of auger piles is important to assure pile integrity. The data obtained through monitoring of the installation process also provide additional information on the subsurface condition and allow determination of the exact position of

the pile base. Depending on the equipment available, some or all of the following quantities can be measured or calculated during the installation of auger piles: the rate of auger rotation, the rate of auger penetration, the torque, the concrete pumping rate, and the auger extraction rate (Mandolini *et al.* 2002).

Automated monitoring systems are available for the drilled displacement pile rigs as well. These can be used to continuously monitor the depth of penetration, the vertical force, the torque, and the rate of auger/casing penetration and rotation. In the past, quality control (QC) of auger piles was performed mostly by field inspectors, based mainly on the industry standards published by the Deep Foundations Institute (DFI) in the 1990's (Brettmann 2003). Currently, automated systems are attached to pile rigs throughout the world. Although these monitoring systems can provide valuable information on the integrity of the piles, they are not meant to replace qualified field inspectors. Automated QC monitoring techniques are based on measurements of either volume or pressure of the grout/concrete. Typical automated systems measure: i) time, depth and hydraulic pressure during drilling, and ii) time, depth, grout/concrete volume or grout/concrete pressure during casting. Continuous, real time graphs of relevant data are available to the operator during the installation of DD piles (this facilitates any impromptu adjustments that may be needed). These files can also be stored electronically for future reference (Brettmann and NeSmith 2005).

NeSmith and NeSmith (2006a, 2006b, 2009) described an automated data acquisition system used for APGD piles and indicated that the recorded data can be useful in characterizing the subsurface profile and in estimating pile capacity. This automated system measures the depth of penetration, the inclination of the mast of the drilling platform, the drilling stem rotation, the grout flow and pressure (measured at the top of the drilling stem), and the hydraulic pressure applied to the motor that controls the rotation of the drilling tool. The torque applied during drilling is calculated from the recorded hydraulic pressure. In addition, the drilling time is recorded through an internal time counter in the main control unit of the data acquisition system.

A specific energy or installation energy term can be calculated from the variables mentioned

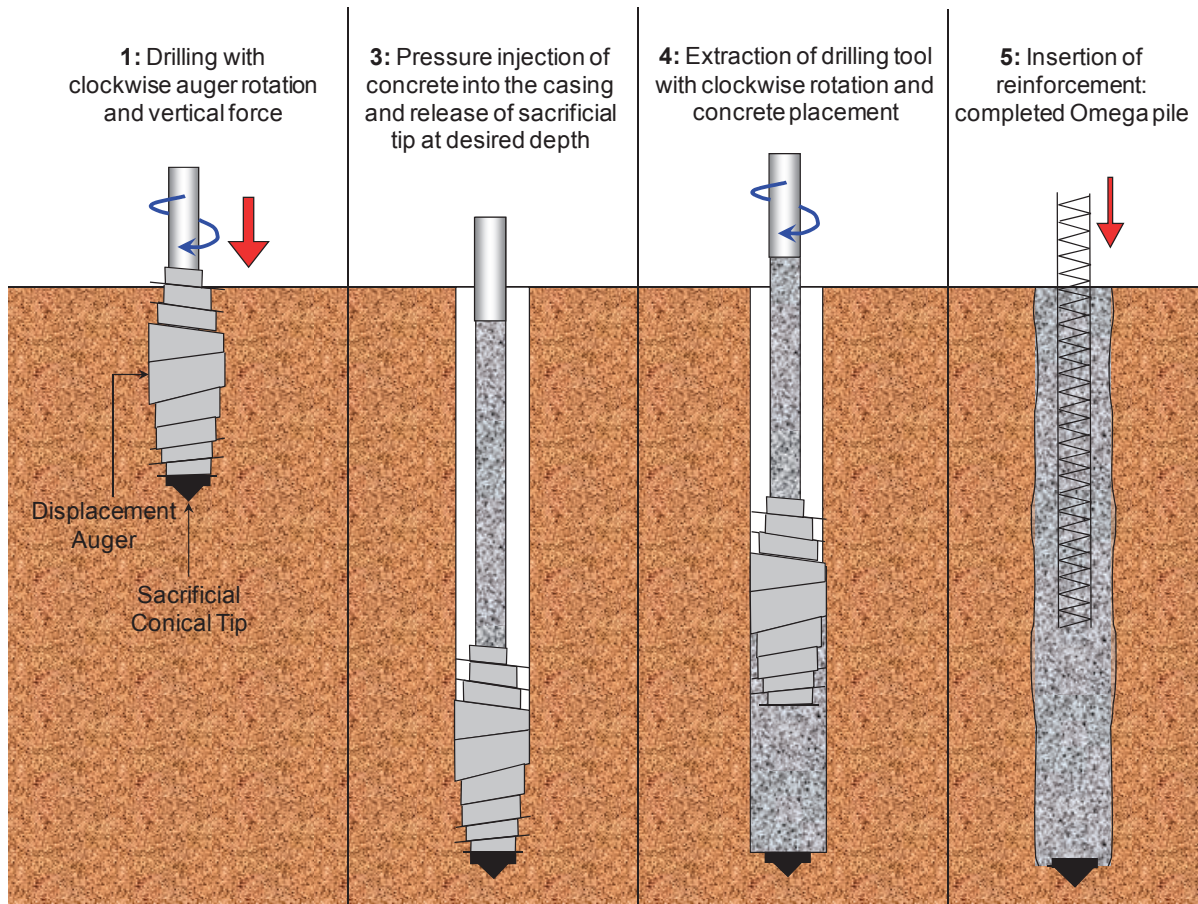


[FIG. 7] Installation stages for the Omega pile.

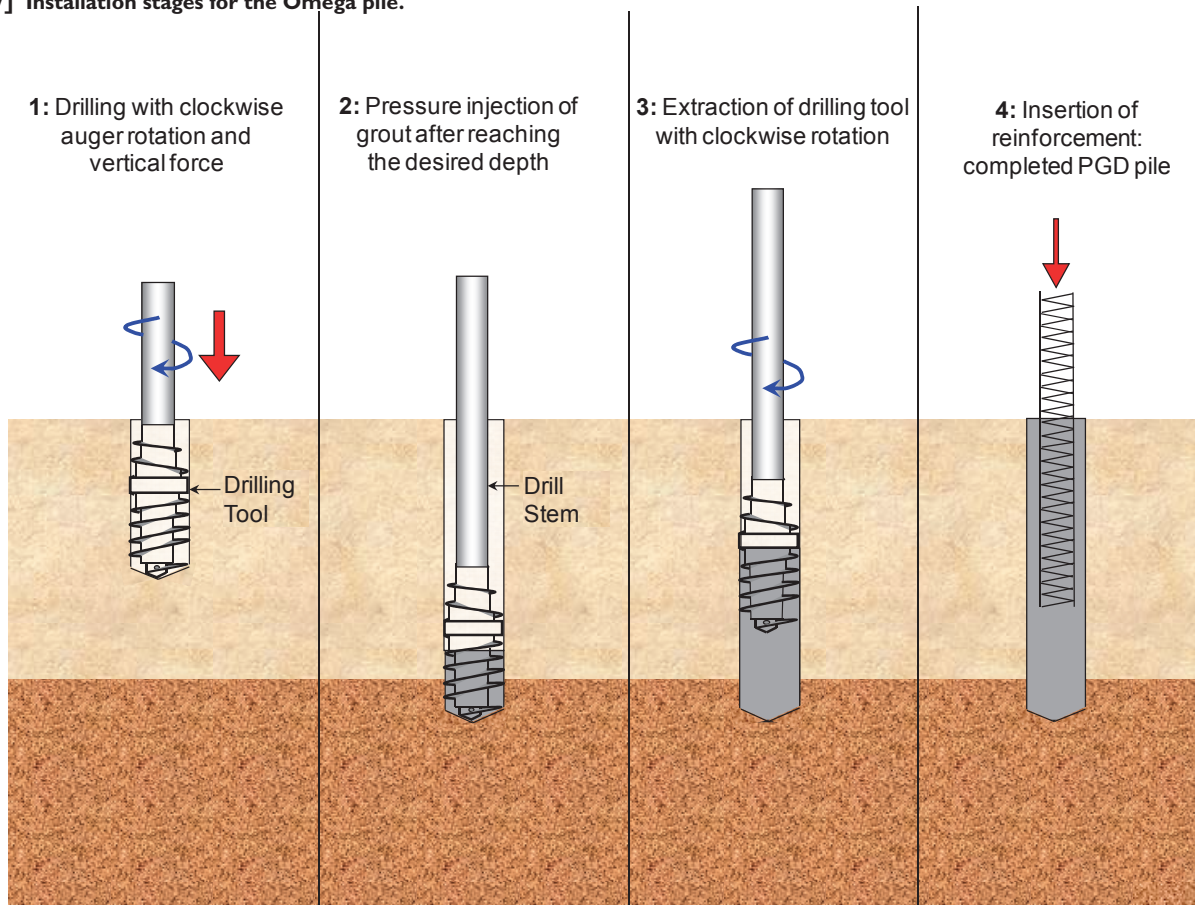


[FIG. 8] Installation stages for the PGD pile.

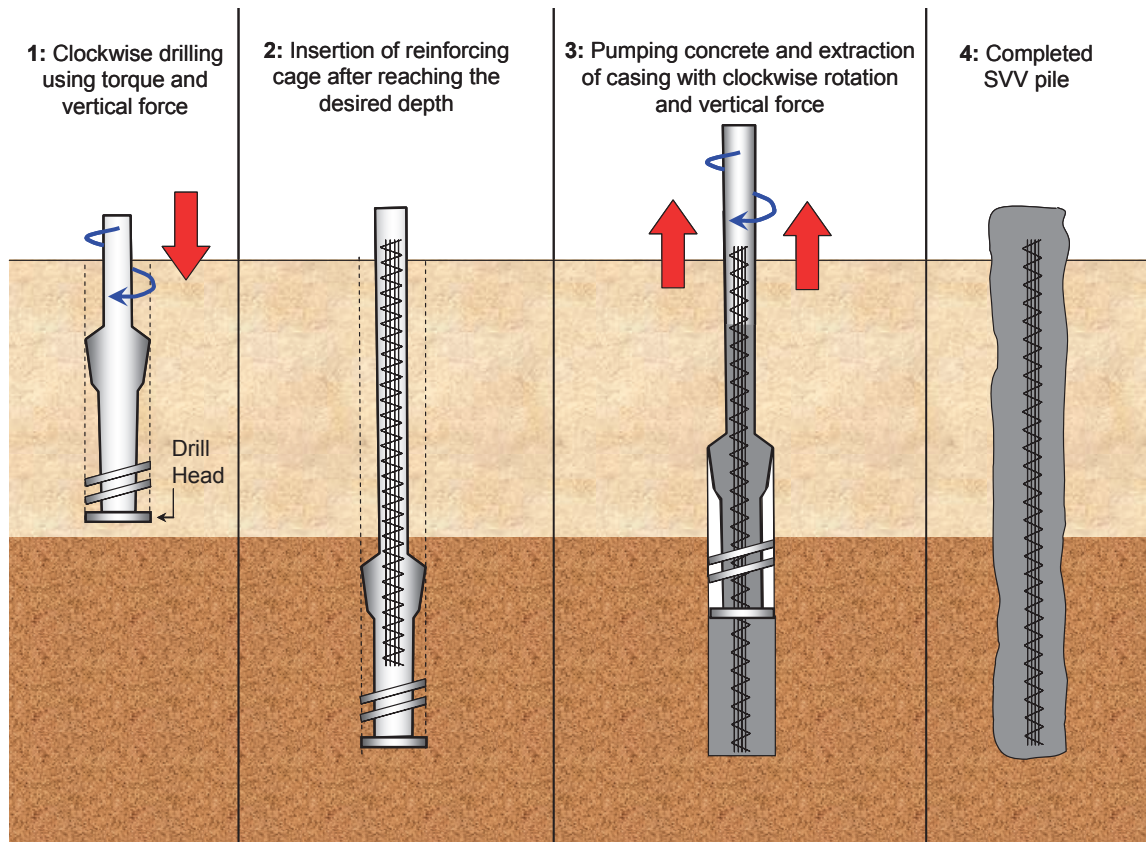


[FIG. 9] Installation stages for the SVV pile.

above and other machine-specific installation parameters (Bottiau et al. 1998). The specific energy along the depth of the pile can be correlated with *in situ* test results; it can potentially be used to interpret the effects of pile installation and to help predict pile load capacity (De Cock and Imbo 1994). NeSmith (2003) also proposed that an installation effort parameter (IE; defined as the product of normalized values of torque and drilling tool penetration rate) be used as an indicator of the capacity of DD piles. However, research on this topic is very limited and caution is necessary when using these methodologies.

DESIGN METHODS

General Framework

The ultimate pile capacity Q_{ult} can be expressed as:

$$Q_{ult} = Q_{b,ult} + Q_{sL} \quad (1)$$

where $Q_{b,ult}$ and Q_{sL} are the ultimate base and limit shaft capacities. These quantities are calculated from:

$$Q_{b,ult} = q_b A_b \quad (2)$$

$$Q_{sL} = A_s \sum_{i=1}^n q_{si} h_{si} \quad (3)$$

where the subscript i represents a given soil layer ($i = 1, 2, 3, \dots$) for which shaft capacity is calculated; n is the total number of layers crossed by the pile; q_b and q_{si} are the unit base and shaft resistances; $A_b (= \pi D_b^2/4)$ is the representative pile base area; $A_s (= \pi D_s)$ is the pile shaft perimeter; D_b and D_s are the nominal diameters of the pile base and shaft respectively; and h_{si} is the thickness of the i^{th} soil layer.

According to the guidelines provided by Huybrechts and Whenham (2003), the nominal shaft and base diameters depend on the drilling tool geometry. For the Atlas and Olivier piles, D_b and D_s are assumed to be equal to the measured maximum diameter D_f of the drilling auger screw blade (see Fig. 10). Bustamante and Gianceselli (1993, 1998), however, suggested that the nominal diameter of the Atlas pile is equal to $0.9D_f$, except for the thick-flanged Atlas piles, for which they suggested a nominal diameter equal to D_f . For the Fundex pile, D_b is equal to the measured maximum diameter of the conical auger tip, and D_s is equal to the measured maximum diameter of the casing/tube (Huybrechts and Whenham 2003). For other DD piles that also have a nearly smooth shaft, such as the De Waal and Omega piles, both D_s and D_b are taken as the diameter of the soil displacement body (which is equal

to the maximum diameter of the screw blade; Huybrechts and Whenham 2003). Since the nominal pile diameter depends on the drilling tool geometry, the different coefficients proposed (in different design methods) for pile capacity calculations reflect the way in which they were determined, including the nominal dimensions of the pile. No specific guidelines are given in the literature on nominal diameter values for use in the design of other types of DD piles.

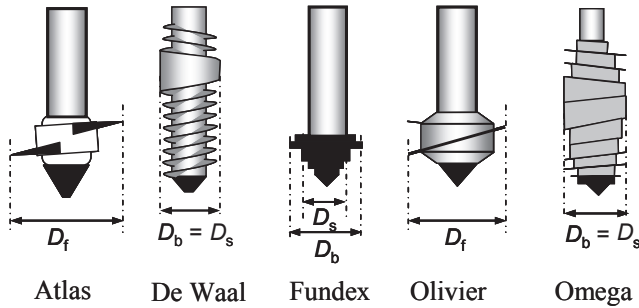


[FIG. 10] Design dimensions for some DD piles.

Calculation of unit base and shaft resistances

Available design methods for DD piles are mostly based on *in situ* test results. The unit base and shaft resistances of piles are typically related to the cone penetration test (CPT) tip resistance q_c , the standard penetration test (SPT) blow count N and the pressuremeter test (PMT) limit pressure p_l .

Method A

This design methodology was developed in the U.S. based on load tests performed on 28 APGD piles (NeSmith 2002; Brettmann and NeSmith 2005). The Geotechnical Engineering Circular No. 8 (published by Federal Highway Administration) recommends this method for the calculation of the axial capacity of DD piles in the U.S. (Brown *et al.* 2007). The ultimate load (defined as the 'interpreted failure load' by NeSmith 2002) was defined as the minimum of the loads corresponding to (i) a pile head settlement of 25.4 mm (1 in) or (ii) a pile displacement rate of 0.057 mm/kN (0.02 inch/ton). The specified value of the pile head settlement (i.e., 25.4 mm = 1 inch) is equal to about 6% of the diameter of the piles tested [pile diameters ranged from 0.36 m to 0.46 m (14-18 in), with 80% of the piles having a diameter equal to 0.41 m (16 in). According to NeSmith (2002), the settlement-based criterion (pile head settlement equal to 25.4 mm or 1 in) controlled the determination of the ultimate load (or the 'interpreted failure load'). Therefore, in this

design method, the ultimate pile load capacity is based on a relative settlement of 6% (i.e., the load corresponding to a pile head settlement equal to 6% of the pile diameter). The unit base resistance q_b is given by:

$$q_b \text{ (MPa)} = 0.4 q_{cm} + w_b \quad \text{for } q_{cm} \leq 19 \text{ MPa} \quad (4a)$$

or

$$q_b \text{ (MPa)} = 0.19 N_m + w_b \quad \text{for } N_m \leq 50 \quad (4b)$$

where q_{cm} and N_m are representative values of q_c and uncorrected SPT blow count N in the vicinity of the pile base, and w_b is a constant that depends on soil gradation and angularity. For soils containing uniform, rounded particles with up to 40% fines, $w_b = 0$ and the upper limit of q_b is 7.2 MPa (1,044 psi). For soils with well-graded, angular particles having less than 10% fines, $w_b = 1.34$ MPa (195 psi) and the upper limit for q_b is 8.62 MPa (1,250 psi). Interpolation (based on percentage of fines) is suggested to determine the values of w_b for other types of soils (NeSmith 2002). q_{cm} and N_m are determined from the following equations (Fleming and Thorburn 1983):

$$q_{cm} = 0.25q_{c0} + 0.25q_{c1} + 0.5q_{c2} \quad (5a)$$

$$N_m = 0.25N_0 + 0.25N_1 + 0.5N_2 \quad (5b)$$

where q_{c0} and q_{c1} are the average and minimum cone resistances over a length of $4D_b$ below the pile base, respectively, and q_{c2} is the average cone resistance over a length of $4D_b$ above the pile base after eliminating values greater than q_{c1} (NeSmith 2002). N_0 , N_1 and N_2 refer to the corresponding uncorrected SPT values (equivalent to q_{c0} , q_{c1} , and q_{c2}).

The unit shaft resistance for any soil layer i is given by:

$$q_{si} \text{ (MPa)} = 0.01 q_{ci} + w_s \quad \text{for } q_{ci} \leq 19 \text{ MPa} \quad (6a)$$

or

$$q_{si} \text{ (MPa)} = 0.005 N_i + w_s \quad \text{for } N_i \leq 50 \quad (6b)$$

where w_s is a constant similar to w_b , q_{ci} is the CPT cone resistance for soil layer i , and N_i is the uncorrected SPT blow count for soil layer i . For soils containing uniform, rounded particles with up to 40% fines, $w_s = 0$ and the limiting value of q_{si} is 0.16 MPa (23 psi). For soils with well-graded, angular particles having less than 10% fines, $w_s = 0.05$ MPa (7 psi) and the limiting value of q_{si} is 0.21 MPa (30 psi). Interpolation of w_s is suggested for intermediate

soils. This shaft capacity calculation method is recommended only for sandy soils, where pile installation results in soil densification. Brettmann and NeSmith (2005) recommended the use in Eqs. (5b) and (6b) of energy-corrected SPT blow count N_{60} values.

Method B

Bustamante and Ganeselli (1993, 1998) developed a design method based on the results of 24 load tests on Atlas piles. They defined the ultimate pile load capacity as the load corresponding to 10% relative settlement (i.e., the load corresponding to a pile head settlement equal to 10% of the pile diameter).

According to this method, the unit base resistance is given by:

$$q_b = K\alpha \quad (7)$$

where K is a coefficient that depends on the soil type (Table 1), and α represents an average of the *in situ* test results within an influence zone extending from a distance a above to a below the pile base (Table 2). For the SPT-based design, the parameter α is the average (geometric mean) of N_1 , N_2 and N_3 (see Table 2). For the PMT-based design, the parameter α is the average (geometric mean) of p_{11} , p_{12} and p_{13} (see Table 2). To obtain α from a CPT profile, the *in situ* q_c profile is modified within the influence zone. This is done in four successive stages: (i) the *in situ* q_c profile is smoothed to remove local irregularities within the influence zone, (ii) an arithmetic mean q_{ca} is calculated within the influence zone, (iii) a q_{ce} profile is obtained within the influence zone by applying bounds to the minimum and maximum resistances in the q_c profile: for the zone above the pile base, the resistance values are clipped

[TABLE 1] Values of K for different soil types (Bustamante and Ganeselli 1998).

Soil Type	In situ Tests		
	PMT	CPT	SPT
Clay	1.6-1.8	0.55-0.65	0.9-1.2
Sand	3.6-4.2	0.50-0.75	1.8-2.1
¹ Gravel	≥ 3.6	≥ 0.5	-
¹ Marl	2.0-2.6	≥ 0.7	≥ 1.2
¹ Chalk	≥ 2.6	≥ 0.6	≥ 2.6

¹Conservative values are reported due to inadequacy of test results

between $0.7q_{ca}$ and $1.3q_{ca}$, and for the zone below the pile base, an upper bound of $1.3q_{ca}$ is applied, and (iv) the arithmetic mean q_{ce} value is calculated from the q_{ce} profile obtained in (iii).

To estimate the unit shaft resistance q_{si} , a design curve (Q_1 , Q_2 , Q_3 , Q_4 or Q_5) is first selected depending on the soil type and the guidelines given in Table 3. Fig. 11 is then used to estimate q_{si} from the design curve selected.

[TABLE 2] Values of α and a for different *in situ* tests (Bustamante and Ganeselli 1998).

In situ Tests	Description of α (MPa)	a	
SPT	$^a 1000 \times \sqrt[3]{N_1 \times N_2 \times N_3}$	0.5m	
CPT	Arithmetic Mean of q_{ce}	$1.5 D_b$	
PMT	$\sqrt[3]{p_{11} \times p_{12} \times p_{13}}$	0.5m	

^aThe factor 1000 is used to maintain consistency between units.

The q_c value used to develop this method was obtained from penetration tests using an M1-type mechanical cone. When an electrical CPT cone is used, a correction factor β was recommended:

$$q_{c,mech} = \beta q_{c,elec} \quad (8)$$

where $q_{c,mech}$ is the cone resistance measured with a mechanical cone, and $q_{c,elec}$ is the cone resistance measured with an electrical cone. The coefficient β is in the 1.4-1.7 range for clayey soils and is equal to 1.3 for saturated sands (Bustamante and Ganeselli 1993).

[TABLE 3] Guidelines for selection of a design curve to estimate q_s from Fig. 11 (Bustamante and Ganeselli 1998).

Soil Type	Limit pressure from PMT (MPa)	Cone Resistance (MPa)	Curves	
			C	M
Clay / Clayey Silt / Sandy Clay	< 0.3	< 1.0	Q1	Q1
	> 0.5	> 1.5	Q3	Q2
	≥ 1.0	≥ 3.0	Q4	Q2
Sand / Gravel	< 0.3	< 1.0	Q1	Q1
	> 0.5	> 3.5	Q4	Q2
	≥ 1.2	> 8.0	Q5	Q2
Marl	< 1.2	< 4.0	Q4	Q2
	≥ 1.5	≥ 5.0	Q5	Q2
Chalk	> 0.5	> 1.5	Q4	Q2
	≥ 1.2	> 4.5	Q5	Q2

C = Cast-in-place screw piles, M = Screw piles with lost casing

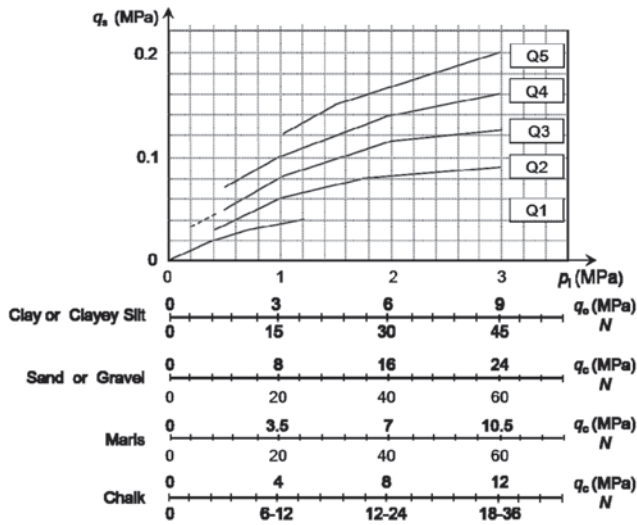


[FIG. 11] Values of unit shaft resistance q_s as a function of p_i , q_c or N (Bustamante and Gianeselli 1993, 1998).

Method C

In the Belgian pile design practice, the capacity of DD piles is calculated using empirical expressions that were developed based mainly on CPT and pile load test results (Van Impe 1986, 1988, 2004; Bauduin 2001; Holeyman *et al.* 2001; De Vos *et al.* 2003; Maertens and Huybrechts 2003a). The design practice for DD piles was strongly influenced by the results of the pile load tests performed at the Sint-Katelijne-Waver and Limelette test sites (Holeyman 2001; Maertens and Huybrechts 2003b; Van Impe 2004); these load tests were supported by the Belgian Building Research Institute (BBRI). This method is applicable to all types of DD piles. The current Belgian practice follows the guidelines developed for the implementation of Eurocode 7 (Application de l'Eurocode 7 en Belgique 2008). The ultimate unit base resistance corresponding to 10% relative settlement is given by:

$$q_b = \lambda \alpha_b \varepsilon_b q_{b,CPT} \quad (9)$$

where λ is a reduction factor accounting for what was referred to as the "soil relaxation" that may take place around the shaft during the drilling process due to the presence of an enlarged base, α_b is an empirical factor that accounts for the pile installation technique and soil type, ε_b is a scaling coefficient (accounting for fissuring of the soil) expressed as a function of the ratio of the diameter of the pile base D_b to that of the standard electrical CPT cone d_{CPT} ($= 35.7$ mm), and $q_{b,CPT}$ is the representative base resistance calculated from a CPT resistance q_c profile obtained according to the method

proposed by De Beer (De Beer 1971; Van Impe 1986; Van Impe *et al.* 1988).

According to the recent guidelines presented in the Application of Eurocode 7 in the Belgian practice (Application de l'Eurocode 7 en Belgique, 2008), the factor $\lambda = 1$ for all the DD piles considered in this paper, except for the Fundex pile. For the Fundex pile, the value of λ is obtained from :

$$\lambda = \begin{cases} = 1.0; & \left(\frac{D_b}{D_s}\right)^2 \leq 1.5 \\ = 1 - 0.429 \left[\left(\frac{D_b}{D_s}\right)^2 - 1 \right]; & 1.5 < \left(\frac{D_b}{D_s}\right)^2 < 1.7 \\ = 0.7; & \left(\frac{D_b}{D_s}\right)^2 \geq 1.7 \end{cases} \quad (10)$$

The factor α_b varies between 0.7 and 0.8 (see Table 4). The coefficient $\varepsilon_b = \max [1.0 - 0.01(D_b/d_{CPT} - 1); 0.476]$ for stiff, fissured tertiary clay, while, for all other soil types, $\varepsilon_b = 1.0$.

The unit shaft resistance q_{si} for the i^{th} soil layer is related to the average cone resistance q_{ci} (obtained using a standard electrical cone) of that layer by:

$$q_{si} = \alpha_{si} \eta_p^* q_{ci} \quad (11)$$

where α_{si} and η_p^* are empirical factors. α_{si} depends on the method of installation in a particular soil and the roughness of the pile shaft (see Table 4). Table 5 shows the values of η_p^* , which are a function of soil type and q_{ci} . Beyond a certain value of q_{ci} , a maximum design value is prescribed for q_{si} (Table 5). Note that, in the shaft capacity calculations, the

[TABLE 4] Values of α_b and α_{si} for use in Eqs. (9) and (11) (Application de l'Eurocode 7 en Belgique 2008).

Pile Types	α_b		α_{si}	
	Tertiary Clay	Other Soils	Tertiary Clay	Other Soils
Piles cast <i>in situ</i> using concrete	0.8	0.7	0.9	1.0
Piles cast using lost casing	0.8	0.8	0.6	0.6

contributions of soil layers with $q_{ci} < 1\text{MPa}$ (145 psi) are neglected.

The Belgian practice for DD piles, as described above, relies on q_c values obtained using an electrical cone. A reduction factor ω is suggested (see Table 6) for q_c values obtained from CPTs performed in tertiary clay using a mechanical cone (i.e., $q_{c,elec} = q_{c,mech}/\omega$).

[TABLE 5] Values of η_p^* for use in Eq. 11 (modified after Application de l’Eurocode 7 en Belgique 2008).

Soil Type	Average Cone Resistance q_{ci} (MPa)	η_p^*	Maximum q_{si} (MPa)
Clay	1-4.5	0.0333	0.150 for $q_{ci} > 4.5$ MPa
Silt	1-6	0.0167	0.100 for $q_{ci} > 6$ MPa
Sandy Silt/ Clay or Clayey Silt/ Sand	1-10	0.0125	0.125 for $q_{ci} > 10$ MPa
Sand	1-10	0.0111	-
	10-20		0.110 + 0.004 ($q_{ci} - 10$)
	> 20	-	0.150

[TABLE 6] Reduction factor ω (Application de l’Eurocode 7 en Belgique 2008).

Type of Mechanical Cone	Tertiary Clay	Other Types of Soil
M1	1.3	1.0
M2	1.3	1.0
M4	1.15	1.0

CAPACITY CALCULATIONS USING THE DIFFERENT DESIGN METHODS

We selected the soil profiles of two well documented pile load test sites to evaluate the different methods of pile capacity calculation described above. The first test site is at Limelette, Belgium; this site was used for the load test program supported by the BBRI. The second test site is located at the Georgia Institute of Technology campus; this test site was used for a load test program on drilled shafts.

Test site at Limelette, Belgium

The pile load test site at Limelette, Belgium, consists of a silty and sandy clay layer down to a depth of 8.2 m (27 ft); this layer is underlain by a clayey sand layer (Van Alboom and Whenham 2003). The water table at the site is located at a depth well below the base of the test piles. Five different types of DD piles were installed and subjected to static load tests (SLTs). The pile geometries, (D_b , D_s and length L_p), as obtained from Huybrechts and Whenham (2003), are given in Table 7. All the test piles, except the Fundex piles, have the same nominal shaft and base diameters (D_s and D_b) for calculation of base and shaft resistances (the nominal design diameters were selected following the guidelines described previously).

We used the average cone resistance profiles [obtained from CPTs done with an electrical cone (for use in Methods A and C) and a mechanical M1-type cone (for use in Method B)], reproduced in Fig. 12, to calculate the ultimate pile capacities. Fig. 12 also shows the $q_{b,CPT}$ profile (calculated using De Beer’s Method) for use in design method C. The calculated ultimate capacities of the test piles are given in Table 8, which also includes the reported ultimate capacities of the piles obtained from the SLTs (Maertens and Huybrechts 2003a). For piles A2, B3, B4, C1 and C2, the SLTs could not be continued up to a pile head settlement of 10% of the pile diameter. For these piles, Chin’s method of extrapolation (Chin 1970) was used to extend the load-settlement curves; the ultimate capacities of these piles were

[TABLE 7] Pile geometries (Huybrechts and Whenham 2003).

Pile Tag	Pile Type	D_s	D_b	L_p
		(m)	(m)	(m)
B3	Atlas	0.51	0.51	9.43
B4				
A4	DeWaal	0.41	0.41	9.53
C4				
A1	Fundex	0.39	0.45	9.59
C1				9.65
A2	Olivier	0.55	0.55	9.20
C2				9.13
A3	Omega	0.41	0.41	9.45
C3				

obtained from the extrapolated curves as the loads corresponding to a pile head settlement equal to 10% of the pile diameter (Maertens and Huybrechts 2003a).

As can be seen in Table 8, the smallest base capacity estimates were obtained with Method A (originally developed for APGD piles). Note that method A could not be used for shaft capacity calculations at this site because the test piles were installed mostly in clayey soils, for which method A is not applicable. Base capacity estimates obtained with method B, (originally developed for the Atlas pile) were larger (by 26-38%) than those calculated using method C. However, the shaft capacity estimates of methods B and C were in good agreement (within 3%).

The total ultimate capacities calculated using method B are consistently higher than the capacities obtained from the SLTs; the maximum difference was obtained for the DeWaal and Olivier piles (for these two pile types, the total ultimate capacities estimated using method B were larger than the SLT capacities by 17% and 20%, respectively). For the Olivier pile A2, the total ultimate capacity calculated using method C is in good agreement (the difference is ~1%) with the ultimate capacity obtained from the extrapolated load-

settlement curve. For the Atlas, Omega and Fundex A1 piles, the total ultimate capacities estimated using method C were smaller (by 11%, 13% and 14%, respectively) than the SLT capacities. For the DeWaal piles, the total ultimate capacities obtained with method C were larger (by 5%) than the SLT capacities.

Test site at Georgia Institute of Technology

We used the residual soil profile at the Georgia Institute of Technology test site to calculate and compare the capacities of a DD pile (using design methods A, B and C), a full-displacement pile and a nondisplacement pile. Subsurface information for this site is available from the results of *in situ* and laboratory tests performed to characterize the test site (FHWA Technical Report 1993). The subsurface at this site consists of a silty sand (SM) layer extending down to depths ranging from 15.8 m to 19.7 m (52 to 65 ft); this silty sand layer is underlain by a partially weathered rock bed. A fill layer 0.6-3.7 m (2-12 ft) thick comprised mostly of silt and sand, is present above the silty sand layer. The ground water table was recorded (at the time of site characterization) at depths ranging from 16.7 m to 19.1 m (55.0 to 62.7 ft) from the ground surface. Particle size analysis of the collected samples revealed that the site consists

[TABLE 8] Ultimate capacities of different drilled displacement piles at the Limelette test site, Belgium.

Pile Tag	Pile Type	Calculated Base Capacity (kN)			Calculated Shaft Capacity (kN)		Calculated Total Capacity (kN)		Capacity Obtained from SLTs (kN)
		Different Design Methods							
		A	B	C	B	C	B	C	
B3	Atlas	1220	2160	1460	1648	1671	3808	3131	^a 3528
B4									^a 3454
A4	DeWaal	832	1456	1079	1351	1363	2807	2442	2400
C4									2248
A1	Fundex	992	1776	1312	1300	1309	3076	2621	2988
C1			1808	1344	1313	1318	3121	2662	^{a, b} 1778
A2	Olivier	1440	2496	1560	1714	1757	4210	3317	^a 3354
C2		1416	2400	1488	1694	1742	4094	3230	^{a, b} 2908
A3	Omega	806	1456	1079	1333	1350	2789	2429	2786
C3									2723

^a Values (corresponding to a pile head settlement equal to 10% of the pile diameter) were obtained from extrapolated load-settlement curves (Maertens and Huybrechts 2003a)

^b Low ultimate capacities of C1 and C2 are attributed to the segregation of concrete and structural rupture (Maertens and Huybrechts 2003a)

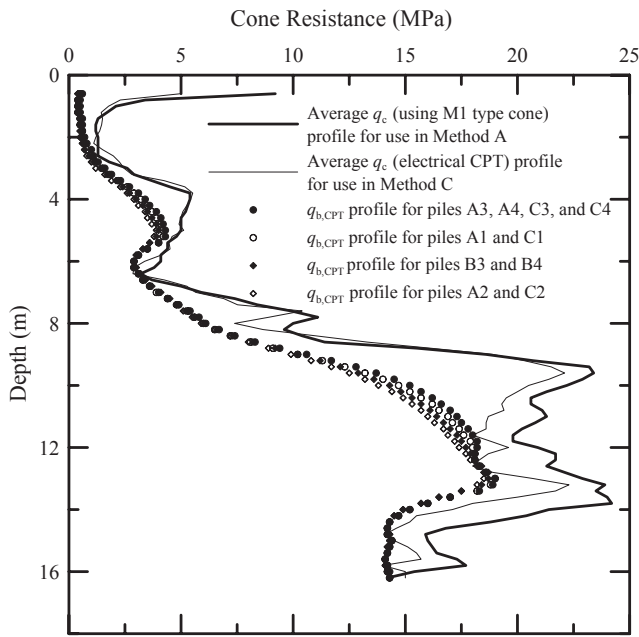


[FIG. 12] Average cone resistance and $q_{b,CPT}$ profiles at the Limelette test site.

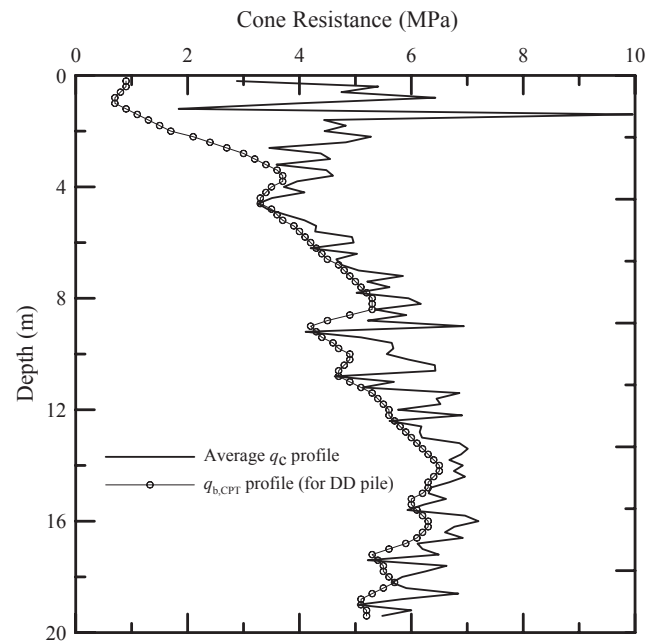


[FIG. 13] Average cone resistance and $q_{b,CPT}$ profiles at the Georgia Institute of Technology test site.

[TABLE 9] Calculated capacities for a DD pile, a full-displacement pile, and a nondisplacement pile (soil profile of the Georgia Institute of Technology test site).

Pile Types	Shaft Capacity (kN)			Base Capacity (kN)			Total Capacity (kN)		
	Method			Method			Method		
DD Pile	A	B	C	A	B	C	A	B	C
	596	955	668	236	459	387	832	1414	1055
Full-displacement Pile	Schmertmann (1978)			Aoki and Velloso (1975)			-		
	704			427			1131		
Nondisplacement Pile	Lopes and Laprovitera (1988)			Franke (1989)			-		
	251			151			402		

of mostly uniform sand particles (median $D_{50} = 0.14$ mm) with 33% fines. The average total unit weight assumed in calculations was 19.2 kN/m^3 ($3,300 \text{ lb/cu yd}$) (FHWA Technical Report 1993). Fig. 13 shows an average CPT profile of this site; this figure also shows the $q_{b,CPT}$ profile (calculated using De Beer's Method) for use in design method C.

The DD, full-displacement, and nondisplacement piles were assumed to be 10 m (33 ft) long with nominal base and shaft diameter equal to 0.4 m (15.75 in). We used CPT-based methods (Aoki and Velloso 1975; Schmertmann 1978; Lopes and Laprovitera 1988; and Franke 1989) to calculate the base and shaft capacities of the full-displacement

and nondisplacement piles in sand. Table 9 shows the calculated capacities for all these piles. It is interesting to note that the capacity of the DD pile calculated using method B is larger than that of the full-displacement pile with the same geometry. The DD pile capacity obtained with method A, however, lies between the capacities calculated for the full-displacement and nondisplacement piles (this is in agreement with the notion that the soil displacement produced during the installation of a DD pile is within the range of that of a partial- to that of a full-displacement pile). The DD pile capacity calculated using method C matches closely the capacity of the full-displacement pile calculated with the Aoki and Velloso (1975)

and Schmertmann (1978) methods. Note that general conclusions can not be reached based on the calculations presented in Table 9; they provide only a site-specific comparison of predicted capacities.

SUMMARY AND CONCLUSIONS

Drilled displacement piles are increasingly used in geotechnical practice. The advantages of these piles are that their construction is fast, economical and environmentally friendly. Depending on the method of installation, DD piles can be classified as partial-displacement piles, with capacities sometimes approaching that of full-displacement piles.

Pile capacity calculation methods do not always predict field capacities with acceptable accuracy. One of the reasons for the difficulty in making good predictions is that the degree of soil disturbance caused by pile installation cannot be assessed properly in the field. Different DD pile installation methods (with different drilling tools) change the soil state differently, leading to different pile load-carrying capacities. Additionally, for the same degree of soil disturbance, a screw-shaped shaft may develop a larger shaft capacity than a smooth shaft. The design methods described in this paper were developed based on pile load tests performed at particular test sites. Consequently, these methods have biases and may not be applicable to other sites without proper calibration. There is also the need for the design methods to be more precise, going beyond just textbook soils (sand and clay).

In order to illustrate the capabilities of currently available design methods, we used these methods to estimate the capacities of the DD piles load-tested at the Limelette test site in Belgium. Additionally, we compared the capacities of DD, full-displacement and nondisplacement piles for a residual soil profile of granite. The comparisons of the calculated and measured pile capacities show that improvements in the design methods are necessary. In particular, future improvement of DD pile design methods should include (1) parameters that reflect the pile installation method and their impact on the state of the soil around the pile; (2) interaction of the pile and soil in a way that reflects the stress-strain response of the soil; (3) limit states that must be prevented. Development of a database containing *in situ* test results (performed before and after pile installation) and pile load

test results can help improve the prediction capability and consistency of design methods for DD piles. These load tests should be extended to large pile settlements (certainly in excess of 10% of the pile diameter), the piles should preferably be instrumented (so that, at a minimum, base and shaft resistances may be separated) and the test sites must be well characterized. Modeling of the pile installation process in conjunction with well designed field load tests and systematic monitoring of pile installation is needed for meaningful advances in the analysis and design of DD piles.

ACKNOWLEDGMENTS

Dr. Irem Zeynep Yildirim assisted with the drafting of some of the figures presented in this paper. The authors greatly appreciate her helpful efforts. The authors also thank the reviewers for their valuable comments.

REFERENCES

1. American Pile Driving, Inc. <americanpiledriving.com > as seen on March 2, 2007.
2. Aoki, N., and Velloso, D. A. 1975. An Approximate Method to Estimate the Bearing Capacity of Piles. Proceedings of the 5th Pan-American Conference of Soil Mechanics and Foundation Engineering, Buenos Aires, Vol. 1, pp. 367-376.
3. Application de l'Eurocode 7 en Belgique : Directives pour le dimensionnement en ELU de pieux sous charge axiale en compression, Version de mars 2008.
4. Bauduin, C. 2001. Design procedure according to Eurocode 7 and analysis of the test results. Screw Piles - Installation and Design in Stiff Clay, Holeyman (ed.), Swets and Zeitlinger, Lisse, pp. 275 - 303.
5. Bottiau, M., 2006. Recent evolutions in deep foundation technologies. *Proceedings of the DFI/EFFC 10th International Conference on Piling and Deep Foundations*, 2006, Amsterdam, The Netherlands.
6. Bottiau, M., Meyus, I. and Callens, S. 2008. Screw-in energy measurement for on-site control of the bearing capacity of Omega piles. *Proceedings of the 7th International Conference and Exhibition on Piling and Deep Foundations*, 2008, Vienna, Austria.
7. Brettmann, T. and NeSmith, W., 2005. Advances in auger pressure grouted piles:

- design, construction and testing. *Advances in Designing and Testing Deep Foundations*. Geotechnical Special Publication No. 129, ASCE, pp. 262-274.
8. Brettmann, T., 2003. Constructibility of augered cast-in-place piles. *Geo-Strata*, 8 - 11.
 9. Brown, D. A., 2005. Practical considerations in the selection and use of continuous flight auger and drilled displacement piles. Advances in auger pressure grouted piles: design, construction and testing. *Advances in Designing and Testing Deep Foundations*. Geotechnical Special Publication No. 129, ASCE, pp. 251-261.
 10. Brown, D. A., Dapp, S. D., Thompson, W. R. and Lazarte, C.A. 2007. Design and construction of continuous flight auger piles. FHWA Geotechnical Engineering Circular No. 8. FHWA.
 11. Brown, D. and Drew, C., 2000. Axial capacity of augered displacement piles at Auburn University, *New Technological and Design Developments in Deep Foundations, Proceedings of sessions of Geo- Denver 2000*, Geotechnical Special Publication No. 100, ASCE, pp. 397-403.
 12. Bustamante, M. and Gianceselli, L., 1993. Design of auger displacement piles from in-situ tests. *Deep Foundations on Bored and Auger Piles, BAP II*, Balkema, Rotterdam, pp. 21-34.
 13. Bustamante, M. and Gianceselli, L., 1998. Installation parameters and capacity of screwed piles. *Deep Foundations on Bored and Auger Piles, BAP III*, Balkema, Rotterdam, pp. 95-108.
 14. Chin, F. V. 1970. Estimation of ultimate load of piles not carried to failure. *Proc. 2nd Southeast Asian Conference on Soil Engineering*, 81-90.
 15. De Beer, E. Méthodes de déduction de la capacité portante d'un pieu à partir des résultats des essais de pénétration. Bruxelles, Journal des Travaux publics de Belgique, volume 72, no 4 (p. 191-268), no 5 (p. 321-353) & no 6 (p. 351-405), 1971-1972.
 16. De Vos, M., Bauduin, C. and Maertens, J. 2003. The current draft of the application rules of Eurocode 7 in Belgium for the design of pile foundations. *Belgian Screw Pile Technology - Design and Developments*, Maertens and HuyBrechts (eds.), Swets and Zeitlinger, Lisse, pp. 303 - 325.
 17. De Cock, F. and Imbo, R., 1994. Atlas screw pile: a vibration-free, full displacement, cast-in-place pile. *Transportation Research Record* 1447, pp 49-62.
 18. FHWA Technical Report No. 41-30-2175. 1993. Axial load-displacement behavior of drilled shaft foundations in piedmont residuum.
 19. Fleming, W. G. K. and Thorburn, S., 1983. Recent piling advances, state of the art report. *Proceedings of the International Conference on Advances in Piling and Ground Treatment for Foundations*, ICE, London, pp 1-16.
 20. Franke, E. 1989. Co-report to discussion, session 13: large-diameter piles. *12th International Conference on Soil Mechanics and Foundation Engineering*, Rio de Janeiro.
 21. Geoforum <http://www.geoforum.com/info/pileinfo/class_list.asp?Method=4> as seen on November 25, 2008.
 22. Holeyman, A. E. 2001. Screw piles - installation and design in stiff clay. *Proceedings of the Symposium on Screw Piles*, Brussels, Belgium. Swets and Zeitlinger B. V., Lisse, The Netherlands.
 23. Holeyman, A., Bauduin, C., Bottiau, M., Debacker, P., De Cock, F. A., Dupont, E., Hilde, J. L., Legrand, C., Huybrechts, N., Mengé, P., Miller, J. P., and Simon., G. 2001. Design of axially loaded piles - 1997 Belgian practice. *Screw Piles - Installation and Design in Stiff Clay*, Holeyman (ed.), Swets and Zeitlinger, Lisse, pp. 63 - 88.
 24. HuyBrechts, N. and Whenham V., 2003. Pile testing campaign on the Limelette test site and installation techniques of screw piles. *Belgian Screw Pile Technology - Design and Developments*, Maertens and HuyBrechts (eds.), Swets and Zeitlinger, Lisse, pp. 71 - 130.
 25. Lopes, F. R., and Laprovitera, H. (1988). On the Prediction of the Bearing Capacity of Bored Piles from Dynamic Penetration Tests. *Deep Foundations on Bored and Auger Piles*, W. Van Impe (ed.), Balkema, Rotterdam, pp. 537-540.
 26. Maertens, J. and Huybrechts, N., 2003a. Results of the static pile load tests at the Limelette test site. *Belgian Screw Pile Technology - Design and Developments*, Maertens and HuyBrechts (eds.), Swets and Zeitlinger, Lisse, pp. 167 - 214.

27. Maertens, J., and Huybrechts, N. 2003b. Belgian screw pile technology design and recent developments. *Proceedings of the 2nd Symposium on Screw Piles*, Brussels, Belgium. Swets and Zeitlinger B. V., Lisse, The Netherlands.
28. Mandolini, A., Ramodini, M., Russo, G. and Viggiani, C., 2002. Full scale loading tests on instrumented CFA piles. *Proceedings of the International Deep Foundations Congress 2002*, Geotechnical Special Publication No. 116, Vol. 2, ASCE, pp. 1088-1097.
29. NeSmith, W. M., 2002. Static capacity analysis of augured, pressure-injected displacement piles. *Proceedings of the International Deep Foundations Congress 2002*, Geotechnical Special Publication No. 116, Vol. 2, ASCE, pp. 1174-1186.
30. NeSmith, W. M., 2003. Installation effort as an indicator of screw pile capacity. *Proceedings of Deep Foundations on Bored and Augered Piles (BAPIV)*, Van Impe (ed.), Rotterdam: Millpress, pp. 177-181.
31. NeSmith, W. M., and NeSmith, W. M. 2006a. Anatomy of a data acquisition system for drilled displacement piles. *Proceedings of the GeoCongress 2006: Geotechnical engineering in the information technology age*, ASCE, pp. 1-6.
32. NeSmith, W. M., and NeSmith, W. M. 2006b. Application of data acquired during drilled displacement pile installation. *Proceedings of the GeoCongress 2006: Geotechnical engineering in the information technology age*, ASCE.
33. NeSmith, W. M., 2003. Advancements in data acquisition based design for drilled displacement piles. *Contemporary Topics in Deep Foundations: Geotechnical Special Publication No. 185*, ASCE, pp. 447-455.
34. Prezzi, M. and Basu, P. 2005. Overview of construction and design of auger cast-in-place and drilled displacement piles. *Proceedings of DFI's 30th annual conference on deep foundations*, Chicago, U.S.A., pp. 497 - 512.
35. Siegel, T. C., NeSmith, W. M., NeSmith, W. M., and Cargill, P. E. 2007. Ground improvement resulting from installation of drilled displacement piles. *Proceedings of DFI's 32nd annual conference on deep foundations*, Colorado Springs, U.S.A., pp. 129-138.
36. Schmertmann, J.H. 1978. Guidelines for Cone Penetration Test, Performance and Design. *U.S. Department of Transportation*, FHWA-TS-78-209.
37. Van Alboom, G. and Whenham, V., 2003. Soil investigation campaign at Limelette (Belgium): results, Belgian Screw Pile Technology - Design and Recent Developments, Maertens and HuyBrechts (eds.), Swets and Zeitlinger, Lisse, pp. 21 - 70.
38. Van Impe, W. F. (1986). Evaluation of deformation and bearing capacity parameters of foundations, from static CPT-results. *Proceedings of the Fourth International Geotechnical Seminar: Field Instrumentation and In Situ Measurements*, NTI, Singapore, pp 51-70.
39. Van Impe, W. F. (1988). Considerations in the auger pile design. *Proceedings of the 1st International Geotechnical Seminar on Deep Foundations on Bored and Auger Piles, BAP I*, Balkema, Rotterdam, pp. 193-217.
40. Van Impe, W. F. (2004). Two decades of full scale research on screw piles : An overview. Published by The Laboratory of Soil Mechanics, Ghent University, Belgium.
41. Van Impe, W. F., De Beer, E., and Lousberg, E. (1988). Prediction of the single pile bearing capacity in granular soils out of CPT results. *Proceedings of the International Symposium on Penetration Testing (ISOPT I)*, Speciality Session, Orlando, pp 1-34.

Analysis of a Deep Excavation In Calgary, Alberta

Thomas Lardner, Geotechnical Research Centre, University of Western Ontario, London, Ontario, Canada; 519-661-2139; tlardner@uwo.ca

Matthew Janes, Isherwood Associates, Mississauga, Ontario, Canada

K.Y. Lo, Geotechnical Research Centre, University of Western Ontario, London, Ontario, Canada

Guangfeng Qu, Geotechnical Research Centre, University of Western Ontario, London, Ontario, Canada

Silvana Micic, Geotechnical Research Centre, University of Western Ontario, London, Ontario, Canada

ABSTRACT

Excavation for The Bow, EnCana, in downtown Calgary, occurred between May 2007 and September 2008. A monitoring programme was used to determine the behaviour of the shoring wall, soil and bedrock during the excavation for the 21 metre (69 ft) deep excavation with a footprint of approximately 17,000 m² (183,000 sq ft). Results from the inclinometer readings indicated that significant horizontal movement due to a weak rock layer and shear band effect. These modes of movement account for up to 100 mm (4.0 in) and 45 mm (1.8 in) of lateral deflection, respectively.

Based upon the results of the monitoring programme, rock samples were collected from the weak mudstone bedrock, with great difficulty, to determine the strength and deformation parameters. Results from the uniaxial compression tests indicate a UCS around 830 kPa (120 psi) and elastic modulus between 80 and 180 MPa (11 and 26 ksi). Mohr-Columb parameters were determined to be $c' = 340$ kPa (49 psi) and $\phi' = 24^\circ$. Residual strengths were determined to be $c'_r = 0$ and $\phi'_r = 15^\circ$.

Using the results of the laboratory tests and field investigation records, an initial finite element analysis was conducted. Results of the analysis show good correlation when compared with the observed monitoring deformation, indicating accurate portrayal of rock parameters. Additional analysis and investigation is required to determine the principal horizontal stresses in magnitude and direction.

INTRODUCTION

The Bow office complex in downtown Calgary, Alberta, will consist of a 54-storey office complex with six levels of underground parking. Installation of the shoring system and excavation for the six storeys of parking began in May 2007 and was completed in September, 2008. The excavation has a footprint of approximately 17,000 m² (183,000 sq ft), a shored face of 13,200 m² (142,000 sq ft), and a depth of 20.5 metres (67.3 ft). Fig. 1 shows the location of the site in Calgary, between 5th and 7th Avenues at Centre Street. Neighbouring the excavation are the Telus building to the north, the PetroCanada Centre to the west, and the Historic Royal Canadian Legion No. 1 and Calgary Light Rail Transit line to the south. Given the proximity of the neighbouring structures, horizontal movement during excavation was a significant concern.

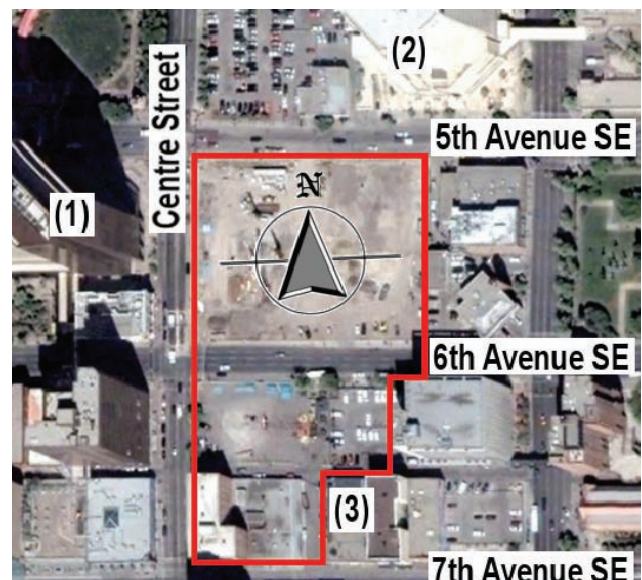


[FIG. 1] Google Earth™ mapping service image with The Bow job site outlined in red, the PetroCanada Centre (1), Telus Centre (2), and Historic Royal Canadian Legion (3).

General site stratigraphy consisted of a thin layer of fill overtop 6 to 7 metres (20 to 23 ft) of well graded gravel and cobble. The bedrock, part of the Porcupine Hills Formation, is composed of layered mudstone, siltstone, and sandstone. Large horizontal movements in the bedrock had been observed during previous deep excavations in Calgary. An extensive monitoring programme was therefore incorporated into the design of the support system so that appropriate measures could be taken in case large horizontal movement occurred.

The shoring design consisted of an anchored secant caisson wall embedded a minimum of 2 m (6.6 ft) into the bedrock with shotcrete shoring on the rock face below. A typical cross section is shown in Fig. 2. The design incorporated a monitoring program composed of 12 inclinometers, 6 extensometers, and precision survey monitoring at neighbouring buildings, the top of each pile, and along the face of the shoring. The monitoring program played an integral role in identifying the magnitude and location of movement during construction.

To better understand the mechanics behind observed movement, rock samples of the host material were taken and subjected to extensive testing by the Geotechnical Research Centre at the University of Western Ontario and Golder Associates. Results of the tests indicate the rock is weak with cohesion of 340 kPa (49 psi),

internal angle of friction of 24°, an elastic modulus between 80 and 170 MPa (11 and 25 ksi), and has some swelling potential. The Geotechnical Research Centre also conducted additional analysis of the monitoring results, and compared these results to preliminary finite element modeling using parameters taken from the post-construction testing.

GEOTECHNIQUE

AMEC Earth and Environmental performed geotechnical investigations at the site in 2005 and 2006. The ground surface at the site is generally level, with elevations ranging between 1045.5 and 1046.3 metres (3,430 and 3,433 ft). The site consists of 0 to 1.0 m (0 to 3.3 ft) of fill over 5.5 to 7.0 m (18 to 23 ft) of well graded, well rounded, fluvial gravel and cobble. Bedrock was encountered between elevations 1039 and 1041 metres (3,409 to 3,415 ft), with localized areas reaching 1035 to 1036 metres (3,396 to 3,399 ft). Groundwater is located in the gravels and varies seasonally from 1 to 3.5 m (3.3 to 11.5 ft) in depth above the rock surface.

The bedrock consists of horizontally bedded mudstone, siltstone and sandstone of the Porcupine Hills Formation of the Cretaceous or Paleocene Age (Jackson and Wilson 1987 and Osborn and Rejwicz 1998). The siltstone and sandstone form indurated, lenticular layers of varying thickness and extent. The mudstone Formed as lacustrine deposits, the cementing agent of the mudstones and siltstones is clay,

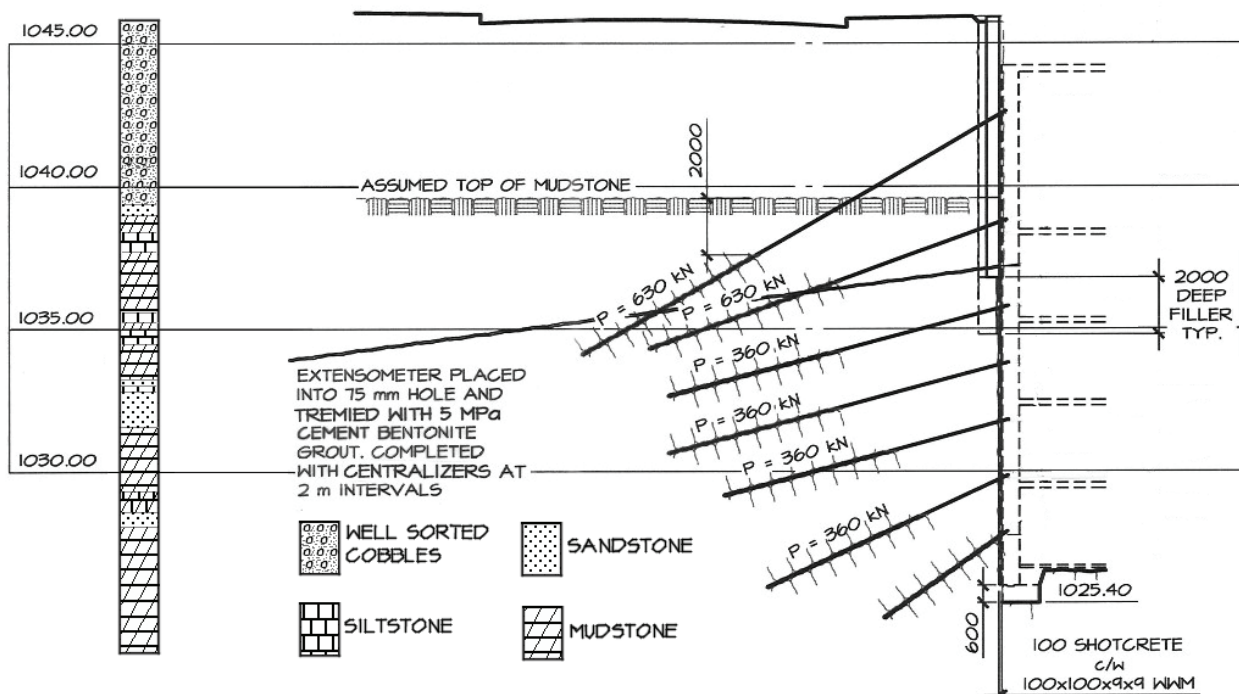


[FIG. 2] Typical cross section.

giving these formations a more soil-like quality than the sandstone lenses. The mudstone varies from very weak to medium strength, with point load axial tests recording strengths typically ranging from 0.16 to 0.8 MPa (23 to 116 psi). The siltstone and sandstone layers have medium to high strengths, with point load axial tests recording between 0.16 and 5.14 MPa (23 to 745 psi) in the siltstone, and 1.7 up to 8.1 MPa (247 to 1,175 psi) in the sandstone. The mudstone is prone to rapid weathering with the addition of oxygen and water after excavation. Based upon borehole logs, the rock mass quality is poor due to the Rock Quality Designation ranging from 0 to 95%, with an average value of 45%. Within the mudstone, zones of rock showing slickensides were reported throughout the geotechnical investigation.

At the time of design, little was known in regards to the bedrock properties. It was known that the bedrock was the cause of large horizontal movements during excavation in Calgary, with the two leading theories being an elevated in-situ stress ($k_0 = 2.0$), or a shear band phenomenon. The shear band phenomenon is suspected of occurring when the stresses due to excavation cause larger displacement of a thin weak layer of rock (AMEC 2006). There was minimal published data available on the strength and deformation properties of the various bedrock layers.

RESULTS OF THE MONITORING PROGRAMME

The monitoring programme at The Bow consisted of 12 inclinometers, 6 extensometers, and survey targets at the top of every pile, throughout the shotcrete wall, and on neighbouring structures. The location of the inclinometers and extensometers are shown in Fig. 3. Inclinometers were drilled separately from the piles and generally to a depth of 10 metres (33 ft) below the final excavation elevation. This was to ensure observations of any deep seated movement. The three monitoring methods were used to ensure accurate monitoring. Inclinometer readings successfully recorded deformations of the rock profile at the shoring face, and extensometers confirmed that the deformation extended beyond the soils and rock immediately adjacent to the wall.

Results from the monitoring indicated that horizontal movement is primarily caused by two methods: shear band movement and a

weak rock zone. These types of movement are shown readily in Inclinometers 4, 5, and 8. Inclinometers 4 and 8 show the behaviour of the shoring wall and rock mass under the influence of a shear band. All three show evidence of a weak rock layer in the upper portion of the bedrock.

Inclinometer 4 indicates the presence of a shear band at the approximate elevation of 1021 m (3,350 ft). Fig. 4 shows the movement observed in Inclinometer 4 over the duration of the excavation. Original grade, final excavation elevation, and current excavation elevation at the time of reading are also shown. Movement observed in Inclinometer 4 reached a maximum of 57.5 mm (2.3 in) at the end of excavation. Over half of this movement, 35 mm (1.4 in), occurs over a 0.6 to 1.2 m (2.0 to 4.0 ft) thick section of rock experiencing the shear band phenomena. Of particular interest is the elevation of the shear band. The movement occurs up to 5 metres (16 ft) below the final excavation elevation.

Inclinometer 5 is located on the east wall, at the north end. Despite the proximity to Inclinometer 4, it does not show any sign

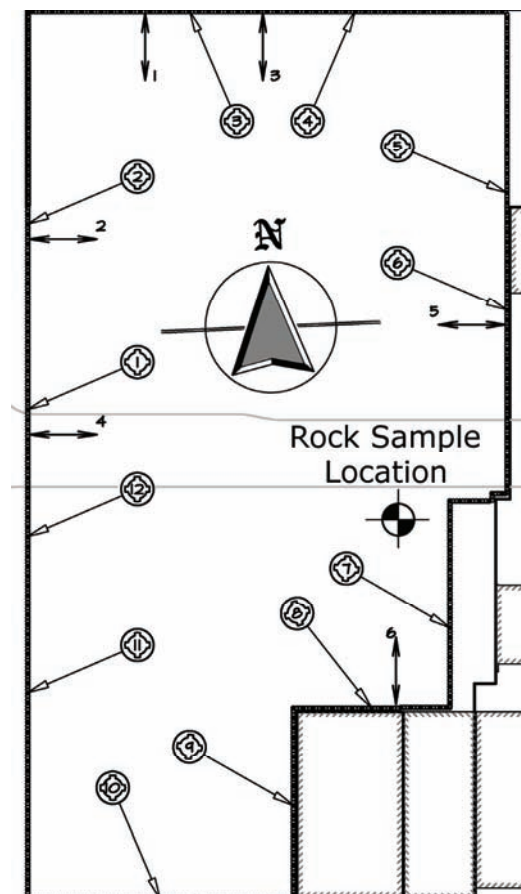


[FIG. 3] Location of inclinometers, extensometers, and rock samples

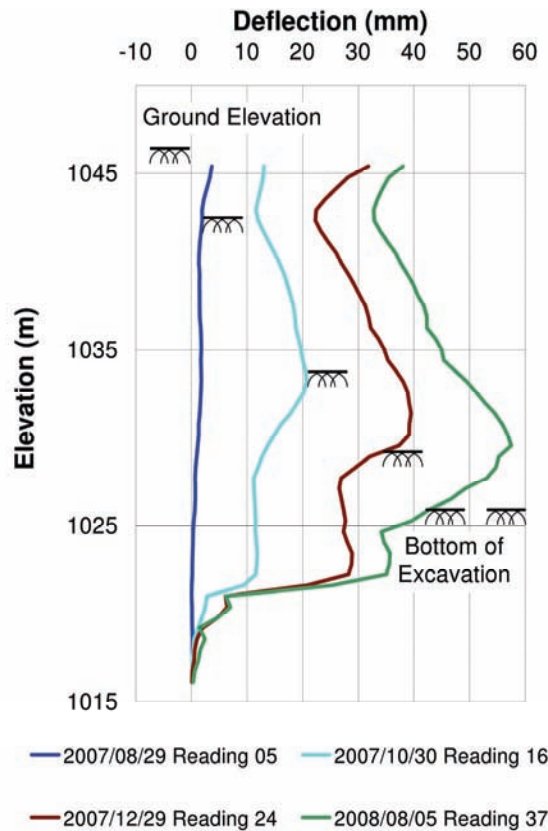


[FIG. 4] Results from Inclinator 4.

of shear band movement, and is instead representative of typical sites. Movement during excavation is shown in Fig. 5. The maximum recorded movement at the end of excavation was 46.5 mm (1.83 in). It should be noted that the inclinometers show some signs of movement at their base, indicating that the total movement could be greater than that recorded.

Comparing the results of Inclinator 5 to Inclinator 4 shows a similar curved protrusion occurring around elevation 1030 metres (3,379 ft). This indicates that similar mechanisms in rock behaviour are acting in the north-east corner, and that there is a possible direction dependency of the shear band phenomenon, as both inclinometers were affected by similar rates of excavation.

The movement during excavation, as observed in Inclinator 4, was compared directly to the rate of excavation, as shown in Fig. 6. This figure shows the movement along the shear band increasing, as the excavation level decreases. From observation, there appears to be a direct correspondence between the rate of excavation and the rate of movement experienced at the shear band. Of particular note, movement of the shear band begins

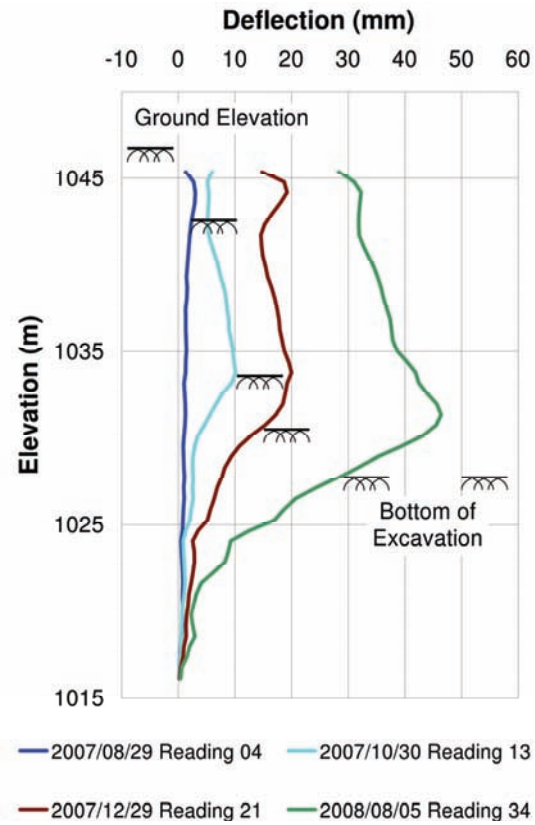


[FIG. 5] Results from Inclinator 5.

shortly after excavation into the rock. The shear band had experienced up to 3 mm (0.12 in) of movement when the excavation was still 12 m (39 ft) above.

The extent of deformation of the rock mass was measured with extensometers. Extensometer 1 is located on the north wall to the west of Inclinator 3. The extensometer consisted of five sensors placed at 5 metre (16.4 ft) intervals, and measured the amount of lateral deformation in the rock mass. Results from Extensometer 1 are shown in Fig. 7. The maximum horizontal extension measured was 19.6 mm (0.77 in) at the time of final excavation.

The extensometer was installed at elevation 1035.0 m \pm (3,396 ft \pm), shortly after excavation into the rock began. By comparing the amount of movement observed in Inclinator 3 and 4 at the time of installation, it can be seen that the extensometer did not capture the total movement. Inclinator records at that elevation indicate that up to 20 mm (0.79 in) of movement at the face of shoring was not captured by the extensometers.

The extent of movement beyond the shoring face can also be inferred by the extensometer records. The non-zero slope between the last two monitoring points indicates that movement

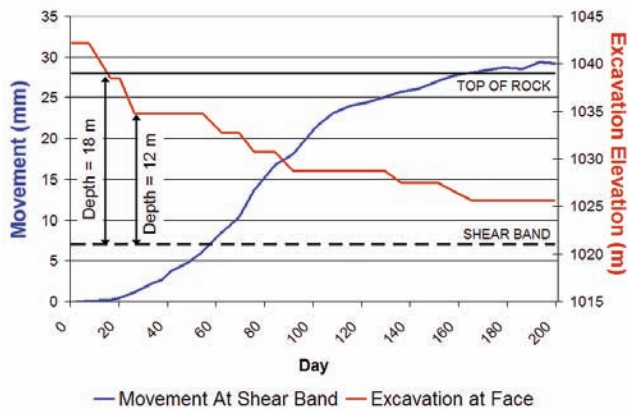


[FIG. 6] Movement at the shear band at Inclinerometer 4 over the course of the excavation.

is occurring past the 25 metre (82 ft) reach of the extensometer. The results of the extensometers are currently being studied.

Inclinometer 8 results are shown in Fig. 8, and show shear band movement around elevation 1028 m (3,373 ft), and a weak rock zone between 1031 and 1036 m (3,383 and 3,399 ft). Inclinometer 8 is useful in that it clearly shows a weak rock zone and a shear band, the two modes of large horizontal movement. Of the maximum 37.5 mm (1.48 in) into site movement, the shear band was responsible for up to 20 mm (0.8 in), and the weak rock for approximately 15 mm (0.6 in).

Readings indicate that the shear band shown in Inclinerometer 8 was located at approximate elevation 1028 m (3,373 ft), which daylighted into the excavation face. Unfortunately, the inclinometer was damaged during construction of the wall, so thorough readings could not be taken over the full course of the excavation. Inspection of the rock face at this elevation showed a 150 to 250 mm thick band (6 in to 10 in) of black mudstone, with some slickensides.

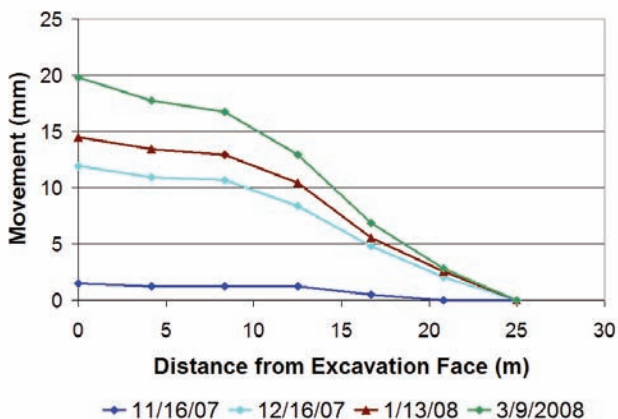


[FIG. 7] Readings from Extensometer I.

However, similar layers had been observed throughout the site during excavation, and were only occasionally correlated with shear band movement in the inclinometer readings.

Such descriptions bear some similarity to the bentonite layers encountered during the excavation for the Edmonton Convention Centre, as described in Chan and Morgenstern's 1987 paper. The paper states that such layers, with enough continuity, would control the excavation stability. However, the detailed mechanics of the movement may be different.

The Geotechnical Research Centre investigated the occurrence of the weak rock layer by compiling the axial and diametric point load test results and plotted them by elevation. The results are shown in Fig. 9. For most of the depth of the excavation, the axial load tests indicate good scatter. However, both tests show a zone that is predominantly the weak mudstone. This zone, between elevations 1028 and 1033 m (3,373 to 3,389 ft) correlates to the larger intrusions shown in the inclinometers, including the results from 4, and 5, above.

ROCK TESTING AND RESULTS

Results from the monitoring program prompted the collection of additional bedrock samples. Block samples were collected at between elevations 1027 and 1028 m (3,370 to 3,373 ft) near the east wall, just south of 6th Avenue SE, and north of Inclinerometer 7. The rock samples were taken from a thin, black, slickensided mudstone layer, similar to that observed at the location of the shear band in Inclinerometer 8. These samples were sent to Golder Associates for shear box testing, and the Geotechnical Research Centre for extensive testing of rock properties. Tests conducted by the GRC include uniaxial compressive tests, multi-stage direct shear tests, hydrostatic compression tests, semi-confined swell tests, null-swell tests, water content tests, Atterberg limits tests, unit weight tests, calcite content tests, and rock salinity tests. This paper will concentrate on the results of the first three test types. For full coverage of the tests, please see the 2009 paper by Lo and Micic.

Extraction of the block samples proved to be difficult. The weak, fissile nature of the rock required extreme caution when excavating. Attempts at producing large block samples proved ineffective. The use of machines was prohibitive, as the vibrations caused the rock to disintegrate. Recovered hand samples were

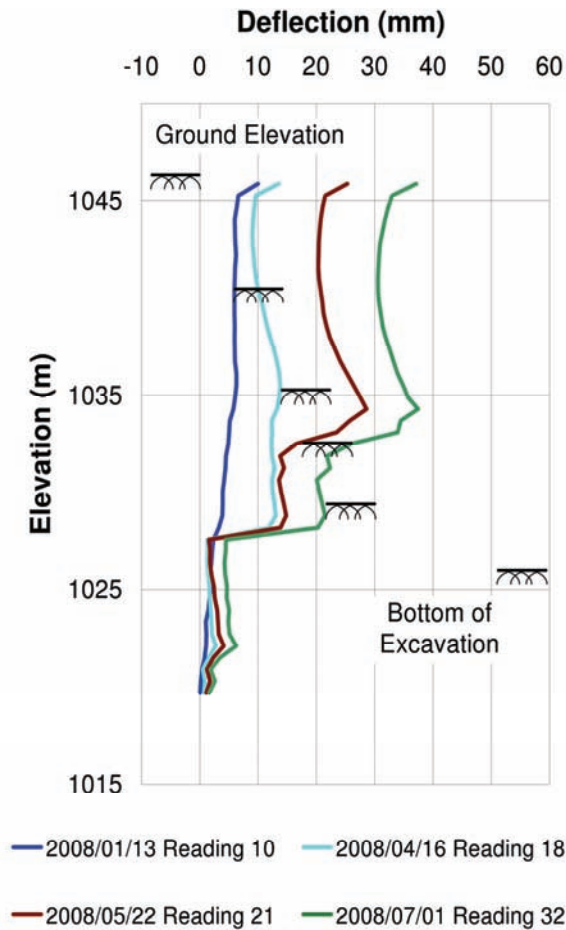


[FIG. 8] Results from Inclinometer 8.

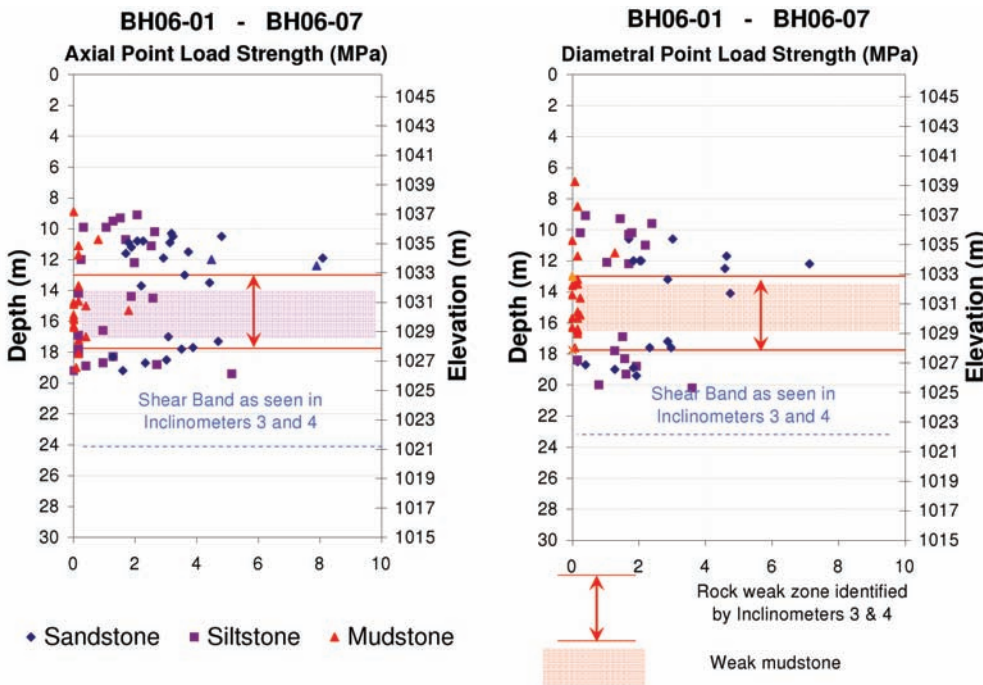


[FIG. 9] Point and Diametric Load test data indicating weak zones.

irregularly shaped, and immediately wrapped in plastic cling-wrap and coated in wax, to ensure no loss of moisture. However, the weak nature of the rock allowed for only square-prism

shaped test samples to be extracted from the larger block samples.

The Geotechnical Research Centre conducted 5 uniaxial compression tests, and five multi-stage direct shear tests. Results from the uniaxial compression tests are shown in Table 1. The combined results are plotted in Fig. 10.

Table 1 indicates a UCS ranging between 560 and 1230 kPa (81 to 178 psi), with a modulus of elasticity at 50% of ultimate strain (E50) between 80 and 170 MPa (11.6 to 24.7 ksi). Chan and Morgenstern (1987) estimated the clay shales to have a modulus of 137.9 MPa (20.0 ksi), and the bentonite layers 49 MPa (7.1 ksi). Results from the GRC uniaxial compression tests indicate that the weak mudstone is closer to the clay shale observed in Edmonton.

The results shown in Fig. 10 indicate that the intact rock has a cohesion value of approximately 340 kPa (49 psi), with an angle of internal friction of 24°. The residual strength parameters drop to zero cohesion and an angle of 15°. The scattering of results could be a result of the inevitable disturbance of the weak mudstone prior to testing. Triaxial compression test results and shear test results by Golder provide results consistent with the testing.

A hydrostatic test was completed to determine the bulk modulus of the rock. The sample was performed in a triaxial compression cell on a square sample of rock. Volume changes in the sample were recorded during the increase in pressure. The results of the test are shown in Fig. 11 and indicate two distinct regions. The first region shows a large change in volume over a very small increase in pressure is attributed to the closing of fissures in the sample. The second region is attributed to the deformation of the rock and is used to derive the

bulk modulus (Goodman 1980). Results show a bulk modulus, K, of approximately 80 MPa (11.6 ksi), which is consistent with the results from the uniaxial compression tests, assuming

[TABLE 1] Results of uniaxial compressive tests.

Test Number	Uniaxial Compressive Strength (kPa)	Modulus (MPa)	
		E_t	E_{50}
UCT 1	720	138	122
UCT 2	1070	180	170
UCT 3	570	85	80
UCT 4	560	135	132
UCT 5	1230	168	160

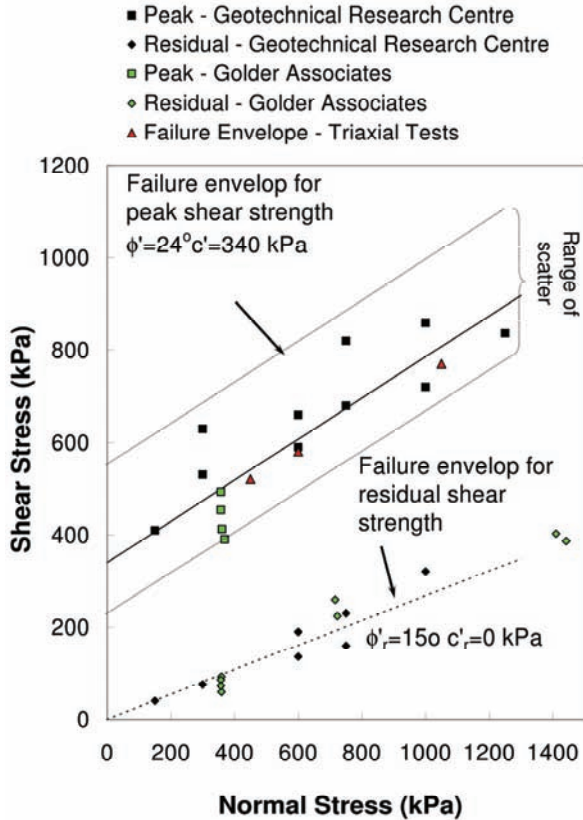


[FIG. 10] Results of multi-stage direct shear tests.

that the Poisson's ratio varies from 0.15 to 0.3 by the equations of elasticity.

Additional tests indicated that the average unit weight of the rock was 22.24 kN/m³ (3,823 lb/cu yd).

POST CONSTRUCTION MODELING

Using the parameters gained from the testing, numerical analyses were performed and the results compared to the deflection measurements observed over the course of the excavation.

The 2D finite element analysis was completed with PHASE2, using a cross section similar to that shown in Fig. 2. This section appropriately

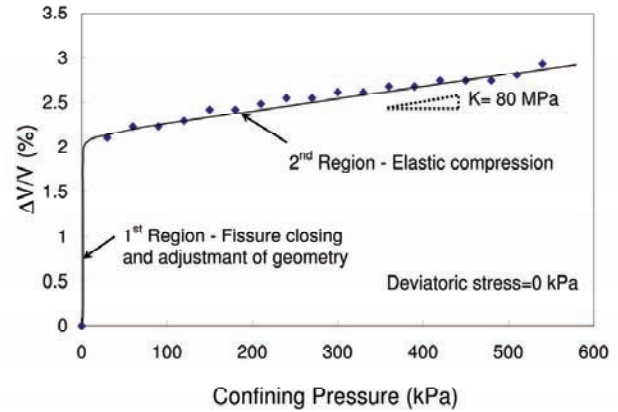


[FIG. 11] Results of the hydrostatic compression test.

represents the as-built shoring wall at Inclinometers 4 and 5. The model considered a mesh with a width of 190 m (623 ft) and a depth of 80 m (262 ft). The boundary conditions consisted of a rough and rigid elements along the bottom, and rigid, smooth elements on the sides. The model used beam elements for the caisson wall and anchor elements for the rock anchors. Material properties were matched with those shown on the shoring construction drawings. The beams were modeled as W460X68 (W18X45) piles. Loads were applied to the anchors as shown on Fig. 2, and in accordance with stressing records from the site. Soil and rock parameters were derived from the test results, as well as from past experience in similar geological conditions. These parameters are outlined in Table 2, and have been separated into five layers: soil, upper rock, weak rock, lower rock and the shear band.

Soil parameters were chosen based upon experience in the area. The weak rock properties were based upon the results of the multi-stage direct shear tests, as shown in Fig. 9. The elastic modulus was chosen as 165 MPa (24 ksi) based upon median values from the uniaxial compression tests. The shear band was chosen to have the residual values derived from the testing. The upper and lower rock layers were assigned a higher friction angle value and elastic modulus. This was based upon the higher axial and diametric point load test values, as shown in Fig. 8. The lower rock was modeled with an elastic modulus that increased by 5 MPa/m (226 psi/ft) with depth. Due to the poor quality of the rock samples, the Poisson's ratio was not able to be measured. As such, it was assumed to be 0.3 for all rock layers. Unit weight was also based upon results from the laboratory tests.

Vertical in-situ stresses were determined through the unit weights described above. Horizontal stresses in the soil were determined assuming a $k_0 = 0.8$. In the rock, it was assumed that there is a transition zone that increased from 0.145 MPa (21 psi) at the bedrock surface to 1.5 MPa (218 psi) at the top of the weak rock zone. From that elevation down, the stress was held constant. For this analysis, it was assumed that the horizontal stresses in the rock were isotropic.

Using the above parameters, the finite element analysis was used to model the stress and strain of the soil, rock, and shoring wall during excavation. Shoring installation, excavation rates, and anchor loading were modeled using field inspection records from the north wall. The results of the analysis, as well as the soil and rock layering and horizontal stresses, are shown in Fig. 12.

The results of the analysis are shown with readings from Inclinerometers 3 and 4, located along the north wall. The analysis accurately reflects the magnitudes and behaviour of the sudden shear band movement, and the bulging of the weak rock. It is noted that the inclinometer readings assumed zero movement at the inclinometer toes, whereas the modeling indicates up to 6 mm (1/4 in) of movement at this elevation. The model results were then compared with the remainder of the inclinometer readings, as shown in Fig. 13.

Several observations are made based upon these results. Inclinometer readings show two general types of movement in the soil, either cantilever style, or as a significant top retaining effect, such as in Inclinerometers 3 and 4. The model indicated movement similar to the former style. The cause of the discrepancy is still being investigated.

The extent of the movement beyond the excavation face was also investigated. Fig. 14 shows the horizontal movements calculated in

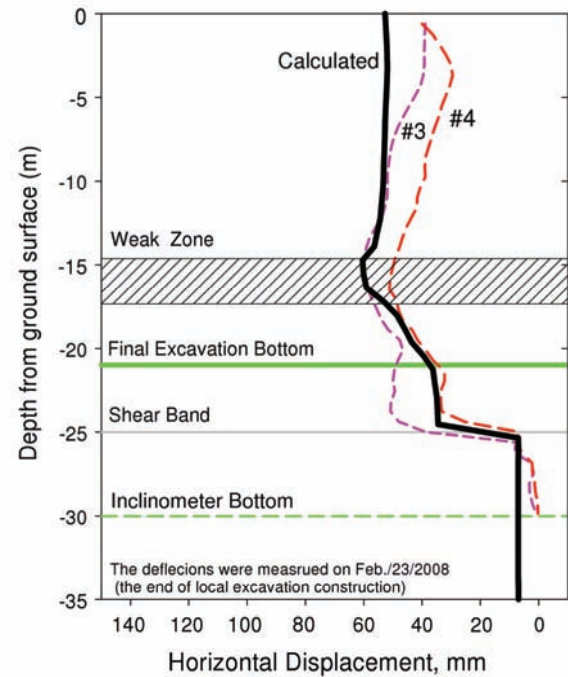


[FIG. 12] Results of preliminary finite element modeling.

the rockmass at the time of final excavation. The figure, using results from the previously mentioned analysis, outlines the extents of the model, the rockmass layers, and the horizontal movement, shown in 10 mm (0.4 in) intervals. From the figure, the FEA results indicate that the effect of the shear band is to propagate movement much farther away from the excavation than is normally observed. The results indicate that horizontal movement is occurring 60 metres (197 ft) or more from the excavation, a distance of 3 times the depth of the excavation. The results can also be compared with the readings from Extensometer 1. Horizontal movement at 25 metres (82 ft) from the excavation face are around 10 mm (0.4 in), which is similar to the amount of movement expected at the end of the extensometer, as previously discussed. The results of the extensometer readings and the

[TABLE 2] Parameters used in initial finite element modeling.

Layer	Unit Weight (kN/m ³)	E (MPa)	c' (kPa)	φ'	c' _r (kPa)	φ'	v
Soil	21	150	10	40	0	15	0.3
Weak Rock	22	165	340	24	0	15	0.3
Shear Band	22	165	-	-	0	15	0.3
Upper Rock	22	825	340	40	0	15	0.3
Lower Rock	22	825	340	40	0	15	0.3

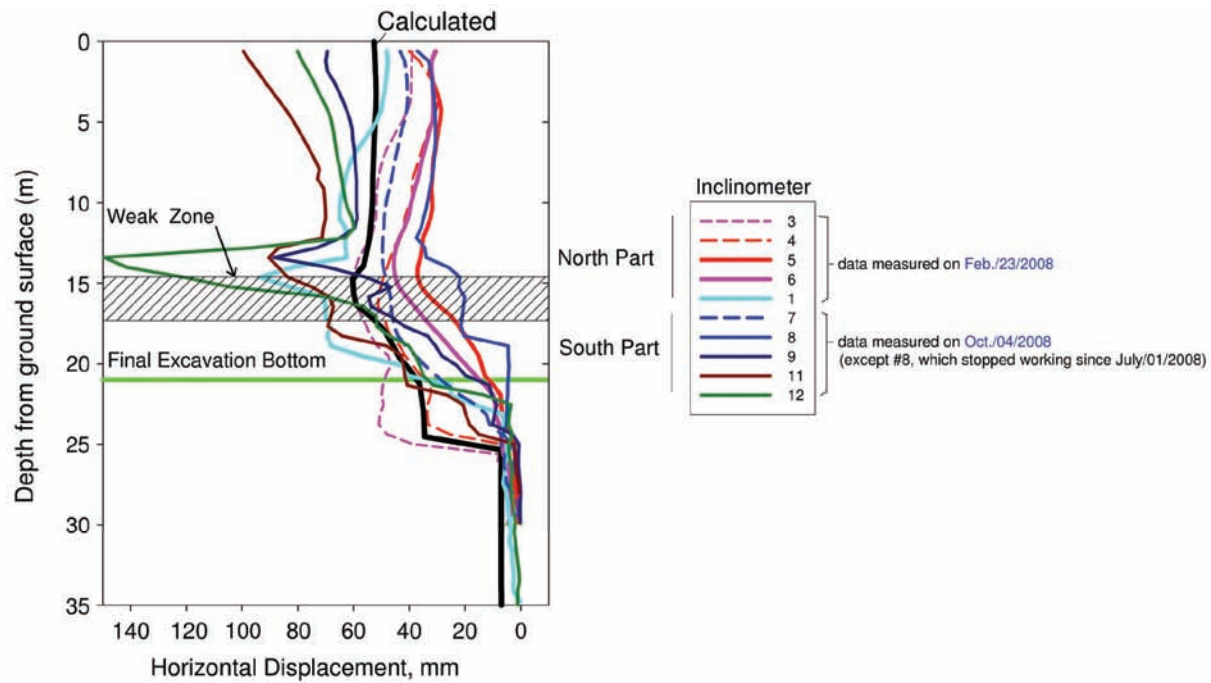


[FIG 13] Cumulated inclinometer results.

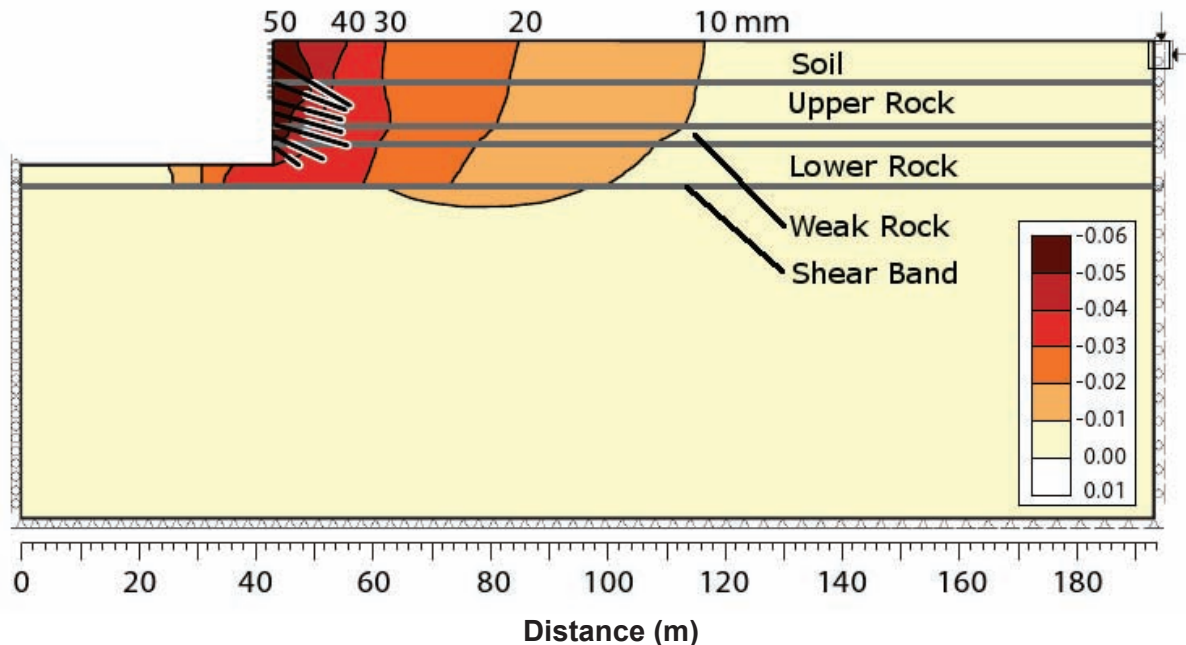


[FIG. 14] FEA results showing the horizontal movement in 10 mm contours.

corresponding FEA are currently undergoing further study.

CONCLUSIONS

Inclinometer monitoring during the 21 m (69 ft) deep excavation for The Bow in downtown Calgary, Alberta, indicated that large lateral deflections in the bedrock are due to a weak rock layer, and the shear band effect in a thin rock layer. Total lateral movement measured ranged between 45 mm and 150 mm (1.8 in and 6.0 in). Movement due to the shear band along the north wall was a maximum of 45 mm

(1.8 in). The weak rock was observed to cause as much as 100 mm (4 in) of deflection, as shown in Inclinometer 12 (Fig. 13). Due to the monitoring results, mudstone samples were collected for laboratory testing. Despite the difficulty in obtaining samples from the field and preparing them for the testing, several rock parameters were measured.

These include:

- a. The uniaxial compression tests indicate that the elastic modulus ranges from 80 to 180 MPa (11.6 to 26.1 ksi) and the uniaxial compressive strength ranges

between 560 MPa and 1230 MPa (81 and 178 ksi). Representative values for the elastic modulus and the UCS could be 160 MPa and 830 MPa (23 ksi and 120 ksi), respectively.

- b. Results from multi-stage direct shear tests indicated that $c' = 340$ kPa (49 psi) and $\phi' = 24^\circ$. Residual strengths were found to be $c'_r = 0$, and $\phi'_r = 15^\circ$.
- c. Results from the hydrostatic compression tests showed that the bulk modulus was approximately 80 MPa (11.6 ksi). This value was in the range of moduli derived from the uniaxial compression tests.

Finite element modeling was conducted based upon results of the laboratory tests, field records of construction, past experience in similar geology, and compared to the movements observed along the north wall. This initial analysis indicated that:

- a. Using the above mentioned parameters and information, magnitude and location of lateral movement along the north wall was modeled with sufficient accuracy.
- b. The presence of the weak rock layer resulted in large lateral movements, and should be considered in future excavations.

It should be noted that a limited number of laboratory tests of the mudstone were completed, and that more are required to accurately determine the rock parameters. No samples were taken of the siltstone and sandstone. Due to the weak and fragile nature of the samples, the Poisson's ratio was not measured. This important parameter should be determined, either through additional laboratory tests, or through in-situ testing.

A significant feature of the mudstone to be recognized is its swelling characteristics (Lo et al. 2009). Both laboratory tests and monitoring results indicated that the rock expanded with time similar to shale formations in Southwestern Ontario and adjoining United States. Swelling of the rock could result in higher than expected stresses on final structures, leading to undesired deformations and damage.

The mechanics behind the shear band effect are also currently not well defined. The current theory is that the shear band is a thin layer of rock that undergoes a large amount of plastic strain due to the effects of excavation. The undetermined mechanics of the shear band prevents the prediction of its manifestation. Layers of rock identified as hosting shear bands were found throughout the site, yet only a few

manifested shear band behaviour. This issue underlines the importance of field monitoring in deep excavations in soft rock.

REFERENCES

1. AMEC 2006. Supplementary geotechnical investigation proposed EnCana Tower 5 Avenue SE and Centre Street S Calgary, Alberta, AMEC Earth & Environmental, Calgary, Alberta.
2. ASTM D 4318. 2005. Standard test methods for liquid limit, plastic limit, and plasticity index of soils. ASTM.
3. Brachman, R.W.I., Moore, I.D, and LO, K.Y., 1998. Analysis and performance of a shoring system with tie-back anchors. *Proceedings of the 51st Canadian Geotechnical Conference, Edmonton, Alberta*, vol. 1, pp 439-446.
4. Brendley, G.W., 1951. X-ray identification and crystal structure of clay minerals. Taylor and Francis Ltd., London, UK.
5. Chan, D. H., and Morgenstern., N.R., 1987. Analysis of progressive deformation of the Edmonton Convention Centre excavation. *Canadian Geotechnical Journal*, volume 24, pp. 430-440.
6. Dreimans, A., 1962. Quantitative gasometric determination of calcite and dolomite using Chittick Apparatus. *Journal of Sedimentary Petrology*, vol. 32, pp. 520-529.
7. Goodman, R.E., 1980. Introduction to rock mechanics. John Wiley & Sons, New York, NY, USA, pp. 64 and 68.
8. Hoek, E., Kaiser, P.K., and Bawden, W.F., 2005. Support of underground excavations in hard rock. Taylor and Francis, New York, New York, USA, pp. 103.
9. Hudson, J.A., and Harrison, J.P., 1997. Engineering rock mechanics - An introduction to the principles. Elsevier Science Ltd., Oxford, UK, pp. 96.
10. Jackson, E.J., and Wilson, C.W., 1987. Geology of the Calgary area. Canadian Society of Petroleum Geologists, Calgary, AB, Canada.
11. Lardner, T., Janes, M. and Halliwell, M. 2008. The Bow, EnCana excavation support system design and performance. *Proceedings from the 61st Canadian Geotechnical Conference & 9th Joint CGS/IAH-CNC Groundwater Conference*, Edmonton, AB, Canada, pp. 63-70.

12. Lee Y.N. and Lo, K.Y., 1993. The swelling mechanism of Queenston shale. *Canadian Tunnelling Journal*, The Tunnelling Association of Canada, pp. 75-97.
13. Lo, K.Y., 1989. Recent advances in design and evaluation of performance of underground structures in rock. *Tunneling and Underground Space Technology*, vol. 4(2), pp. 171-183.
14. Lo, K.Y. and Lee, Y.N., 1990. Time-dependant deformation behaviour of Queenston shale. *Canadian Geotechnical Journal*, vol. 27, pp. 461-471.
15. Lo, K.Y., Cooke, B.H. and Dunbar, D.D., 1987. Design of buried structures in squeezing rock in Toronto, Canada. *Canadian Geotechnical Journal*, vol. 24(2), pp. 232-241.
16. Lo, K.Y., Wai, R.S.C., Palmer, J.H.L. and Quigley, R.M., 1978. Time-dependent deformation of shaly rocks in Southern Ontario. *Canadian Geotechnical Journal*, vol. 15, pp. 537-547.
17. Lo, K.Y., Micic, S., Lardner, T., and Janes, M., 2009. Geotechnical properties of a weak mudstone in downtown Calgary. *Proceedings of the 62nd Canadian Geotechnical Conference*, Halifax, Nova Scotia, pp. 454-462.
18. Martin, R.T., 1955. Glycol retention analyses. *Soil Science Society America Proceedings*, vol. 19(2), pp. 160-164.
19. Moore, D.M. and Reynolds, R.C., 1997. X-ray diffraction and the identification and analysis of clay minerals. Oxford University Press, New York, USA, pp. 227-297.
20. Mohamed, A.M.O., and Antia, H.E., 1998. Geotechnical engineering. Elsevier Science Ltd., Amsterdam, The Netherlands, pp. 75.
21. Osborn, G. and Rajewicz, R., 1998. Urban geology of Calgary. *Geological Association of Canada*, Special Paper 42, Urban Geology of Canadian Cities, pp. 93-115.
22. Rocscience, 2008 PHASE2 v.6.027 user's guide. Rocscience Inc. Toronto, Ont.
23. Wong, R.C.K., 1998. Swelling and soft behaviour of La Biche shale. *Canadian Geotechnical Journal*, vol. 35, pp. 206-221.

Analyzing Drivability of Open Ended Piles in Very Dense Sands

James A. Schneider, University of Wisconsin - Madison, Madison, WI, USA; james@cae.wisc.edu

Ivy A. Harmon, University of Wisconsin - Madison, Madison, WI, USA

ABSTRACT

The successful installation of long piles driven into very dense sands relies on the occurrence of the reduction in local friction with increased pile embedment, a phenomenon known as 'friction fatigue'. The underlying mechanisms controlling friction fatigue are poorly understood, with some design methods including an adjustment for the influence of pile diameter while others do not. This paper back calculates the installation resistance of 0.356m to 2m (14in to 78in) diameter open ended piles driven into very dense sands using wave equation analyses. Cone penetration test data are used to link soil properties to installation resistance. The study illustrates consistent interpretation of a variety of case histories of open ended piles driven in very dense sands using newly developed analysis techniques and normalized parameters. Results provide information on methods for incorporating friction fatigue into drivability studies as well as a discussion of mechanisms related to pipe pile installation resistance in sandy soils.

INTRODUCTION

Observations of the resistance of a pile during installation provides near immediate feedback on assumptions related to design at a given site. Additionally, these measurements can be used to evaluate assumptions inherent in design method formulations. Despite high levels of uncertainty in procedures for back analysis of pile driving records, these data have a significant advantage over static load tests for calibrating design methods. Specifically, the effects of pile length (L), or slenderness ratio (L/D), on soil resistance can be assessed for a large range of values at a single site.

Length or L/D effects are commonly discussed as the phenomenon known as 'friction fatigue'. Friction fatigue is the reduction in pile shaft friction in a given soil horizon that occurs as the pile tip is driven deeper (e.g., Heerema 1980). Friction fatigue has been hypothesized to be most severe for the case of sandy soils (as compared to clayey soils) and some studies imply a greater effect for piles driven into dense sands as compared to loose sands (Alm & Hamre 2001).

There is debate on the appropriate formulation for assessment of friction fatigue; some design methods relate the concept to height of a soil layer above the pile tip (e.g., Heerema 1980; Toolan et al. 1990; Alm & Hamre 2001; Claussen et al. 2005), others relate the behavior to the

height normalized by the pile diameter (e.g., Lehane et al. 1993; Randolph et al. 1994; Jardine et al. 2005, Kolk et al. 2005a), and others consider it to be controlled by the number of installation cycles (or hammer blows) (e.g., White & Lehane 2004; White 2005).

Three case histories with pile diameters varying from 0.356m to 2m (14in to 78in) are back analyzed in this paper. Analyses are focused on the performance of open ended piles in very dense sands, with soil strength and high stress compressibility characterized using results of cone penetration tests (CPTs). A CPT measures the two parameters of cone tip resistance (q_c) and sleeve friction (f_s). Fig. 1 illustrates terminology used in this paper when comparing CPT and pile resistance.

SITES

Three case histories of driving open ended piles in very dense uncemented siliceous sands are back analyzed in this paper; (i) Pigeon Creek (PC), Indiana, USA; (ii) Euripides (Eur-I & Eur-II), The Netherlands; and (iii) Trans Tokyo Bay Bridge (TTB), Japan. Table 1 presents pile, hammer, and installation information for each of the case histories analyzed, with additional information presented by Schneider et al. (2008).

Profiles of CPT tip resistance for each site are shown in Fig. 2. All three sites have relatively soft/loose near surface materials that are

underlain by very dense sands. The Tokyo Bay site includes many more occurrences of low tip resistance, indicating interlayers of soft/loose material. Along the pile shaft, the weighted average apparent relative densities based on normalized cone tip resistance [$q_{cIN}=(q_t/p_{ref})/(\sigma'_{vo}/p_{ref})^{0.5}$] range from 85% for Pigeon Creek to 100% for Euripides and Trans Tokyo Bay. The Eur-I and Eur-II sites may be overconsolidated and have a slightly lower actual relative density, although the overconsolidation ratio is suspected to have a small effect on the correlation between τ_f and q_t (e.g., Foray et al. 1998). Pile driving operations at the Euripides site are shown in Fig. 3.

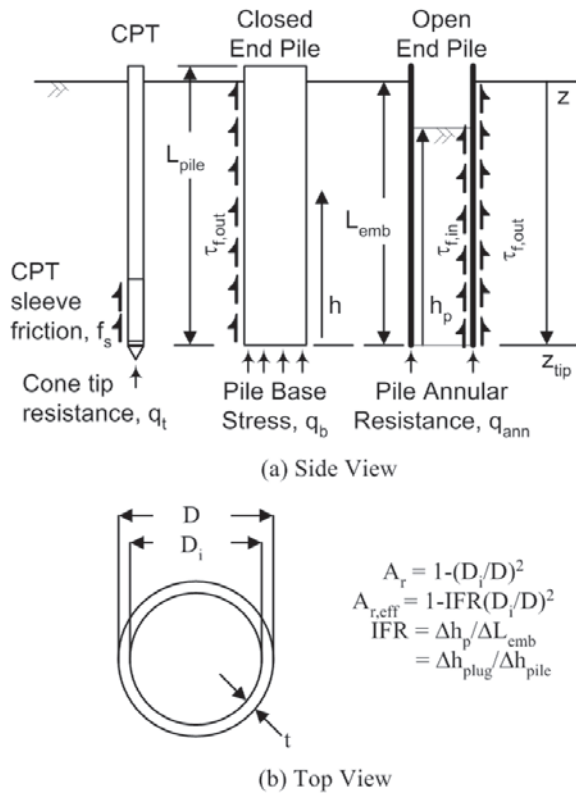


[FIG. 1] Illustrations of cone penetration test (CPT) and pile nomenclature

STATIC RESISTANCE DURING DRIVING

During pile driving the soil resistance will result from static and dynamic components. The dynamic components are related to increases in resistance due to inertial and viscous rate effects (e.g., Randolph 2000), although commonly quantified using damping factors. The static component of the soil resistance during driving (SRD) is similar to the pile static axial capacity, except the resistance often differs due to consolidation, equalization, and ageing, or 'time-effects' (e.g., Tavenas & Audy 1972, Skov

& Denver 1988, Svincken et al. 1994, Randolph 2003), and definition of 'failure' in static load tests. Time effects result from changes in total stress and pore pressures that occur due to soil displacement during the pile installation process, among other factors.

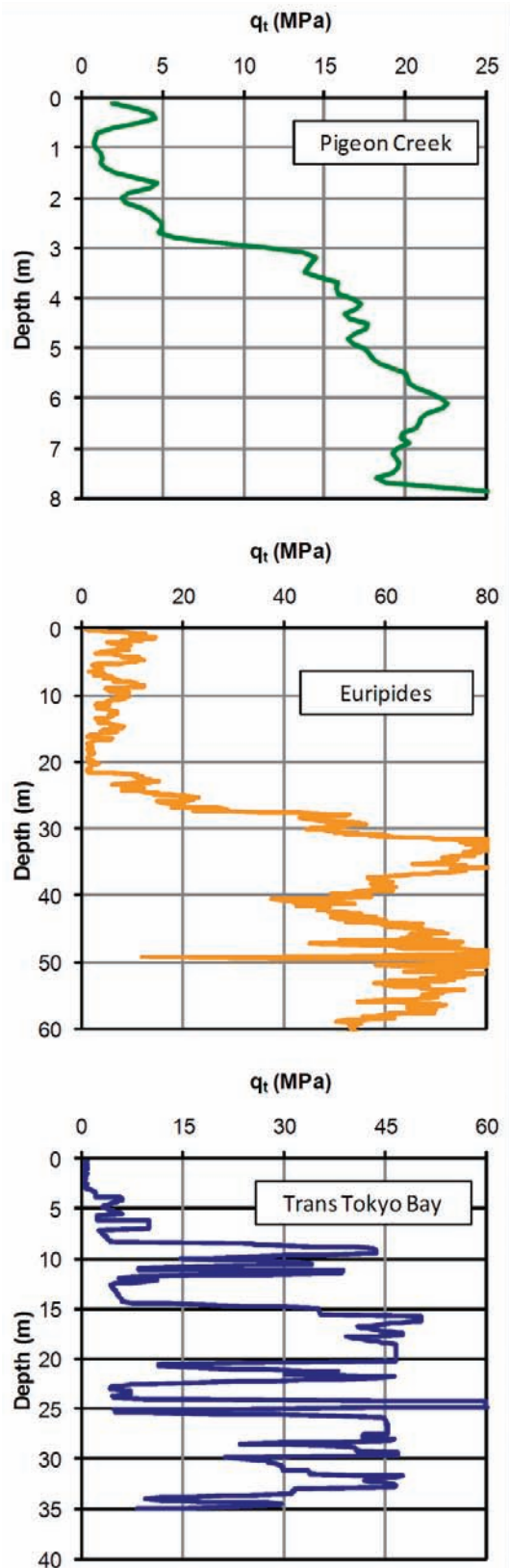


[FIG. 2] CPT q_t profiles for sites analyzed in this paper

[TABLE 1] Characteristics of open ended piles for sites in this study^a (see also Schneider et al. 2008)

Site	ID	D, m	t, mm	z_{tip} , [L _{pile}] m	Water Table, m	Avg IFR	Avg $A_{r,eff}$ [A _r]	Hammer	Enthru ^b [Rated] (kN · m)	Approx. Total Blows	Reference
Pigeon Creek	2	0.356	32	7 [8.24]	3	0.83	0.44 [0.33]	ICE 42-S	19-28.5 [57]	225	Paik et al. 2003
Euripides	I	0.763	36	47 [27, 49.4, 57 ^c]	1	0.96	0.21 [0.18]	IHC S-90	68 [90]	8400	Zuidberg & Vergobbi 1996; Kolk et al. 2005b
Euripides	II	0.763	36	47 [57]	1	0.95	0.22 [0.18]	IHC S-90	71 [90]	8550	
Trans Tokyo Bay	TP	2.0	34	31 [62]	0	1.0	0.07 [0.07]	Menck MRBS 5000	300 [736]	1275	Shioi et al. 1992

^a Nomenclature illustrated in Fig. 1

^b Transferred energy at end of driving [hammer rated energy in brackets].

^c Field welds were made at 27m and 49.4m (89ft and 162ft) for the first installation of the Euripides pile. Initial pile driving (and static load testing at intermediate depths) from 22 March 1995 to 10 May 1995.



[FIG. 3] Pile driving at the Euripides site (photo courtesy Fugro Engineers B.V.)

The ability to predict SRD, as well as static capacity, of an open ended pile is complicated by mechanisms related to soil entering or being displaced by the advancing pile. The relative amount of soil entering an open ended pile can be quantified using the incremental filling ratio (IFR= $\Delta h_{plug}/\Delta h_{pile}$) (e.g., Paikowski et al. 1989). IFR is equal to the change in plug height for an

increment of driving (Δh_{plug}) as compared to the length of pile installed (Δh_{pile}). For large diameter open ended piles in relatively uniform soil deposits the soil within the pile tends to remain near the original ground surface during driving, $\Delta h_{plug} = \Delta h_{pile}$, IFR=1 (e.g., Stevens 1988). Under slow loading conditions, such as a static load test, the soil plug will tend to move with the pile, $\Delta h_{plug} = 0$, IFR=0 (e.g., Randolph et al. 1991).

Considering that the inertia of the soil plug tends to lead to large diameter pipe piles installing in a predominantly coring manner (IFR=1), the unit 'end bearing' (q_b) will occur solely on the pile annulus (q_{ann}) and the pile shaft friction (τ_s) at the time of pile driving will occur both internally ($\tau_{r,in}$) and externally ($\tau_{r,out}$) along the surface area of the pile. The total SRD is the sum of the pile shaft resistance (Q_s) and the pile base resistance (Q_b):

$$SRD = Q_s + Q_b \quad (1a)$$

$$SRD = \pi D \sum_{z_{tip}-L_{emb}}^{z_{tip}} \tau_f \cdot \Delta z + q_{ann} A_{ann} \quad (1b)$$

where A_{ann} is the pile annular area [$=\pi/4(D^2 - D_i^2)$], D is the pile outer diameter, D_i is the pile inner diameter, z is depth, z_{tip} is the pile tip depth, Δz is the change in depth, and L_{emb} is the pile embedded length. It is common to take the internal shaft friction simply as a fraction of the external shaft friction ($\tau_{r,in}/\tau_{r,out}$). Initial analyses in this paper use the assumption that the ratio of $\tau_{r,in}/\tau_{r,out}$ is equal to 0.5 (e.g., lower

bound from Stevens et al. 1982). The effect of $\tau_{f,in}/\tau_{f,out}$ on driving resistance is addressed later in this paper. The differences between internal and external diameter are small compared to the uncertainty in estimating $\tau_{f,in}/\tau_{f,out}$, and are not explicitly considered in this study. The following modified format for SRD is used for is paper:

$$SRD = \pi D \sum_{z_{tip} - L_{emb}}^{z_{tip}} 1.5 \tau_{f,out} \cdot \Delta z + q_{ann} A_{ann} \quad (1c)$$

To quantify the effects of friction fatigue on shaft friction during pile installation, two detailed models for soil resistance are used:

- AH-01 (Alm & Hamre 2001)
- UWA-05 (Lehane et al. 2005, 2007)

The formulations for each model are summarized as follows, and the interested reader is referred to the original references for more detail.

Alm & Hamre (2001) method for sands

The Alm & Hamre (2001) method was calibrated primarily based on drivability studies of large diameter piles in the North Sea. For sands, pile diameters ranged from 2.4m to 2.7m (8ft to 9ft), and pile penetration ranged from 55m to 70m (180ft to 230ft). To minimize additional uncertainty related to selection of soil parameters and modeling changes in radial stress due to pile installation, both q_b and τ_f are correlated to CPT q_t . Shaft friction is estimated to exponentially decay from a maximum ($\tau_{f,max}$) to a residual ($\tau_{f,res}$) value:

$$\tau_f = \tau_{f,res} + (\tau_{f,max} - \tau_{f,res}) e^{-kh} \quad (2)$$

$$\tau_{f,max} = \frac{q_t}{76} \left(\frac{\sigma'_{v0}}{p_{ref}} \right)^{0.13} \tan \delta_f \quad (3a)$$

$$\tau_{f,res} = 0.2 \tau_{f,max} \quad (4)$$

Where h is the height above the pile tip, σ'_{v0} is the initial vertical effective stress, p_{ref} is a reference stress equal to 100 kPa, and δ_f is the soil-pile interface friction angle at failure. The shape factor for the 'rate' of degradation (k) is related to the normalized cone tip resistance:

$$k = \frac{1}{80} \left(\frac{q_t}{\sigma'_{v0}} \right)^{0.5} \quad (5)$$

The result of Equation 2 (through 3a, 4, and 5) is discussed by Alm & Hamre (2001) to be the total internal and external shaft friction. It was recommended by Alm & Hamre to reduce this value by 50% and apply to both the interior and

exterior of the pile, i.e., $\tau_{f,in}/\tau_{f,out} = 1$. Since the analyses in this paper considers $\tau_{f,in}/\tau_{f,out} = 0.5$, the external shaft friction is considered to be 2/3 of the value from Equation 2, such that the total pile friction during installation agrees with the recommendations of Alm & Hamre (2001).

$$\tau_{f,max,out} = \frac{q_t}{114} \left(\frac{\sigma'_{v0}}{p_{ref}} \right)^{0.13} \tan \delta_f \quad (3b)$$

While the ratio of the end bearing of statically loaded closed ended displacement piles to CPT tip resistance (q_b/q_t) is often considered to vary from 0.6 to 1.0 (e.g., White & Bolton 2005, Xu et al. 2008), normalized annular end bearing during installation is estimated to range from 0.35 to 0.55, as:

$$\frac{q_{ann}}{q_t} = 0.15 \cdot \left(\frac{q_t}{\sigma'_{v0}} \right)^{0.2} \quad (6)$$

Equations 2, 3b, and 4 through 6 are combined within Equation 1c and referred to as the AH-01 method for the remainder of this paper.

This allows for ease of comparison of results produced by applying AH-01 to those of other design methods which explicitly separate internal and external shaft friction.

Modified UWA-05 method for uncemented siliceous sands

Unlike the AH-01 method, UWA-05 was developed for estimation of static axial capacity rather than SRD. The database of piles used in calibration of UWA-05 was more representative of onshore conditions than offshore, with a mean diameter of 0.5m (20in) and a mean embedded length of 17m (55ft). The mean time between installation and load testing of the database piles was 9 days. Some differences between shaft resistance at 9 days after installation and that during installation should be expected, but these variations will be addressed later in this paper.

Shaft friction is evaluated using the Coulomb failure criterion:

$$\tau_{f,out} = \sigma'_{rf} \tan \delta_f = (\sigma'_{rc} + \Delta \sigma'_{rd}) \tan \delta_f \quad (7)$$

where σ'_{rf} is the radial effective stress on the external wall of the pile at failure, σ'_{rc} is the radial effective stress on the external wall of the pile after pile installation and equalization, and $\Delta \sigma'_{rd}$ is the change in radial effective stress during pile loading. The radial stress after installation and the change in radial stress are estimated separately, and both typically use correlations to cone tip resistance. For driven

piles in siliceous sands, the radial stress after installation and equalization is estimated as:

$$\sigma'_{rc} = \frac{q_t \cdot A_{r,eff}^b}{a} \left[\max \left(\frac{h}{D}, \nu \right) \right]^{-c} \quad (8a)$$

$$\sigma'_{rc} = \frac{q_t \cdot A_{r,eff}^{0.3}}{33} \left[\max \left(\frac{h}{D}, 2 \right) \right]^{-0.5} \quad (8b)$$

Where (e.g., White 2005, Lehane et al. 2005):

a = parameter to account for the reduction in radial stress behind the pile tip = 33

b = parameter to account for differences between open and closed ended piles = 0.3

c = exponent which accounts for friction fatigue = 0.5

ν = parameter which provides an upper limit on h/D^c at the pile tip = 2

$A_{r,eff}$ is the effective area ratio that explicitly accounts for the differences in radial stress induced by open, closed, and partially plugged piles.

$$A_{r,eff} = 1 - IFR \left(\frac{D_i^2}{D^2} \right) \quad (8c)$$

The incremental filling ratio ($IFR = \Delta h_{plug} / \Delta h_{pile}$) is defined previously. The use of $A_{r,eff}$ in Equations 8a and 8b results in higher shaft friction on closed ended piles as compared to open ended piles, and partially plugged piles have an intermediate value (e.g., White et al. 2005). The pile area ratio, $A_r = 1 - D_i^2 / D^2$, is the same as $A_{r,eff}$ when $IFR = 1$ (fully coring).

The change in radial stress during loading is based on elastic cylindrical cavity expansion theory (e.g., Lehane et al., 1993):

$$\Delta \sigma'_{rd} = \frac{4G\Delta y}{D} \quad (8d)$$

In the absence of sufficiently varied case histories presenting reliable data on changes in radial stress during loading, the recommendations of Jardine et al. (2005) were used by Lehane et al. (2005, 2007) to define $G = G_0$ and $\Delta y = 2R_a = 20\mu m$ for Equation 8d. G_0 is usually estimated from CPT tip resistance:

$$\frac{G_0}{q_t} = K_G \left[\frac{q_t / p_{ref}}{(\sigma_{v0} / p_{ref})^{0.5}} \right]^{-n} \approx 185 \cdot q_{c1N}^{-0.7} \quad (8e)$$

For assessment of annular resistance of open ended piles or end bearing stress of closed ended piles, UWA-05 takes the ratio of pile base stress to properly averaged cone tip resistance (q_b / q_t) as 0.6. For this application to annular resistance of open ended piles during driving, a lower value of q_{ann} / q_t is used, based on discussion in Alm & Hamre (2001):

$$\frac{q_{ann}}{q_t} \approx 0.35 \quad (9)$$

Equations 7 through 9 are applied within Equation 1b and referred to as the modified UWA-05 method for the remainder of this paper.

WAVE EQUATION ANALYSES

The program GRLWEAP (Pile Dynamics 2005) was used for wave equation analyses in this paper. Standard quake values of 2.5mm (0.1in) were used for both the shaft and base resistance (e.g., Roussel 1979; Stevens et al. 1982), with a Smith shaft damping of 0.25s/m and Smith base damping of 0.5s/m applied in the sandy soils. When clay soils were encountered, the shaft damping was increased to 0.65s/m.

It is difficult to use the two previously discussed methods for estimating shaft friction within the program GRLWEAP, in that the shaft friction distribution changes each time the pile tip is advanced. Fig. 4 presents calculated shaft friction distributions for installation of piles at the Pigeon Creek site (e.g., Paik et al. 2003, Table 1). It is observed that the shaft friction distribution based on a pile tip depth of 8m (26ft) will underpredict pile shaft friction when the pile tip is, for example, at 5m (16ft). This is the phenomenon of friction fatigue. To accurately assess the effects of friction fatigue during drivability studies, a separate wave equation analysis would need to be performed for each tip depth.

Alm & Hamre (2001) appear to get around this difficulty by developing a bearing graph using wave equation analyses and then estimating pile blowcount profile from SRD (or SRD from pile blowcount). Three parametric studies of factors influencing site specific bearing graphs are summarized in Fig. 5 for an IHC S-90 hydraulic hammer and pile conditions for the Euripides test (Zuidberg & Vergobbi 1996, Kolk et al. 2005b, Table 1). It is assumed that the pile diameter, wall thickness, and damping parameters (in these uniform soil deposits) will not change, so the major factors influencing the bearing graph are (i) embedded length of the pile; (ii) fraction of resistance from Q_b or Q_c ; and (iii) shape of the distribution of τ_r .

Relatively similar bearing graphs are calculated irrespective of shape of shaft friction distribution or pile length in these parametric studies. Conversely, the fraction of shaft friction does have a significant influence when estimating blowcount from SRD. The use of

bearing graphs is therefore limited since Q_s/SRD will typically increase with pile embedment in uniform deposits, and large variation may also be expected in layered soil deposits.

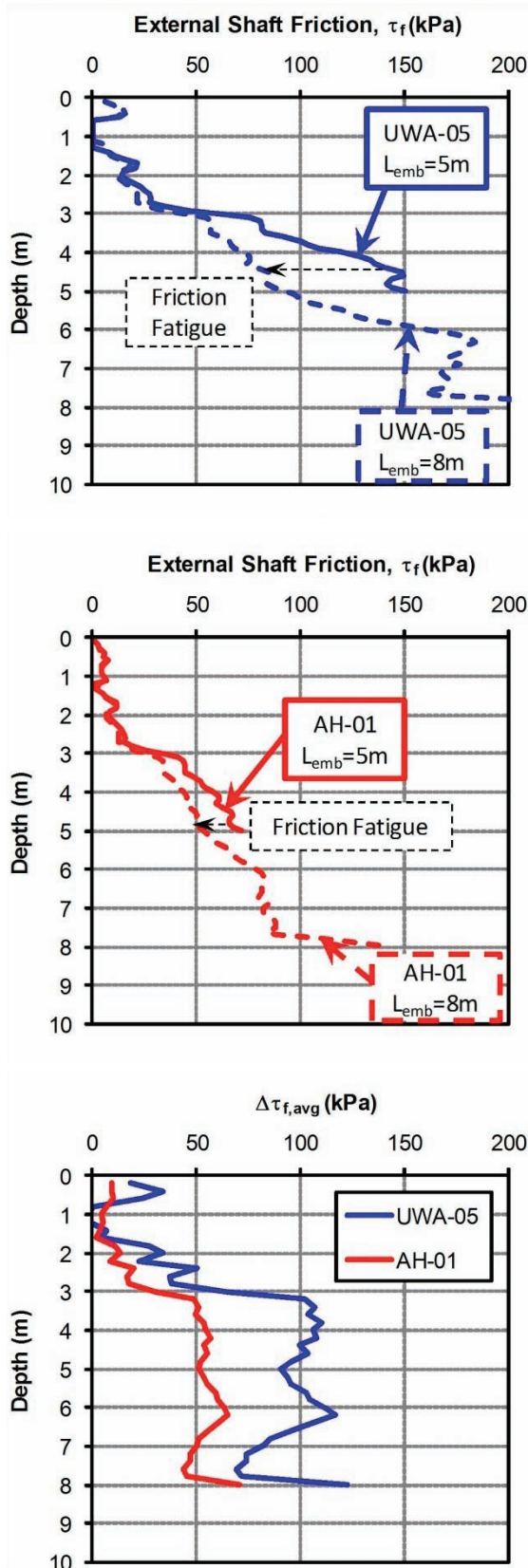


[FIG. 4] Comparison of calculated friction fatigue and pseudo average incremental shaft friction ($\Delta\tau_{f,avg}$) at the Pigeon Creek site

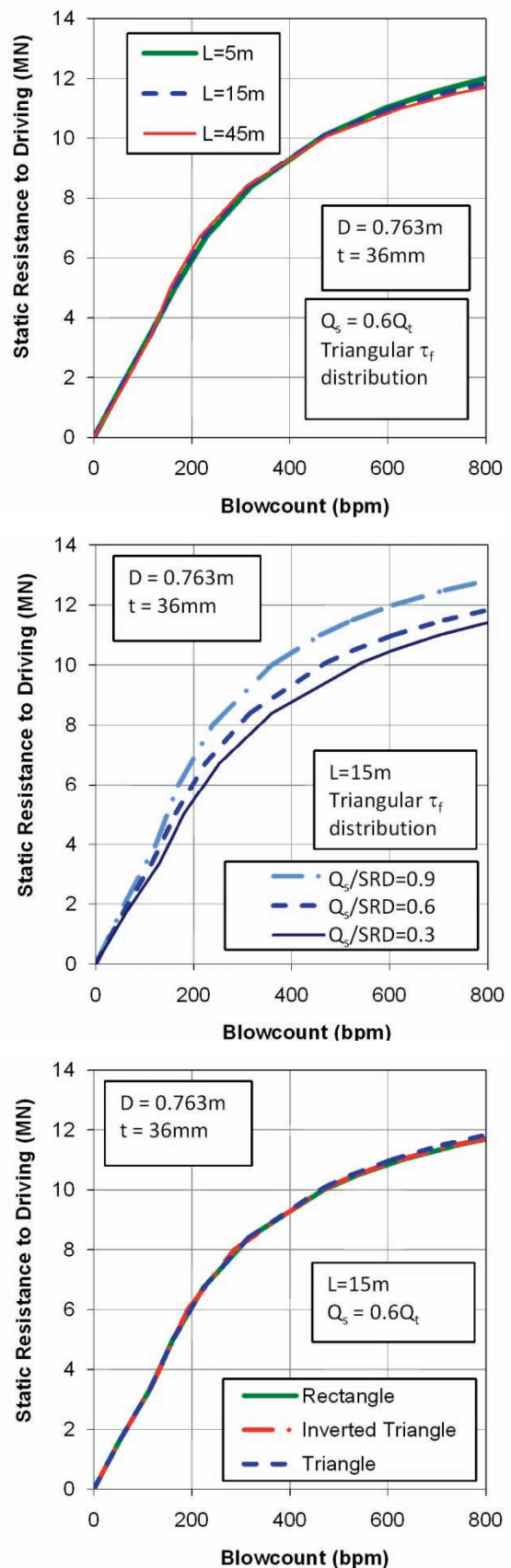


[FIG. 5] Parametric study of the shape of SRD-blowcount curves for an IHC S-90 hammer

The shape of the shaft friction distribution has been shown to have a minimal effect on the bearing graph, so the change in shaft capacity between two increments of driving can be used

to estimate a pseudo average incremental shaft friction ($\Delta\tau_{f,avg}$). The pseudo average incremental shaft friction is calculated as:

$$\Delta\tau_{f,avg} = \frac{\Sigma Q_{s,L} - \Sigma Q_{s,L-1}}{\pi D \cdot \Delta L} \quad (10)$$

where $\Sigma Q_{s,L}$ is the cumulative shaft resistance at the pile tip depth, $\Sigma Q_{s,L-1}$ is the cumulative shaft resistance at the depth of the previous SRD calculation, and ΔL is the length of pile driven between the two sets of calculations. Fig. 4 compares pseudo average incremental shaft friction for the two methods. Due to the effects of friction fatigue, $\Delta\tau_{f,avg}$ is significantly less than τ_f near the pile tip after continued driving in a given layer and $\Delta\tau_{f,avg}$ may even be negative, particularly for small values of ΔL .

It is interesting that the pseudo average incremental shaft friction in Fig. 4 appears to reach a constant value after a 'critical depth' of 3m (10ft) (or 8D). Observations such as these may have led to development of the concepts of 'critical depth' and limiting shaft friction values. It should be stressed that the average shaft friction values will be a function of pile geometry and soil density (among other factors), and a unique limiting shaft friction value for a given sand density is not valid in most situations, particularly in layered deposits.

ANALYSIS AND DISCUSSION

Digitized CPT profiles were used for assessment of τ_f and q_b . Due to similar zones of influence attributed to a CPT and pile annulus, no q_t averaging techniques were employed for these studies. The soil profile was discretized into approximately 100 elements for input into GRLWEAP. The same discretization was used for bearing graph (BG) and drivability analyses.

While the piles for this study (as summarized in Table 1) have a large range of diameters, the wall thickness is relatively consistent at about 34mm (1.34in). This results in the pile area ratio increasing from approximately 0.07 for the Trans Tokyo Bay pile to 0.33 for the smaller diameter Pigeon Creek pile. Since smaller diameter piles tend to plug more than larger diameter piles in uniform soil conditions (e.g., Lehane et al. 2005), the $A_{r,eff}$ of the Pigeon Creek pile is actually 0.44 and is estimated to have an initial radial stress (and thus shaft friction) that is potentially 60% greater than that for the Trans Tokyo Bay pile. The increasing trend of calculated initial radial stress (on the exterior side of a displacement

pile) with area ratio is illustrated in in Fig. 6, with calculations based on White et al. (2005) and Lehane et al. (2005). Since the AH-01 model does not explicitly account for $A_{r,eff}$, the graph is normalized for a typical open ended pile with a D/t ratio of 40, such as those used to calibrate AH-01.

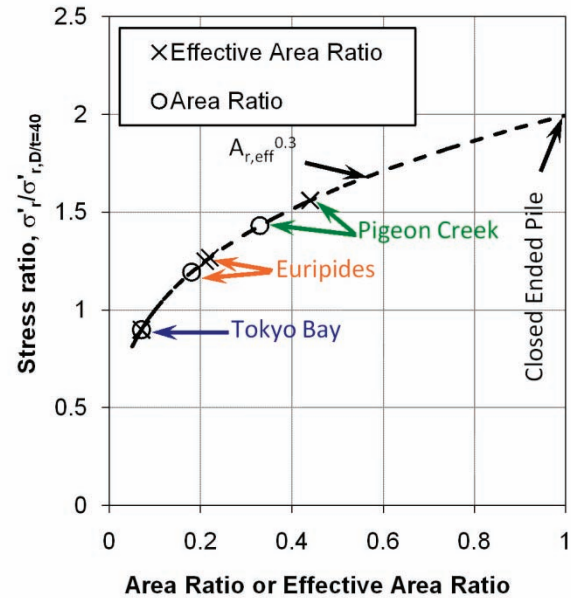


[FIG. 6] Comparison of effective area ratio to inferred influence on maximum shaft friction for test piles in this study (trend from White et al. 2005)

Analysis results are presented as calculated and measured blowcount profiles with depth. Measured resistance is presented as blows per meter of penetration (bpm). Fig. 7 compares calculations based on the method of AH-01 for bearing graph and $\Delta\tau_{f,avg}$ studies. A similar plot is presented for the modified UWA-05 method in Fig. 8.

In general it can be seen from Figs. 7 and 8 that the AH-01 method predicts drivability well for the Euripides and Trans Tokyo Bay piles, while the modified UWA-05 method tends to better predict the drivability response for the small diameter, larger area ratio, Pigeon Creek pile. Similar results are obtained with the bearing graph and $\Delta\tau_{f,avg}$ drivability analyses for both resistance calculation methods (AH-01 & modified UWA-05).

Due to the distinctly different method formulations for AH-01 and modified UWA-05, there are a few reasons that could lead to these similarities and differences:

1. Evaluation of annular end bearing;
2. Evaluation of initial shaft friction behind the pile tip ($a_{avg}/A_{r,eff}^{0.3}$ term from Equation 8a);

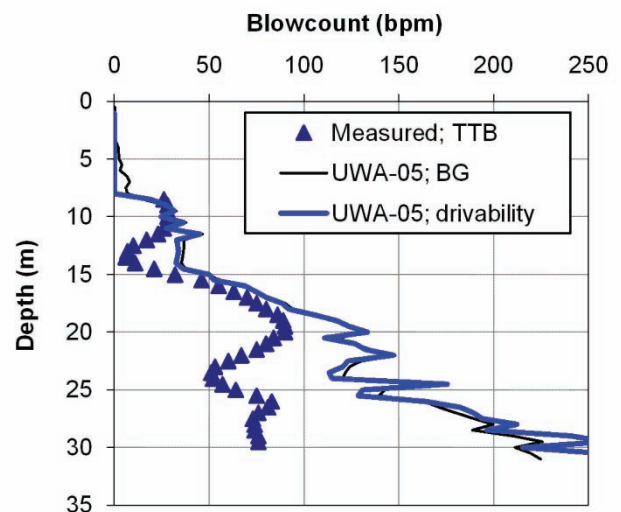
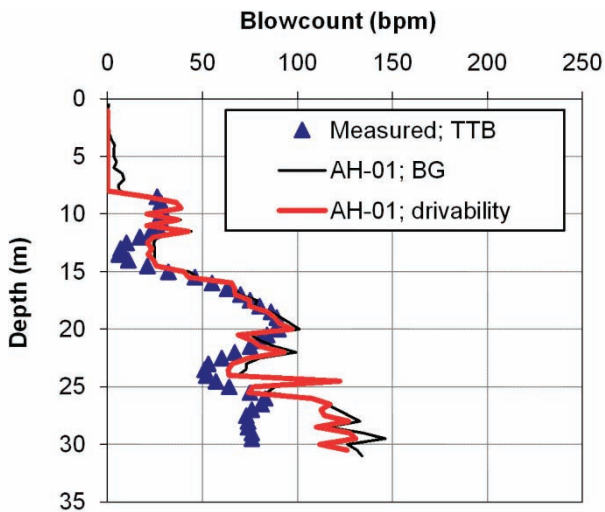
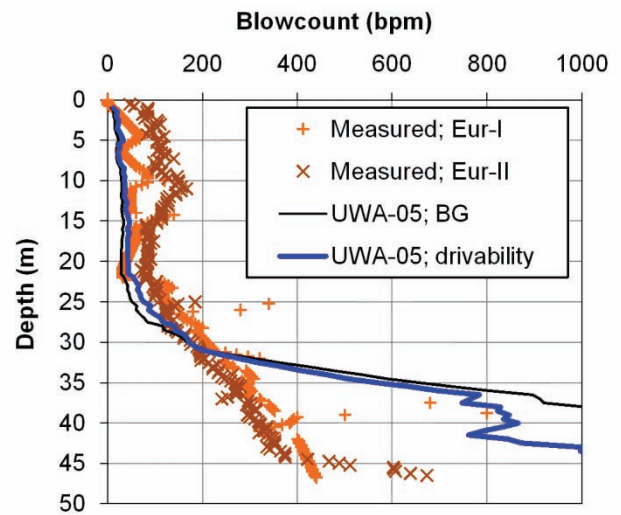
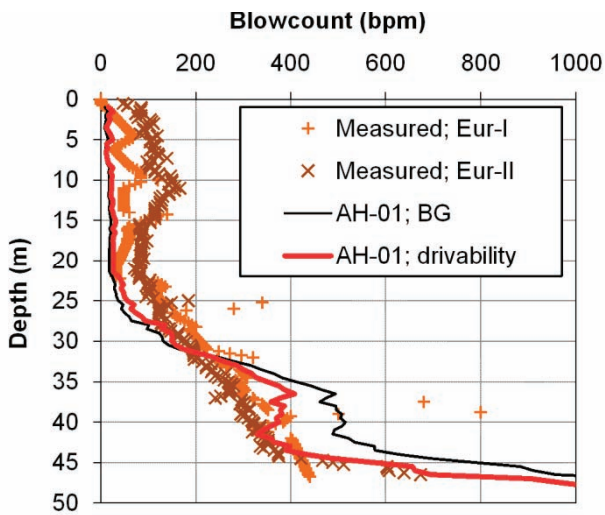
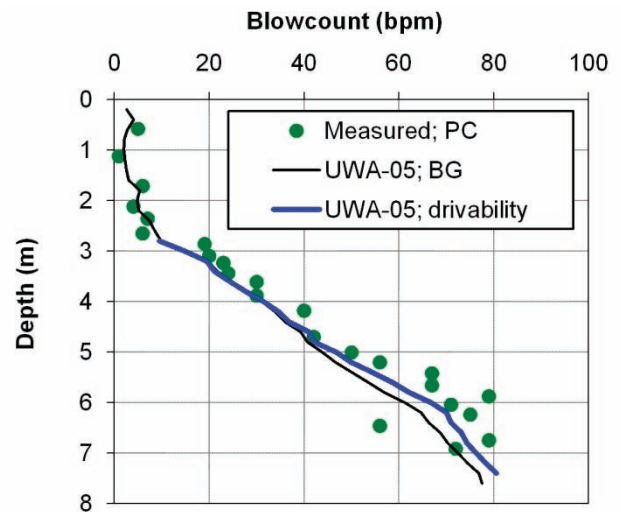
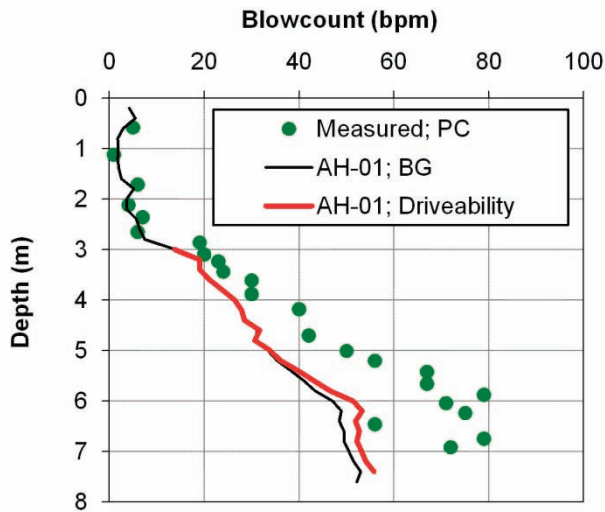


[FIG. 7] Calculated and measured blow counts using AH-01 SRD method

[FIG. 8] Calculated and measured blow counts using modified UWA-05 axial capacity method

3. 'Rate' of friction fatigue.

Factors 1 and 2 are compared in Table 2 and Fig. 9, and Factor 3 is evaluated using Figs. 10 and 11. Despite having a larger end bearing component (q_{ann}/q_t), the AH-01 method gives lower blowcount during driving. Estimation

of τ_f is more significant than q_{ann} , and q_{ann}/q_t appears to have a small effect on these pipe pile drivability analyses. The 'a' parameter is stress dependant within the formulation of AH-01 [$(\sigma'_{v0}/p_{ref})^{0.13}$; Equation 3a/3b], so 'a_{avg}' parameters are presented in Table 2. Area ratio

and plugging are not explicitly included in AH-01, likely since these factors have a small effect on drivability of large diameter piles with a constant D/t. However, these factors are of significant importance for modeling the Pigeon Creek pile. Fig. 9 illustrates that if the shaft friction in AH-01 method is increased using the area ratio correction from Fig. 6, a better estimation of pile driving resistance is achieved.

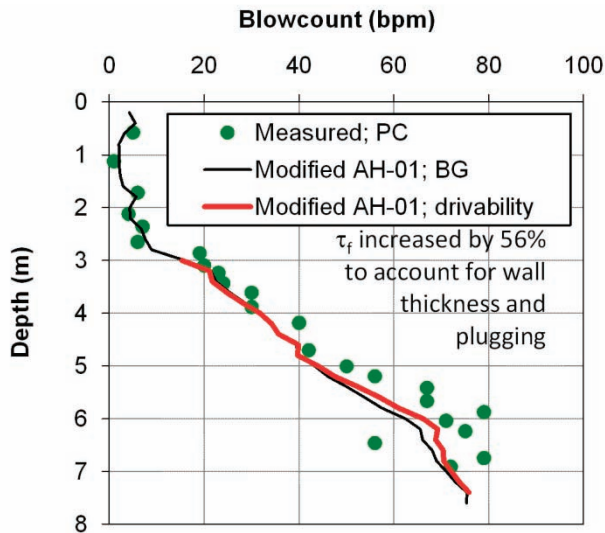


[FIG. 9] Performance of AH-01 method modified for wall thickness and plugging effects for open ended Pigeon Creek pile

[TABLE 2] Summary of analysis results

Site	Pile Tip Depth (m)	$\frac{q_{avg}}{A_{r,eff}^{0.3}}$	$\frac{q_{ann}}{q_t}$	Total Blows [Drive.] ¹
AH-01				
Pigeon Creek	7	126	0.45	155 [185]
Euripides	47	105	0.41	7870 [9580]
Tokyo Bay	30.5	108	0.42	1595 [1715]
Modified UWA-05				
Pigeon Creek	7	42	0.35	200 [245]
Euripides	47	55	0.35	20000+ [20000+]
Tokyo Bay	30.5	74	0.35	2465 [2445]

¹ Total blow counts based on bearing graph calculations, with number in brackets from drivability studies

The 'rate' of friction fatigue is compared in Figs. 10 and 11 for the two methods. The ratio of τ_f/q_t at a given soil horizon is compared to the ratio of τ_f/q_t at the pile tip. This ratio is referred to as the Shear Stress Tip Ratio, or TTR. Shaft friction

and this ratio will decrease with height (h) or h/D behind the pile tip due to friction fatigue.

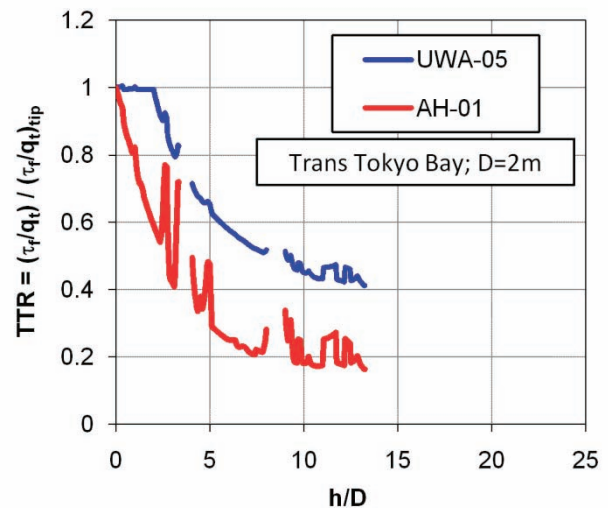
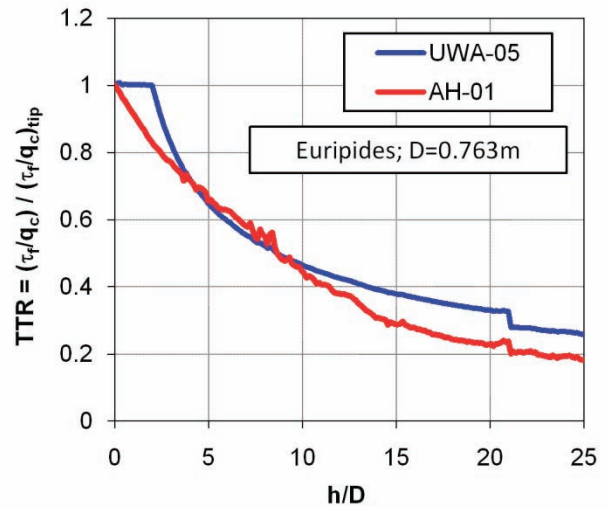
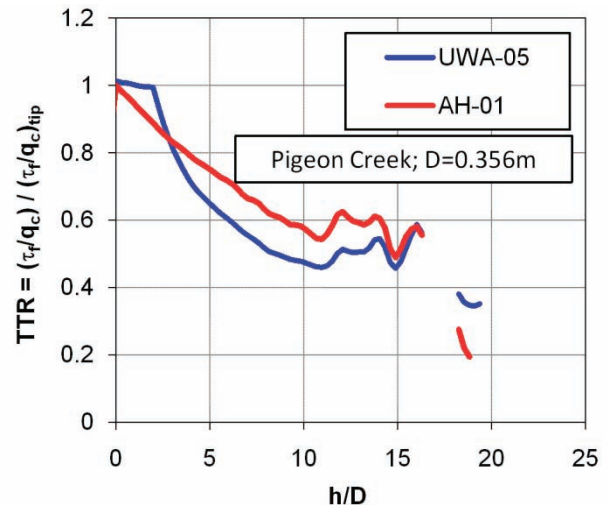


[FIG. 10] Comparison of friction fatigue using ratio of τ_f/q_t at a given height above the pile tip to τ_f/q_t at the pile tip (or 'TTR')

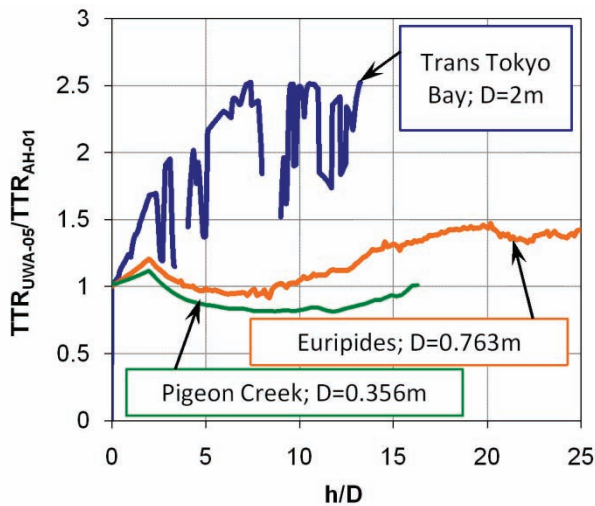


[FIG. 11] Comparison of friction fatigue using 'TTR' at each of the three sites from this paper

Similar values of TTR are observed for the modified UWA-05 and AH-01 for the Pigeon Creek and Euripides piles, but significant differences occur for the Trans Tokyo Bay pile. The 'rate' of friction fatigue predicted using the AH-01 method is more severe than that predicted by modified UWA-05 at TTB. This appears to occur due to the presumed diameter effect within the friction fatigue formulation of modified UWA-05. A larger database and more detailed analyses (e.g., a series of full wave equation analyses such as CAPWAP) should provide insight into this potential diameter effect.

RATIO OF INTERNAL TO EXTERNAL SHAFT FRICTION

The ratio of internal to external shaft friction is uncertain, yet has significant implications on the interpretation of pipe pile drivability. Stevens et al. (1982) recommended performing analyses with $\tau_{f,in}/\tau_{f,out}$ ranging from 0.5 to 1.0. On the contrary, Dutt et al. (1995) suggest that the internal shaft friction (for normally consolidated clays) does not contribute to driving resistance. Alm & Hamre (2001), suggest applying shaft friction equally on the inside and outside of the pile, but recommend using half the static shaft friction for this value. This logic is similar to applying no shaft friction to the inside of the pile and full shaft friction on the outside of the pile.

Figs. 7 and 9 show that the AH-01 method can perform well for the cases in this paper, while Fig. 8 indicates that the modified UWA-05 method tends to overpredict SRD. This overprediction may result from overestimation of shaft friction, since the UWA-05 method is based on resistance at 9 days after installation.

Alternatively, overprediction may result from overestimation of $\tau_{f,in}/\tau_{f,out}$. Fig. 12 shows the sensitivity of pile drivability studies using modified UWA-05 method to the ratio of internal to external shaft friction.

Calculated and measured blowcounts of the larger diameter piles in this study, Euripides I / II and Trans Tokyo Bay, are better correlated when applying modified UWA-05 with $\tau_{f,in}/\tau_{f,out}$ of zero. Blow counts for the partially plugged piles at Pigeon Creek are better correlated when using the modified UWA-05 method and $\tau_{f,in}/\tau_{f,out}$ equal to 0.75. These trends could be interpreted to suggest that the ratio of internal to external shaft friction is much higher for the case of partially plugged piles as compared to the case of coring piles. It is unlikely that the internal shaft friction for the Tokyo Bay and Euripides piles is equal to zero and that the influence of partial plugging at Pigeon Creek has such a significant effect on $\tau_{f,in}/\tau_{f,out}$. It is clear, however, that the assumptions related to internal shaft friction are important to assessment of driving behavior, and experimental studies are required to increase the understanding of underlying mechanisms controlling this resistance. It is likely that current soil models for pile drivability studies involve some level of compensating errors to produce accurate predictions.

CONCLUSIONS

While this study examined a relatively small number of case histories, the large variation in pile size combined with relatively consistent soil conditions at each of the different sites has led to the following conclusions:

- To rationally assess drivability of open ended piles in very dense sands, analyses must incorporate the effects of friction fatigue, pile area ratio, and potential for partial plugging during driving. Each of these factors has been hypothesized to be influenced by pile diameter.
- When using GRLWEAP for drivability studies that include effects of friction fatigue, analyses may be performed using the bearing graph option or a drivability analysis with a shaft friction distribution based on $\Delta\tau_{f,avg}$ (Equation 10). While similar results were achieved in this study (for < 300 bpm or 91 bpf), the drivability ($\Delta\tau_{f,avg}$) analysis is preferred since GRLWEAP can account for effects of the changing ratio of pile shaft friction to total resistance, soil

type dependant damping, as well as variable hammer stroke / fuel setting / efficiency that cannot be accounted for in bearing graph analyses.

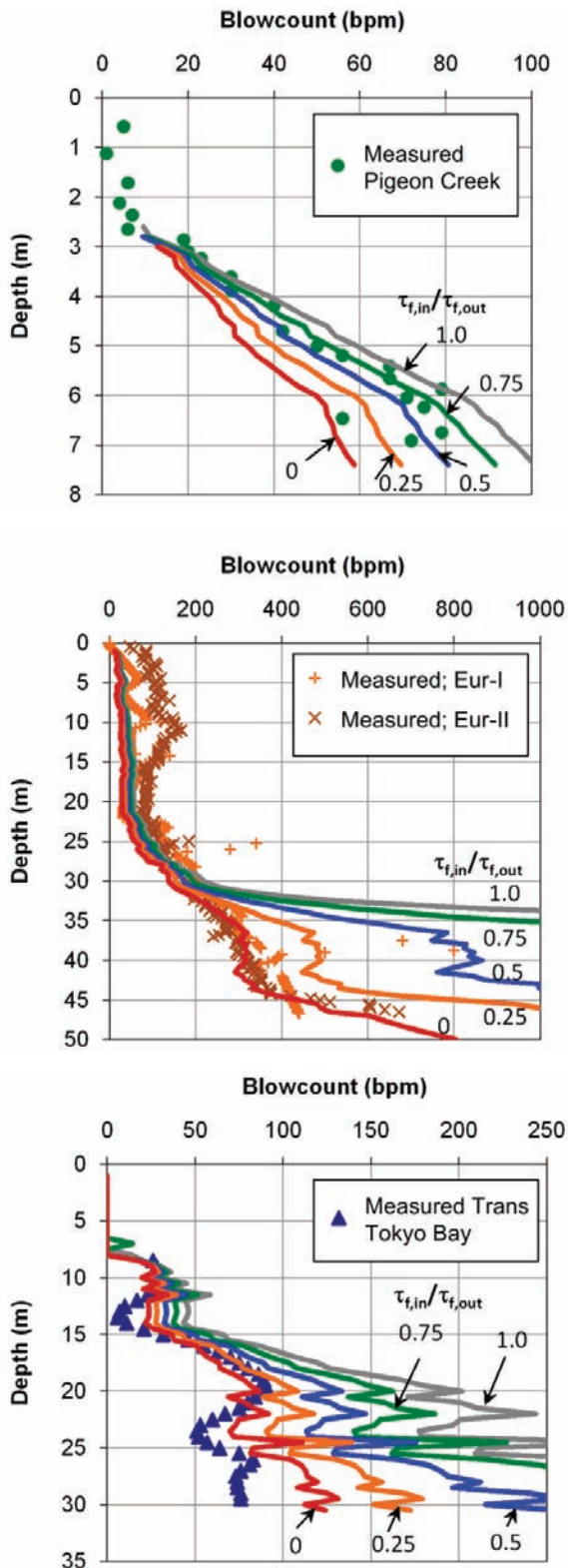


[FIG. 12] Effect of internal shaft friction (quantified using $\tau_{f,in}/\tau_{f,out}$) on drivability assessment using the modified UWA-05 method

- Since the AH-01 method was calibrated based on pile driving records, it performed

well for the range of pile diameters in this study provided that the ratio of pile diameter to pile wall thickness (D/t) was approximately 40. For low values of D/t or partial plugging during installation, application of the effective area ratio correction (Fig. 6) was required to minimize the unconservative bias in the original formulation.

- The modified UWA-05 method tended to overpredict SRD when using $\tau_{f,in}/\tau_{f,out}$ of 0.5 for drivability analyses. This observation is expected since the modified UWA-05 method was calibrated to a database of load tests performed, on average, 9 days after pile driving. Increase in capacity with time after driving needs to be considered for assessment of driving resistance as well as assessment of static capacity based on SRD.

While the analysis procedures discussed in this paper have been useful to highlight mechanisms influencing diameter effects on drivability of piles, an expanded database and more detailed analyses of pile driving records would extend these insights into a broader understanding of friction fatigue for use in pile drivability and static capacity analyses. Additional experimental studies evaluating the ratio of internal to external shaft friction are also warranted.

ACKNOWLEDGEMENTS

Fugro is thanked for access to site characterization, pile installation, and static load test data related to the Euripides project. Pile Dynamics, Inc. is acknowledged for use of the academic version of GRLWEAP during these studies. Reviewers of this paper are thanked for their valuable suggestions and comments.

REFERENCES

1. Alm, T. & Hamre, L. (2001). Soil model for pile drivability predictions based on CPT interpretation. *Proceedings of the 15th International Conference on Soil Mechanics and Geotechnical Engineering*, 2, Istanbul, Turkey, 1297-1302.
2. Clausen, C.J.F., Aas, P.M., & Karlsrud, K. (2005). Bearing capacity of driven piles in sand, the NGI approach. *Proceedings of the International Symposium on Frontiers in Offshore Geomechanics*, Perth, Australia, 677-682.

3. Dutt, R.N., Doyle, E.H., Collins, J.T., & Ganguly, P. (1995). A simple model to predict soil resistance to driving for long piles in deepwater normally consolidated clays. *Proceedings of the 27th Annual Offshore Technology Conference*, OTC 7668, Houston, USA, 257-269.
4. Foray, P., Balachowski, L., & Colliat, J.L. (1998). Bearing capacity of model piles driven in dense overconsolidated sands. *Canadian Geotechnical Journal*, 35(2), 374-385.
5. Heerema, E.P. (1980). Predicting pile driveability: Heather as an illustration of the friction fatigue theory. *Ground Engineering*, 13(3), 15-37.
6. Jardine, F.M., Chow, F.C., Overy, R.F., & Standing, J.R. (2005). *ICP design methods for driven piles in sands and clays*. London: Thomas Telford.
7. Kolk, H.J., Baaijens, A.E., & Senders, M. (2005a). Design criteria for pipe piles in silica sands. *Proceedings of the International Symposium on Frontiers in Offshore Geomechanics*, Perth, Australia, 711-716.
8. Kolk, H. J., Baaijens, A.E., & Vergobi, P. (2005b). Results of axial load tests on pipe piles in very dense sands: the EURIPIDES JIP. *Proceedings of the International Symposium on Frontiers in Offshore Geomechanics*, Perth, Australia, 661-667.
9. Lehane, B.M., Jardine, R.J., Bond, A.J., & Frank, R. (1993). Mechanisms of shaft friction in sand from instrumented pile tests. *Journal of Geotechnical Engineering*, 119(1), 19-35.
10. Lehane, B.M., Schneider, J.A. & Xu, X., (2005). The UWA-05 method for prediction of axial capacity of driven piles in sand. *Proceedings of the International Symposium on Frontiers in Offshore Geomechanics*, Perth, Australia, 683-690.
11. Lehane, B.M., Schneider, J.A. & Xu, X., (2007). Development of the UWA-05 design method for open and closed ended driven piles in siliceous sand. *Contemporary Issues in Deep Foundations, ASCE GSP 158*, 1-10.
12. Paik, K., Salgado, R., Lee, J., & Kim, B. (2003). Behavior of open- and closed-ended piles driven into sands. *Journal of Geotechnical and Geoenvironmental Engineering*, 129(4), 296-306.
13. Paikowski, S.G., Whitman, R.V., & Baligh, M.M. (1989). A new look at the phenomenon of offshore pile plugging. *Marine Georesources & Geotechnology*, 8(3), 213-230.
14. Pile Dynamics, Inc. (2005). *GRLWEAP: Wave Equation Analysis of Pile Driving, Procedures and Models Manual*, Cleveland.
15. Randolph, M.F. (2000). Pile-soil interaction for dynamic and static loading. *Proceedings of the 6th International Conference on Application of Stress Wave Theory to Piles*, Sao Paulo, Appendix, 3-11.
16. Randolph, M.F. (2003). Science and empiricism in pile foundation design. *Géotechnique*, 53(10), 847-875.
17. Randolph, M.F., Dolwin, J., & Beck, R. (1994). Design of driven piles in sand. *Géotechnique*, 44(3), 427-448.
18. Randolph, M.F., Leong, E.C., & Houlsby, G.T. (1991). One-dimensional analysis of soil plugs in pipe piles. *Géotechnique*, 41(4), 587-598.
19. Roussel, H.J. (1979). Pile driving analysis of large diameter high capacity offshore pipe piles. PhD Thesis, Tulane University, New Orleans, LA.
20. Schneider, J.A., Xu, X., & Lehane, B.M., (2008). Database assessment of CPT based design methods for axial capacity of driven piles in siliceous sands. *ASCE Journal of Geotechnical & Geoenvironmental Engineering*, 134(9), 1227-1244.
21. Shioi, Y., Yoshida, O., Meta, T., & Homma, M. (1992). Estimation of bearing capacity of steel pipe pile by static loading test and stress-wave theory (Trans-Tokyo Bay Highway). *Application of Stress Wave Theory to Piles*, Rotterdam, 325-330.
22. Skov, R. & Denver, H. (1988). Time-dependency of bearing capacity of piles. *Proceedings of the 3rd International Conference on Application of Stress Wave Theory to Piles*, Ottawa, Canada, 888-897.
23. Stevens, R.F. (1988). The effect of soil plug on driveability in clay. *Proceedings of the 3rd International Conference on Application of Stress Wave Theory to Piles*, Ottawa, Canada, 861-868.

24. Stevens, R.F., Wiltsie, E.A., & Turton, T.H. (1982). Evaluating pile driveability for hard clay, very dense sand, and rock. *Proceedings of the 14th Annual Offshore Technology Conference*, Houston, USA, 465-469.
25. Svinkin, M.R., Morgano, C.M., & Morvant, M. (1994). Pile capacity as a function of time in clayey and sandy soils. *Proceedings of the 5th International Conference on Piling and Deep Foundations*, Bruges, Belgium, 1.11.1-1.11.8.
26. Tavenas, F.A. & Audy, R. (1972). Limitations of the driving formulas for predicting bearing capacities of piles in sand. *Canadian Geotechnical Journal*, 9(1), 47-62.
27. Toolan, F.E., Lings, M.L., & Mirza, U. A. (1990). An appraisal of API RP2A recommendations for determining skin friction of piles in sand. *Proceedings of the 22nd Annual Offshore Technology Conference*, Houston, USA, 33-42.
28. White, D.J. (2005). A general framework for shaft resistance on displacement piles in sand. *Proceedings of the International Symposium on Frontiers in Offshore Geomechanics*, Perth, Australia, 697-703
29. White, D.J. & Lehane, B.M. (2004). Friction fatigue on displacement piles in sand. *Géotechnique*, 54(10), 645-658.
30. White, D.J., & Bolton, M.D. (2005). Comparing CPT and pile base resistance in sand. *Proceedings of the Institute of Civil Engineers, Geotechnical Engineering*, 158, 3-14.
31. White, D.J., Schneider, J.A., & Lehane, B.M. (2005). The influence of effective area ratio on shaft friction of displacement piles in sand. *Proceedings of the International Symposium on Frontiers in Offshore Geomechanics*, Perth, Australia, 741-747.
32. Xu, X., Schneider, J.A., & Lehane, B.M. (2008). Cone penetration test (CPT) methods for end-bearing assessment of open- and closed-ended driven piles in siliceous sand, *Canadian Geotechnical Journal*, 45(8), 1130-1141.
33. Zuidberg, H.M. & Vergobbi, P. (1996). Euripides, Load tests on large driven piles in dense silica sands, *Proceedings of the 28th Annual OTC*, Houston, 193-206.

Support of Structures in Expansive Shale Using Recycled Plastic Piles

Lance A. Roberts, South Dakota School of Mines and Technology, Rapid City, SD, USA;
lance.roberts@sdsmt.edu

Eric Brandner, South Dakota School of Mines and Technology, Rapid City, SD, USA

ABSTRACT

Expansive soil formations can be found throughout the United States. When subjected to wetting, these formations have the potential to swell and exert large uplift forces on buildings and foundations. Lightly loaded structures, such as single family residences founded in areas of expansive soils, can be significantly damaged due to uplift movement from swelling actions. Designing an economical deep foundation that can resist uplift forces is critical to prevent damage to these structures. The current solutions to control uplift due to swelling soils, such as over-excavation and replacement of the expansive material or the use of drilled shafts can be costly. Piles made from recycled polymer materials could provide a solution. Due to a lower coefficient of friction along the interface of the soil-pile interface compared to traditional pile materials, solid recycled plastic piles can allow expansive soils to move nearly independently from the pile when wetted. This results in a much smaller magnitude of uplift force being transferred to the structure, which minimizes the risk of significant structural damage from excessive movements.

This paper presents the results of research conducted on the use of recycled plastic piles in an expansive shale environment. The preliminary phase of the project involved the installation of six recycled plastic piles at a test site on the South Dakota School of Mines and Technology campus. Two of the piles were subjected to a full-scale compression load test in order to determine ultimate capacity. The remaining four piles were subjected to long-term monitoring of uplift movement during the course of the project. A concrete anchor was also installed at the test site for uplift monitoring. Data gathered during the field and laboratory testing was utilized in a non-linear soil-structure interaction model to predict the displacement behavior and internal stresses within a plastic pile and concrete anchor subjected to uplift forces from the swelling shale. While more research is needed to further understand the application for recycled plastic piles, the results from this research indicate that their use is a viable alternative for support of lightly loaded structures in expansive soil environments.

INTRODUCTION

Expansive soils typically contain minerals such as bentonite. When wetted, these materials attract large quantities of water within their structure, thereby expanding and creating uplift forces on structures and foundations (Das 2002). Expansive soil formations are found throughout the United States, but are most prevalent in the Midwest from Texas, Oklahoma, and the upper Missouri Valley (Das 2006). Lightly loaded structures, such as residences and other single story structures, are particularly vulnerable to damage caused by the uplift forces. Due to the weight and large ground coverage area of these structures, differential movements as small as 1 in. per 20 ft. (25 mm per 6 m) can cause significant damage (Meehan and Karp 1994). This can include cosmetic damage, such as cracking of

interior walls and slabs, serviceability damage, such as inoperable doors and windows, and structural damage of framing systems. While the damage is often caused at a slow rate, the repair cost for these problems can be high. Estimated costs of damages caused by expansive clay are as high as \$7 billion annually (FEMA 1997).

In most instances, the effects of expansive soils are mitigated by over-excavation of the material and replacement with a granular material. The depth of replacement will vary from locale to locale, but is generally 5 to 10 ft. (1.5 to 3 m). For sites with highly expansive soils and movement sensitive structures, a combination of over-excavation and support of the structure with a deep foundation system may be required. Typically, small diameter drilled shafts are used for these applications. This allows the structure

to be supported independently on grade beams with crushable forms to minimize potential uplift forces from the soil. However, Johnson and Stroman (1985) suggest that the uplift forces on drilled shafts installed in expansive soils can be so extreme that drilled shafts have failed due to tensile fractures along their length. Designing an adequate foundation system to accommodate and resist the uplift loads can be a very costly initiative, thus new and innovative methods to address this problem are warranted.

OBJECTIVE AND SCOPE

The objective of this research is to examine the feasibility of utilizing recycled plastic piles for support of lightly-loaded structures, such as single family residences, in an expansive soil environment. The project described herein includes full-scale field and laboratory experimentation, as well as modeling the response of plastic piles in swelling soil conditions. During the course of the project, six solid recycled plastic piles reinforced with fiberglass bars were installed at a field test site. A static load test was performed on two 15 ft. (4.5 m) piles equipped with strain gage and telltale instrumentation. The remaining four piles, instrumented with telltales, were monitored for vertical movement for the duration of one year. Laboratory tests were conducted to determine the characteristics of the in-situ soil at the test site. Field and laboratory data were utilized to develop a non-linear, soil-structure interaction model to predict the displacement response of a plastic pile and drilled shaft due to variations within expansive soil conditions.

RECYCLED PLASTIC PILES

Recycled plastic piles are commonly used in marine applications as an alternative to typical wooden, steel, and concrete piles. Their composition enables resistance against corrosion, marine borers, and deterioration from the sun (FHWA 2006). Ductile characteristics make them ideal as fender piles and bumpers to absorb impact forces from ships and other small marine vessels (Seaward 2009). Recycled plastic piles are produced in many shapes and configurations. Variations include hollow tubes, non-reinforced solid piles, piles mixed with reinforcing fibers, steel reinforced piles, and fiberglass reinforced piles. Since the recycled plastic piles are produced in an extrusion process, they have a relatively

smooth interface when compared to other conventional pile materials, such as steel or concrete. A research hypothesis for this study is that a smooth soil-pile interface would provide a low coefficient of friction, thereby reducing pile displacement induced by the surrounding expansive material. A reduction in pile displacement would in turn lower the magnitude of uplift forces within the pile itself, along with movement transferred to a structure. Since expansive soils can cause significant damage to lightly loaded, single story structures or to the deep foundation elements that support them, the use of recycled plastic piles to carry these buildings is of particular interest. Fig. 1 provides a cross-section of the recycled plastic pile used for this project and identifies the three major components.

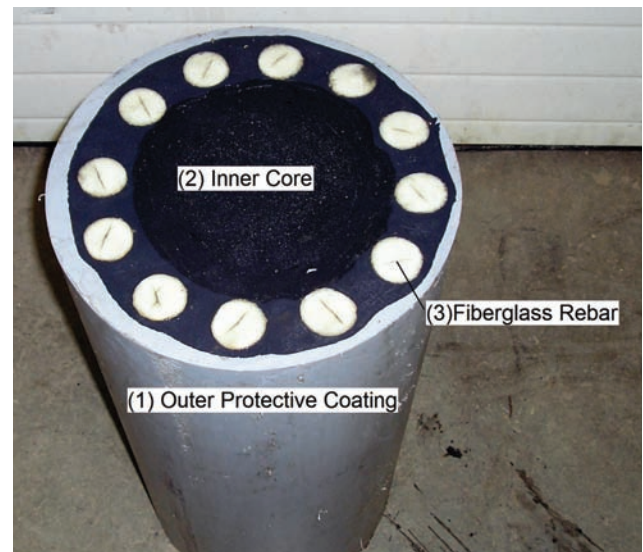


[FIG. 1] Cross-section and components of Seapile® composite marine piling.

FIELD TEST SITE

Full-scale field load testing and long-term uplift monitoring were conducted on several plastic piles installed in an expansive shale site. The field test site was located on the campus of the South Dakota School of Mines and Technology (SDSM&T) in Rapid City, South Dakota. As shown in Fig. 2, the site was located approximately 300 ft. (90 m) north of the corner of E. St. Andrew Street and Hawthorne Avenue. The selection of the test site was based on both the presence of undisturbed highly expansive soil and the absence of developed structures that would be affected by the research efforts. A geotechnical investigation was conducted at the site by drilling three boreholes and obtaining samples of the shale

materials. The site was comprised of Belle Fourche shale with little to no overburden at the surface. Laboratory testing of the shale samples indicated swell pressures over 20 ksf (960 kPa), along with swell percentages of up to 18%. Additional information regarding the site conditions can be found in Brandner et al. (2009).



[FIG. 2] Location of field test site on SDSM&T campus (from Bing™).

FIELD TESTING PILES

Six recycled plastic piles, termed Seapiles® and manufactured by Seaward Engineered Plastics, were installed at the test site for compression load testing and long-term vertical movement monitoring. Four of the piles had a length of 15 ft. (4.5 m), one pile had a length of 20 ft. (6.0 m), and one pile had a length of 25 ft (7.6 m). All recycled plastic piles had a diameter of 13 in. (330 mm) and were reinforced with 12 - 1.5 in. (38 mm) diameter fiberglass reinforcing bars spaced equidistantly around the perimeter of the pile. The reinforcing bars were 0.55 in. (14 mm) from the edge of the pile. Two 15 ft. (4.5 m) piles were subjected to static field load testing. The remaining four piles, along with a concrete anchor, were monitored for vertical movement due to seasonal moisture fluctuations.

All of the recycled plastic piles used in the field testing program were instrumented. Two piles selected for static load testing, designated as Pile 1 and Pile 2, were each instrumented with two Geokon® vibrating wire embedment strain gages, located approximately 8 in. (200 mm) from the toe of the pile and installed on the pile per the manufacturer recommendations. In addition to the strain gages, Pile 1 and 2 were

affixed with four stainless steel telltales. Two of the telltales were attached 8 in. (200 mm) from the toe of the pile while the other two telltales were attached near the mid-point of the pile. The remaining four piles, used to monitor long-term vertical movement, received telltale instrumentation only. One of the 15 ft. (4.5 m) piles, designated as Pile 3, contained four telltales in a similar configuration to that of the load test piles. The remaining 15 ft., 20 ft., and 25 ft. (4.5 m, 6.0 m and 7.6 m) piles, designated as Pile 4, Pile 5, and Pile 6, respectively, contained two telltales each, with one telltale attached near the toe of the pile and another at the mid-point of the pile. Plastic conduit was placed over the telltales to allow independent movement from the surrounding soil. A fully instrumented toe portion of a plastic pile that was used in one of the static load tests is shown in Fig. 3.



[FIG. 3] Strain gages and telltales attached at the toe of a pile.

PILE INSTALLATION

The recycled plastic piles were installed in September 2008. The installation began by selecting the locations of the piles. To reduce the influence that adjacent piles would have on each other during load testing, a minimum spacing of 15 ft. (4.5 m) was utilized. Installation of all plastic piles was similar:

1. An 18 in. (457 mm) diameter dry shaft was drilled to a depth roughly 1 ft. (300 mm) shorter than the length of the pile to be installed;
2. A large diameter clamp, attached to the hoist on the drill rig, was secured to the head of the plastic pile;
3. The drill rig hoisted the pile into a vertical position over the shaft;

4. While the pile was lowered into the shaft, as observed in Fig. 4, telltale extensions were added along the length of the pile, along with plastic conduit over each telltale. The conduit was secured with duct tape. A metal washer was placed behind the plastic conduit for vertical alignment. Strain gage cables were also attached to the perimeter of the pile using duct tape. The plastic pile was lowered into the shaft in such a manner to minimize the amount of loose material knocked from the side of the excavation;
5. Once at the bottom of the shaft, the pile was leveled and repositioned within the shaft to ensure a relatively equal annulus around the perimeter of the pile;
6. A low plasticity clay material was tamped into the annulus to stabilize the pile within the hole and prevent water from flowing into the annulus.



[FIG. 4] Pile being lowered into the shaft.

Clay from the Spearfish Formation near Rapid City was chosen because of its low swell potential, low permeability when compacted, and abundant local availability. The clay was tested for Atterberg limits and found to possess a LL of 30 and a PI of 9. The reuse of the excavation spoils from the drilling process was not considered since adequate compaction of the shale was not feasible. Sand was also eliminated as backfill material due to its high permeability and potential to allow water to

infiltrate the borehole, causing the shale to swell at all depths along the pile and at the toe. Minimal construction equipment was required for installation of the plastic piles. A Production Digger 6030 drill rig with hoist was utilized, along with a skid steer to move material on-site. The installation time per pile varied due to the amount of instrumentation attached to the pile. Total installation time included drilling to the appropriate depth, installing instrumentation, placing/seating the pile, and backfilling the annulus with the low plasticity clay. Pile 1 and Pile 2, which contained strain gages and telltales, required approximately one hour each to install as extreme caution was exercised to ensure no damage to the strain gauges of the telltales. Conversely, Pile 4, Pile 5, and Pile 6, which were instrumented with two telltales each, took only about thirty minutes per pile to install. After installation was completed, verticality measurements were obtained for all plastic piles. The measurements indicated that all piles were within the general plumbness requirements reported in most drilled shaft construction specifications (1/4" per 1 foot or 6 mm per 300 mm). During installation of the plastic piles, drill cuttings from various depths were sampled in order to determine the average in-situ moisture content of the shale versus depth as shown in Table 1.

A cast-in-place, concrete anchor with a diameter of 6 in (152 mm) was placed in October 2008 for uplift monitoring and performance comparison with the recycled plastic piles. The anchor was installed to a depth of 15 ft (4.5 m). A Grade 75, #14 (45 mm) Dywidag threadbar was placed in the center of the anchor for its entire length.

[TABLE 1] In-situ moisture content (%) of shale during installation.

Depth (ft)	Pile					
	1	2	3	4	5	6
5	17.5	16.7	18.4	14.6	15.5	13.5
10	12.7	12.5	13.1	13.0	13.4	12.8
15	13.3	12.8	13.1	12.7	12.5	12.8
20					12.3	12.6
25						13.2

STATIC LOAD TESTING

The static load testing of Pile 1 and Pile 2 took place in November 2008. Four reaction anchors were installed near Pile 1 and Pile 2 to provide adequate resistance for a reaction support frame during the load testing procedure. Each anchor was drilled to a depth of 30 to 35 ft. (9 to 10.5 m) and had a diameter of 6 in. (152 mm). A Grade 75, #14 (45 mm) Dywidag threadbar was inserted into each hole before being tremie grouted with cement grout. The reaction support frame, consisting of built-up steel sections and wood cribbing, was constructed and integrated with the reaction anchors as shown in Fig. 5.



[FIG. 5] Reaction frame setup for static load testing of plastic piles.

The static load testing generally followed Procedure “A” of ASTM D1143. However, the test piles were loaded in increments of 10 kips (44.5 kN) because the ultimate compressive capacity of the plastic piles was unknown. Load was applied by a hydraulic jack with a calibrated pressure gage. The hydraulic jack had a capacity of 1,000 kips (4.5 MN). Vertical head settlement measurements of the test piles were recorded at each loading increment using four dial gage indicators with sensitivity of 0.001 in. (0.025 mm). The dial gages were equidistantly spaced around the head of the test pile and were attached to a reference frame, which was independent from the test pile and test reaction system. Four additional dial gages, with accuracy to 0.001 in., (0.025 mm) were used to measure the movements of the telltales during the compression test of Pile 2. A standard tape measure was used to determine telltale movement during the compression test of Pile 1. Strains within the test pile were measured during each loading increment using

the embedment strain gages. All strain gages were connected to a vibrating wire readout device through a terminal switch box. The movements of the four telltales were monitored and recorded at each loading increment. Vertical movements of the reaction anchors were monitored using an automatic level and level rod.

Pile 2 was tested first due to its location at the test site. While attempting the first load increment of 10 kips (44.5 kN), Pile 2 experienced a total settlement of nearly 3 in. (75 mm). The excessive settlement was theorized to be the result of loose drill cuttings and other unconsolidated material beneath the toe of the pile from the installation. The application of load against Pile 2 continued until resistance was observed via the pressure gage attached to the hydraulic jack. Once a 10 kip (44.5 kN) load was attained, the pile was completely unloaded and the dial gauge instrumentation was reset. The load test then progressed as originally planned. A load-settlement plot of Pile 2 is shown in Fig. 6. The hydraulic jack was “bumped” at each load to compensate for loss in pressure and creep. This resulted in increased vertical displacement at each bump in the hydraulic jack pressure.

The load testing of Pile 2 provided valuable information for development of a load testing procedure for Pile 1 as follows:

1. Apply a seating load of 10 kips on the pile to ensure that the pile was properly seated at the toe. Maintain this load on the pile for at least 30 minutes;
2. Unload the pile completely and set all dial gauge instrumentation;
3. Perform the load test by applying the load in 10 kip (44.5 kN) increments. Do not bump the hydraulic jack to maintain the load;
4. Record head settlement, telltale, and strain gage readings at each load increment after the pressure gauge on the hydraulic jack has stabilized.

Pile 1 was loaded until plunging was evident and the hydraulic jack was no longer able to register an increase in pressure. The load-settlement plot of the Pile 1 load test data is shown in Fig. 7. Pile 1 was allowed to set overnight unloaded and was reloaded the next morning without the seating procedure. The load-settlement plot for the reloading of Pile 1 is also shown in Fig. 7.

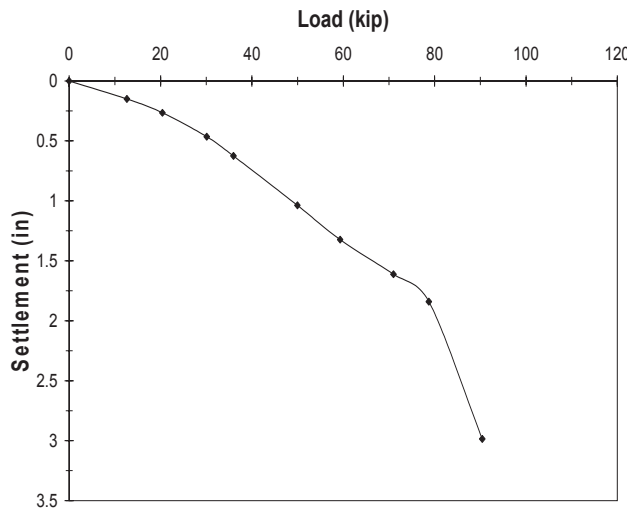


[FIG 6] Load-settlement curve for Pile 2.

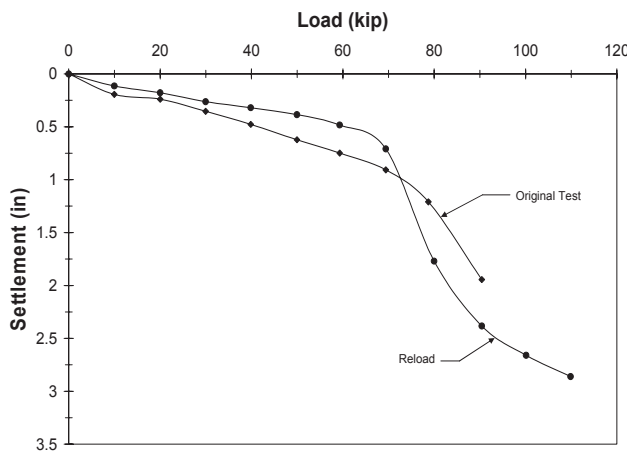


[FIG. 7] Load-settlement curve for Pile 1 (original load test and reload test).

The design load for a single deep foundation element supporting a lightly-loaded structure is typically on the order of 25 to 35 kips (110 to 155 kN). It is observed from Figs. 6 and 7 that the plastic piles are able to adequately support a design load of this magnitude with a head settlement of approximately 0.25 in. (6 mm). It is evident from Fig. 7 that the load-unload-reload of Pile 1 caused an increase in the stiffness of the soil at the toe, but that the pile achieved its plunging load much sooner compared to the original load test. The static load tests demonstrated that adequate cleanout of loose material from the shaft bottom, along with seating of the pile during placement of the pile in the shaft, appears to be critical in order to ensure acceptable load-settlement and ultimate capacity performance.

ANALYSIS OF LOAD TEST DATA

There are a number of methods to compute the ultimate capacity of a deep foundation using

field load test data. A review of the relevant literature resulted in the identification of more than ten different criteria (Fellenius 1990, Salgado 2006). Although many of these criteria were developed for specific deep foundation systems, the use of varying criteria often results in a different ultimate capacity for the deep foundation (Yang 2008). A method that can interpret the results of the field load test data without bias toward the predicted ultimate capacity is beneficial to ensure efficiency in the design. To that end, the field load test data was analyzed using the t-z model approach.

The t-z model approach has been widely utilized for analytical and numerical modeling of deep foundation load-settlement behavior (Randolph and Wroth 1978, Scott 1981, Misra and Chen 2004, Reese et al. 2006). In the t-z model, axial resistance along the interface of a deep foundation and at the toe is represented by a spring-slider system. The spring-slider system is assumed to behave in either an ideal elasto-plastic or hyperbolic manner, and each spring is assigned a strength and stiffness magnitude. Along the interface, the spring-slider system represents the annular band of soil that participates in the axial resistance, as shown in Fig. 8, and thus an imperfect interface is assumed (i.e. movement of foundation and interface soil are not equal). The foundation itself is assumed to behave elastically throughout considering that the load required to reach yield of the interface is much smaller than that to yield the foundation material.

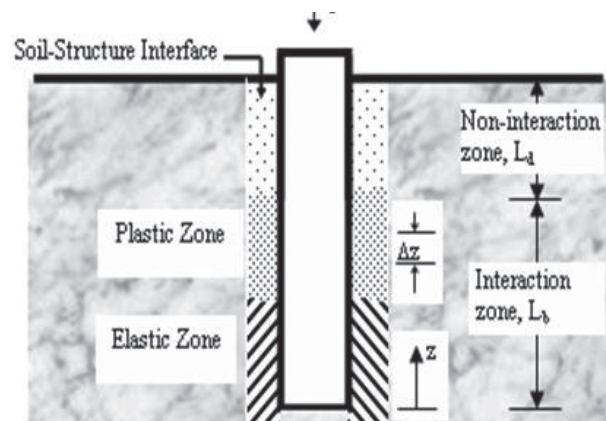


[FIG. 8] Schematic of foundation when describing behavior using t-z model.

In the t-z model, the following equilibrium equation is solved (Reese et al. 2006):

$$K_m \frac{d^2 u}{dz^2} - Ku(z) = 0 \quad (1)$$

where, $u(z)$ is the deep foundation deformation, K_m is the deep foundation axial stiffness, and K is the shear modulus of soil-structure interface sub-grade reaction.

The solution to the equilibrium equation, assuming non-linear behavior of the spring-slider system, is presented elsewhere (Misra and Roberts 2006). However, for completeness, there are a number of additional parameters necessary to utilize the t-z model approach. Under a compression load, the deep foundation will develop a toe force, P_t , proportional to the toe displacement, u_t , given by:

$$P_t = K_t u_t \quad (2)$$

where, K_t is the toe soil stiffness. Based on theories for rigid punch bearing upon elastic half-space, the initial tangent stiffness of the toe soil, K_{ti} , may be related to foundation diameter and the elastic properties of the toe soil as follows (Misra and Roberts 2006):

$$K_{ti} = \frac{0.3\pi D E_s}{(1 - \mu_s^2)} \quad (3)$$

where, E_s is the modulus of soil sub-grade reaction, μ_s is toe soil Poisson's ratio, and D is the diameter of the foundation element.

As an axial load is applied to the head of the deep foundation, the springs will displace based on their strength and stiffness properties and the deep foundation element will settle. As the applied axial load increases, yielding of the springs begins in the uppermost elements and progresses to the toe. At some load, all springs yield and the deep foundation will fail by plunging. The ultimate capacity of the toe soil can be determined assuming a punching shear failure from the following equation:

$$P_{utip} = q_t A_m \quad (4)$$

where, q_t is the unit tip bearing resistance and A_m is the cross sectional area of the foundation element. The use of a t-z model approach therefore results in the development of a load-settlement curve that represents the behavior of the deep foundation over a wide range of applied axial loads.

In Fig. 9, the force-displacement behavior for a nonlinear (hyperbolic) spring-slider system is shown. In Fig. 9, K_{init} is the initial tangent shear modulus of soil-structure interface, and q_o is the ultimate (asymptotic) strength of the soil-structure interface given by the product of the

deep foundation perimeter and the ultimate shear strength of the soil-structure interface, τ_u , in drained or undrained conditions. The toe soil force-displacement curve can be similarly represented using the initial tangent tip soil stiffness, K_{ip} , and the ultimate (asymptotic) strength of the tip soil, q_p , in drained or undrained conditions. The soil-structure interface strength and stiffness parameters are related to the deep foundation type, construction techniques, and the properties of the soil strata. The toe soil strength and stiffness parameters are generally only related to the deep foundation type and properties of the soil at the toe.

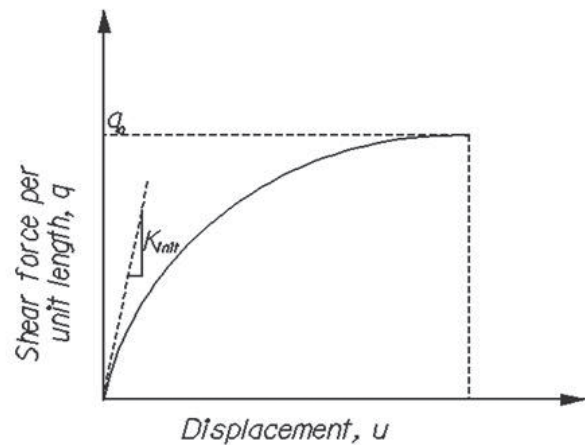


[FIG. 9] Interface force-displacement curve for a hyperbolic spring-slider system.

A t-z model back-computation procedure using load test data is described extensively in Roberts et al. (2008). The method is an iterative process where the load-settlement and strain magnitude predicted by the t-z model is matched to the load-settlement and strain magnitudes of the deep foundation using the load test data. Software has been developed at SDSM&T to perform the t-z back-computation. The back-computation procedure using the t-z model and the load test data from Pile 1 is shown in Figs. 10 and 11. In Fig. 10, head-settlement measurements recorded from the field load test (points) are superimposed on the predicted head-settlement curve from the t-z model (solid line). In Fig. 11, the telltale movement at the pile toe from the field load test (points) is superimposed on the predicted toe movement from the t-z model (solid line). By fitting the t-z model to the head-settlement and telltale data, the strength and stiffness parameters for the interface and toe soil springs were back-computed. Non-linear (hyperbolic)

displacement behavior was assumed for all springs in the back-computation process. In addition, the composite elastic modulus of the plastic piles was assumed as 450 ksi (3,100 MPa) (Seaward 2009), the non-interaction zone length was taken as 1 ft. (305 mm) due to potential ground disturbance, and the Poisson's ratio of the shale at the pile toe was assumed as 0.30. The back-computed t-z model strength and stiffness parameters are reported in Table 2.

[TABLE 2] Strength and stiffness parameters of the t-z model interface and toe springs.

Interface Springs		Toe Spring	
Strength	Stiffness	Strength	Stiffness
psi	ksi	ksf	ksf
0.75	0.5	100	2000

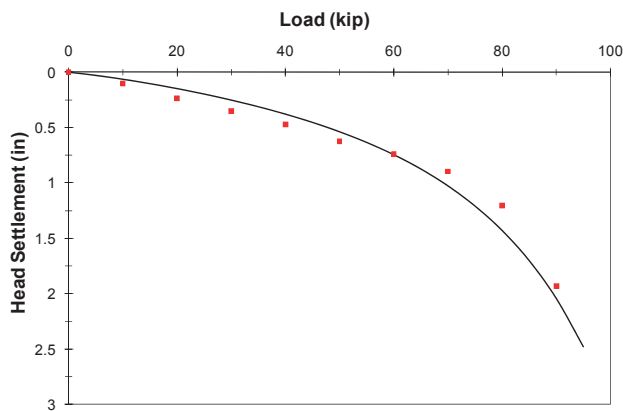


[FIG. 10] Measured head settlement versus predicted head settlement from t-z model.

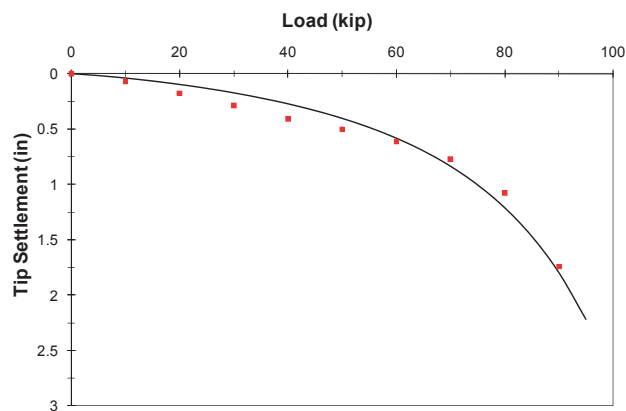


[FIG. 11] Measured telltale pile toe movement versus predicted toe movement from t-z model.

As shown in Table 2, the pile interface strength and stiffness parameters are minimal and that a majority of the pile resistance is due to the spring at the pile toe. This confirms that the combination of the pile installation method, along with the low coefficient of friction of

the pile, should allow for a reduction in uplift forces due to the expansion of the shale at the site. Interestingly, approximately 30% of the total head settlement at any given load is due to elastic shortening of the pile as the composite elastic modulus of the plastic pile is on the order of 10% that of conventional concrete.

It is important to note that in Figs. 10 and 11, differences between the measured values from the field load tests (points) and predicted values from the t-z model (solid line) are realized. Discrepancies of this nature are often due to slight errors in the field measurements. In the back-computation process, the predicted values from the t-z model are within $\pm 10\%$ of the field measured values.

SOIL SWELL MODEL

The swell potential of soil varies between different geological formations (Das 2002). Key factors characterizing the magnitude of swell pressure include the in-situ void ratio, e_o , and change in the degree of saturation, ΔS , of the soil. During the subsurface investigation of the test site, laboratory tests were conducted to determine the swell pressure at 5 ft. (1.5 m) intervals along the entire depth of the exploratory borings. Using the in-situ void ratio, change in the degree of saturation, and swell pressure data from this laboratory testing, a potential swell pressure equation was developed to predict the response of the Belle Fourche shale at the test site for a range of in-situ conditions:

$$S_p = 0.458 P_a \Delta S^{0.874} e_o^{-5.016} \quad (5)$$

where, S_p is the swell pressure (psf) and P_a is the atmospheric pressure. The value of ΔS in Eq. 5 is taken as a decimal. The equation was developed using multiple variable linear regression and was found to have a correlation coefficient of 0.98, indicating a strong correlation within the test data.

Using Eq. 5, the swell pressure for the shale at the test site was predicted for different field conditions by: (1) varying e_o while maintaining a constant value of ΔS as shown in Fig. 12, and (2) varying ΔS while maintaining a constant value of e_o , as shown in Fig. 13. From Fig. 12, it is observed that as e_o increases, the swell pressure of the material will decrease sharply. This is expected and caused by an increase in the volume of air and water in the three phase soil element. This in turn allows for greater

expansion of the soil particles as the soil particles must expand farther to exert pressure against others. From Fig. 13, it is observed that as ΔS increases, the swell pressure will also increase. This is also expected since the greater the change in the degree of saturation, the greater the amount of water that is absorbed into the soil system and thus the greater the expansion. When comparing Figs. 12 and 13, the in-situ void ratio, e_o , has a significantly greater impact on the swell pressure over the change in the degree of saturation, ΔS .

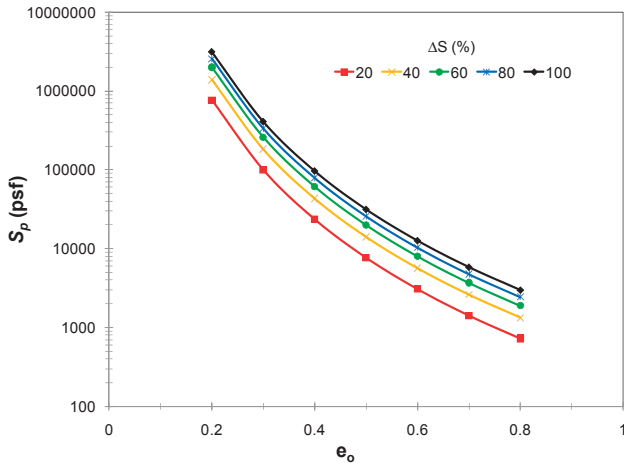


[FIG. 12] Swell pressure versus e_o for various magnitudes of ΔS .

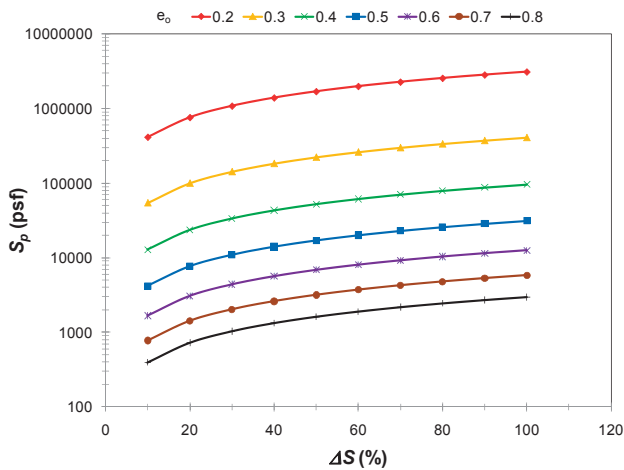


[FIG. 13] Swell pressure versus ΔS for various magnitudes of e_o .

PILE MODEL USING SWELL EQUATION

The diameter and length of drilled shafts used in the mitigation of expansive soil will vary; however, the minimum size typically used in expansive shale environments in South Dakota is a 24 in. (610 mm) diameter shaft with a length of 25 ft. (7.6 m). As mentioned previously, the uplift force exerted on a drilled shaft due to the expansion of soil can be large enough to cause

a tensile fracture failure of the drilled shaft (Johnson and Stroman 1985). Therefore, the internal forces and uplift movement of a drilled shaft were modeled to observe whether tensile fracture failure could occur due to the internal pile forces from soil expansion. In addition, a similar model was developed for a recycled plastic pile with a diameter of 13 in. (330 mm) and length of 15 ft. (4.5 m). A comparison of the two models allows for improved understanding of the behavior of these deep foundation systems in expansive soil and permits easy parametric analyses and performance prediction studies to be conducted.

The deep foundation model was developed using the t-z model method. For the drilled shaft, τ_u and K_{mit} for the t-z springs were assumed as 20 psi (138 kPa) and 5 ksi (34.5 MPa), respectively, based on the characteristics of the shale at the site and using criteria given in Coduto (2001) and FHWA (1999). For the plastic pile, the strength and stiffness values for the t-z springs were assigned the back-computed values from the field load test. A compressive load of 30 kips (133 kN) was applied to each model to simulate the typical design load for a foundation element within a lightly loaded structure. Swell pressures were computed using Eq. 5 for various values of e_o along the foundation interface, while assuming that ΔS was 100% at the ground surface and linearly decreased to 0% at the depth of wetting. An upward swell force was applied at each discretized nodal element along the length of the foundation. The upward swell force, SF, at each element was determined as follows:

$$S_F = S_p \pi D \Delta z \beta \quad (6)$$

where, Δz is the discretized element length and β is a factor to account for the soil-pile interface friction angle and in-situ coefficient of earth pressure (FHWA 1999). All additional variables have been defined previously. A β value of 1.10 and 0.10 was assigned to the drilled shaft and plastic pile, respectively, during the swell force modeling. The β value for the plastic pile was based on the t-z back-computation of the field load test data, while the β value for the drilled shaft was based on typical values for intermediate geomaterials given in Coduto (2001) and FHWA (1999). The swell forces along the foundation interface provided resistance to the applied head load of 30 kips (133 kN)

(along with the weight of the foundation), while uplift resistance from the shale acted only along the soil-structure interface below the depth of wetting. It was assumed that the toe did not contribute any uplift resistance due to suction. Lastly, a perfect interface between the shale and clay was assumed which would allow for full transfer of the developed swell pressure from the expansive shale through the clay annulus to the foundation element in order to satisfy strain compatibility of the radial soil.

Using the developed deep foundation soil expansion model described above, the internal axial stresses within a drilled shaft and plastic pile subjected to an uplift force were computed for a range of in-situ void ratios. The computed axial stresses are shown in Figs. 14 and 15 for the drilled shaft and plastic pile, respectively. It is observed in Fig. 14 that as the magnitude of the in-situ void ratio, e_o , decreases, significant axial stresses are developed within the drilled shaft at the depth of wetting. The magnitude of the axial stress is such that tensile fracturing of normal strength concrete is highly likely, thereby confirming observations by Johnson and Stroman (1985) and Chapel and Nelson (2000). In Fig. 15, the axial stresses developed within the plastic pile also increase as e_o decreases. However, the axial stresses within the plastic pile are always compressive and thus structural failure of the plastic pile due to tensile stress is not a concern.

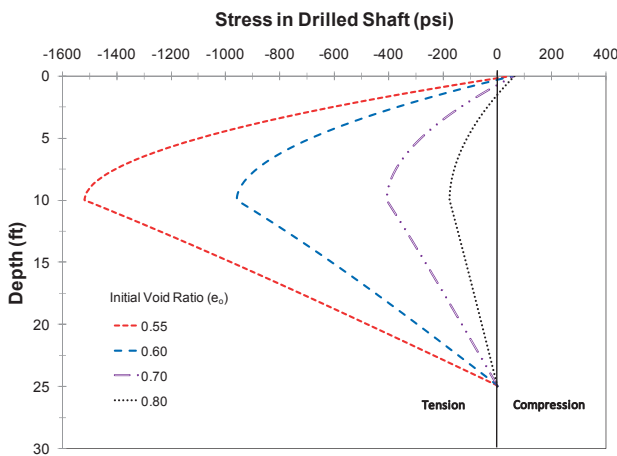


[FIG. 14] Internal stresses developed in drilled shaft under expansive shale uplift forces.

Head displacements for the drilled shaft and plastic pile were also determined using the deep foundation soil expansion model. Fig. 16 shows the predicted head displacement for both the drilled shaft and plastic pile when subjected to variable swell pressures under a

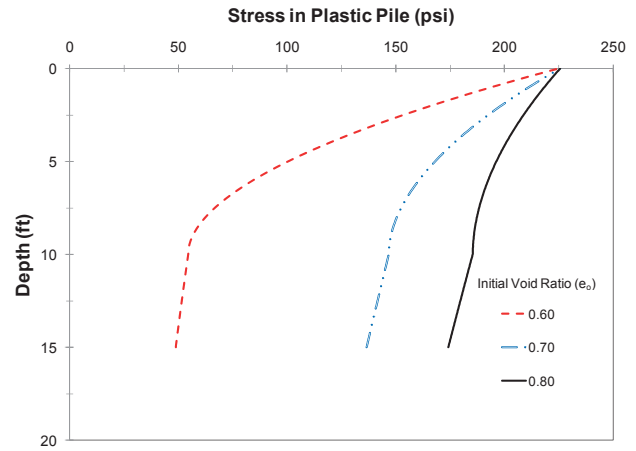


[FIG. 15] Internal stresses developed in plastic pile under expansive shale uplift forces.

design load of 30 kips (133 kN). Overall, both the drilled shaft and plastic pile exhibited upward movement and the movement of the drilled shaft is always greater than the neutral point. As e_o decreases, the overall rate of upward displacement between the plastic pile and drilled shaft is nearly equal, but the upward displacement of the plastic pile reaches infinity sooner than the drilled shaft. Based on these results, the research team is examining various methods to increase the side resistance of the plastic pile near the toe to help control the magnitude of uplift.

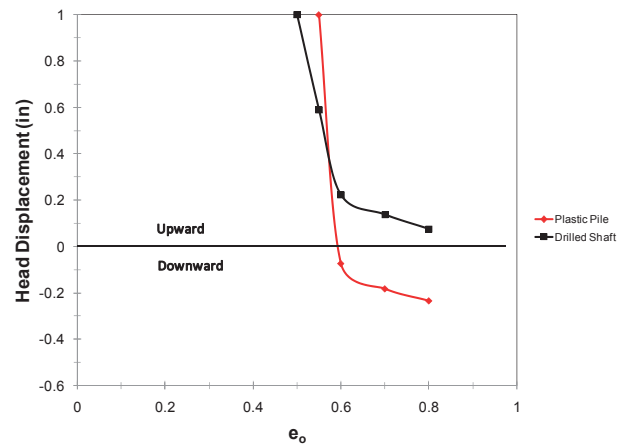


[FIG. 16] Head displacement for drilled shaft and plastic pile under expansive shale uplift forces.

PILE UPLIFT MONITORING AND SITE FLOODING

Pile movement due to seasonal moisture fluctuations was a crucial component for this project. To monitor uplift, weekly surveys using a conventional surveying level and rod, with an accuracy of 0.01 ft. (3 mm), were conducted over the course of one year.

Surveys included pile head elevation and pile elongation measurements from the telltales. Precipitation totals during each weekly survey interval were also recorded. Establishing a benchmark was especially difficult at the site due to the presence of the expansive shale and the potential for movement of a temporary benchmark placed in the ground. For this reason, a fire hydrant located near the site was used and the survey datum was established from one of the bolts connecting the bonnet to the barrel of the hydrant.

Overall, the plastic piles and concrete anchor experienced minimal vertical movement during the one year monitoring period, as shown in Fig. 17. Due to the accuracy of the surveying equipment, it is possible that most of the apparent vertical movement may actually be measurement error, as all plastic piles and the concrete anchor generally moved the same magnitude (upward or downward) at each measurement as shown in Fig. 17. However, the plastic piles did appear to settle within the first couple of months likely due to the presence of loose drill cuttings and other material beneath the toe of the pile. Pile 6 settled the most, with a magnitude of 0.13 ft. (40 mm). It is unclear why Pile 6 settled such a large magnitude.

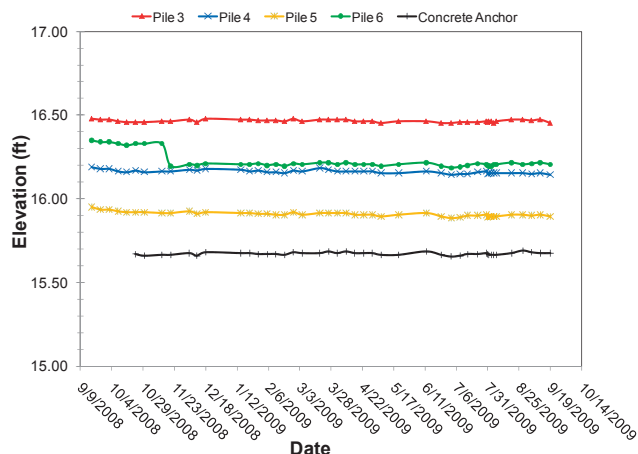


[FIG. 17] Observed maximum and minimum elevations of the plastic piles and anchor.

The small apparent magnitude of vertical movement observed during the monitoring period encouraged the researchers to examine a worst case scenario of moisture variation at the test site. This was accomplished by flooding a portion of the site. To control the area of water infiltration, an earth berm was constructed around Piles 3, 4, 5, 6, and the concrete anchor. The thicker vegetation and miscellaneous debris

was removed from the interior of the berm area prior to flooding. To fill the area within the berm, 10,500 gallons (40,000 litres) of water was required.

Site flooding occurred in July 2009. Prior to flooding, moisture samples were taken near the outer edge of the berm using a hand soil sampler. Samples were obtained at depths ranging from 0.5 to 4 ft. (0.15 to 1.2 m) The use of the hand sampler limited the depth at which samples could be obtained. The degree of saturation of the samples was determined and found to increase from 65% at the surface to 94% at 4 ft. (1.2 m). Elevations of the plastic piles and concrete anchor were determined prior to site flooding.

Flooding the test site took approximately two hours. Standing water was present at the conclusion of the flooding process with an average water depth of about 6 in. (150 mm) as shown in Fig. 18. The overcast and cool weather conditions during the day limited the amount of evaporation. Complete infiltration into the shale took approximately 12 hours. The next day, moisture samples were taken inside the berm to a depth of 4 ft. (1.2 m). The degree of saturation of all samples was found to be 100%. As before, the use of a hand sampler limited the depth of the sampling.



[FIG. 18] Flooding the test site.

Pile head elevations were recorded for a period of one week after the site flooding. However, as shown in Fig. 17 during this period, very minor head movements were recorded for the plastic piles and concrete anchor. In order to confirm the site observations, the potential head displacement of the plastic piles and concrete anchor

were computed using the developed deep foundation soil expansion model described previously, along with the magnitudes of ΔS given in Table 3 for the upper 4 ft. (1.2 m) of the shale due to the flooding activities. Substituting these ΔS values into Eq. 5, along with a constant value of $e_o = 0.60$, provides the magnitude of swell pressure at these depths. The swell pressures, provided in Table 3, were substituted in Eq. 6 to compute the swell forces within the shale zone. The swell forces were applied linearly along each discretized element of the t-z model within the upper 4 ft. (1.2 m) of the shale. All assumptions regarding the interface behavior of the plastic piles and concrete anchor within the t-z model from the previous modeling exercise were maintained. Based on this analysis, the upward head displacement of the plastic piles and concrete anchor were predicted to be 0.034 in. (0.86 mm) and 0.047 in. (1.19 mm), respectively. These magnitudes are significantly below the accuracy of the surveying equipment used on this project. Interestingly, if the depth of wetting was actually 10 ft. (3 m), the upward head displacement of the plastic piles and concrete anchor would be approximately 0.073 in. (1.85 mm) and 0.055 in. (1.40 mm), respectively, given the saturation conditions at the site. To that end, obtaining actual uplift measurements was not possible without the use of more sensitive equipment.

[TABLE 3] Degree of saturation before and after flooding test site.

Depth (ft)	S (%)		ΔS (%)	S_p (psf)
	Pre Flood	Post Flood		
0.5	66.4	100	34	4843
1	64.1	100	36	5125
2	70.3	100	30	4348
3	83.4	100	17	2607
4	93.7	100	6	1120

COST AND BENEFIT ANALYSIS

A cost benefit analysis was performed to determine the potential economic impact of using recycled plastic piles. The analysis focused on expansive shale mitigation techniques for residential structures due to an

increase in the number of damaged homes in Rapid City over the last five years. Therefore, the cost analysis assumed a one story, single family dwelling with a basement plan area of 1500 ft² (140 m²). The typical expansive soil mitigation options were examined and included (1) over-excavation and replacement of the expansive shale with a granular material to a depth of 10 ft. (3 m) beneath a slab-on-grade basement floor; (2) use of 24 in. (610 mm) diameter, 25 ft. (7.6 m) long drilled shafts supporting a structural floor/grade beam system placed on crushable forms; and (3) use of 13 in. (330 mm) diameter, 15 ft. (4.6 m) long recycled plastic piles supporting the same structural floor/grade beam system. Based on estimated total loads, it was assumed that 18 plastic piles would be required, while only 12 drilled shafts would be necessary. Using information provided by local contractors, the use of recycled plastic piles could provide a cost savings of nearly 10% and 20% when compared to Option 1 and 2, respectively.

The efficiency of using recycled plastic piles as deep foundation elements was also investigated. A drilled shaft foundation must be long enough to provide necessary resistance to the uplift forces. However, the minimum length required for uplift translates to a relatively high ultimate compressive capacity when compared to the design loads. This over-design may be as high as 11 times depending on the weathering characteristics and unconfined compressive strength of the shale, along with the construction method for the drilled shaft. Recycled plastic piles, however, can adequately support the anticipated design loads with a sufficient factor of safety against ultimate bearing failure, which leads to increased efficiency in the design.

Environmental impact was also considered. An over-excavation and replacement option would likely produce a significant amount of soil waste material, along with the highest emissions from the construction equipment. The difference in the volume of waste material generated from the use of drilled shafts or recycled plastic piles would likely be insignificant and the difference in emissions is not known at this time. However, the use of recycled plastic piles may be considered "green engineering", which may motivate builders and geotechnical engineers to consider this type of foundation system.

CONCLUSIONS

Expansive soil is a problematic material found in the Midwest of the United States from Texas to the upper Missouri Valley. Lightly loaded structures constructed on expansive soils are susceptible to damage due to uplift forces caused by swelling action. This paper examines the potential use of recycled plastic piles for support of such structures. Due to a low coefficient of friction along the pile interface, plastic piles should allow the expansive soil to move independently of the pile without causing significant uplift forces that could be transferred to the structure.

An expansive shale test site was chosen on the SDSM&T campus in order to perform two field load tests and observe the long-term vertical movement of plastic piles. After an initial field investigation consisting of three exploratory borings, the shale was established to have a medium to high potential of swelling. Six recycled plastic Seaward Seapiles® of varying lengths were installed at the site by drilling an oversized hole, inserting the pile and backfilling the annulus between the pile and hole with low plasticity clay. Two of the installed piles were subjected to static load tests. After conducting the field load tests, a t-z model was used to back-compute the strength and stiffness parameters for the shale along the soil-pile interface and at the toe. Vertical movements of the four remaining piles, along with a small diameter concrete anchor, were monitored with weekly surveys for the duration of a one year period. Negligible movement of both the plastic piles and concrete anchor was observed, even after flooding the test site with water, predominately due to the accuracy of the surveying equipment. The field load tests did highlight the importance of ensuring that prior to installation of the piles in the pre-drilled hole, the bottom of the hole must be relatively free of loose drill cuttings and other slough. Since some loose material is likely to reside in the hole regardless of the cleanout method, subjecting the piles to a seating load, potentially applied using the drill rig prior to backfilling the annulus, should ensure adequate resistance and performance of the piles during service life. This was observed during field load testing of Pile 1, which underwent a seating load of 10 kips (44.5 kN) prior to full load testing.

Using swell test data from shale samples collected at the project site, a deep foundation

soil expansion model was developed based on predicted swell pressures. The predicted swell pressures were found to be a function of in-situ void ratio and change in the degree of saturation of the shale. The model was employed to predict the internal stresses and uplift behavior of a plastic pile and drilled shaft under varying degrees of swell pressure. While the model indicated significant differences in the tensile stresses developed within each type of deep foundation system, the model predicted similar magnitudes of vertical movement.

A cost benefit analysis was conducted by examining typical mitigation options for a single family residence. The analysis revealed that the use of recycled plastic piles could result in cost savings of between 10% and 20% over conventional methods. Other potential benefits of using recycled plastic piles include less soil waste, less construction emissions, and better efficiency in terms of capacity.

ACKNOWLEDGEMENTS

This research was made possible by a competitive research grant from the South Dakota Board of Regents and generous donations of time, expertise, and financial support from Hayward Baker Inc. Special thanks are also due to Seaward Engineered Plastics for the donation of the recycled plastic piles, FMG, Inc. for geotechnical exploration and testing services, and B&B Foundation Services for pile installation.

REFERENCES

1. Brandner, E., Roberts, L.A. and Surovek, A. 2009. Investigation of recycled plastic piles for support of structures in expansive shale environments. *Proceedings of the 34th Annual Conference on Deep Foundations*, Kansas City.
2. Chapel, T.A. and Nelson, J.D. 2000. Strain measurements of concrete piers in expansive soils. GSP 106, *Proceedings of Geo-Denver 2000*, Denver, pp. 151-163.
3. Coduto, D.P. 2001. *Foundation design - principles and practices*. Prentice Hall, Upper Saddle River, 883 p.
4. Das, B.M. 2002. *Principles of geotechnical engineering*. Brooks/Cole, Pacific Grove, 686 p.
5. Das, B.M. 2007. *Principles of foundation engineering*. CL-Engineering, Toronto, 794 p.

6. Fellenius, B.H. 1990. Guidelines for the interpretation and analysis of the static load test. Deep Foundations Institute, Hawthorne, NJ.
7. FEMA. 1997. Multi-hazard identification and risk assessment (MHIRA). Subpart B: Geological hazards, Chapter 11: Expansive Soils. *Federal Emergency Management Agency*, pp. 122-128.
8. FHWA. 1999. Drilled shafts: construction procedures and design methods, FHWA-IF-99-025. FHWA, McLean, VA.
9. FHWA. 2006. Behavior of fiber-reinforced polymer composite piles under vertical loads, *FHWA-HRT-04-107*. FHWA, McLean, VA.
10. Johnson, L.D. and Stroman, W.R. 1985. Long-term behavior of a drilled shaft in expansive soil. *Transportation Research Board, Transportation Research Record No. 1032*, pp. 53-59.
11. Meehan, R.L. and Karp, L.B. 1994. California housing damage related to expansive soils. *Journal of Performance of Constructed Facilities*, ASCE, 8(2), pp. 139-157.
12. Misra, A. and Chen, C.-H. 2004. Analytical solutions for micropile design under tension and compression. *Geotechnical and Geological Engineering*, 22(2), pp. 199-225.
13. Randolph, M.F. and Wroth, C.P. 1978. Analysis of deformation of vertically loaded piles. *Journal of the Geotechnical Engineering Division, ASCE*, 104(12), pp. 1465-1488.
14. Reese, L.C., Isenhower, W.M., and Wang S.-H. 2006. Analysis and design of shallow and deep foundations. John Wiley, New Jersey, 574 p.
15. Misra, A. and Roberts, L.A. 2006. Probabilistic analysis of drilled shaft service limit state using 't-z' method. *Canadian Geotechnical Journal*, 43(12), pp. 1324-1332.
16. Roberts, L.A., Misra, A. and Levorson, S.M. 2008. Practical method for Load and Resistance Factor Design (LRFD) of deep foundations at the strength and service limit states. *International Journal of Geotechnical Engineering*, 2(4), pp. 355-368.
17. Salgado, R. 2006. The engineering of foundations. McGraw-Hill, New York, 896 p.
18. Seaward 2002. Seapile® and Seatimber® composite marine products typical performance characteristics.
19. Scott, R.F. 1981. Foundation analysis. First Edition. Prentice Hall, Englewood Cliffs, NJ.
20. Yang, X., Han, J., Parsons, R.L. and Henthorne, R.W. 2008. Resistance factors for drilled shafts in weak rock based on O-Cell test data. *Proceedings of the TRB Annual Meeting 2008*, Transportation Research Board, Washington, D.C.

Peak and Post-Peak Shear Strength of Cement-Bentonite

Paul J. Axtell, P.E., Dan Brown and Associates, Overland Park, Kansas;
paxtell@danbrownandassociates.com

Timothy D. Stark, Ph.D., P.E., University of Illinois

John C. Dillon, P.E., U.S. Army Corps of Engineers, Kansas City District

ABSTRACT

Self-hardening cement-bentontie (c-b) slurry walls were constructed as shear walls to stabilize the downstream slope of Tuttle Creek Dam near Manhattan, Kansas. The slope stabilization was required to protect the existing pressure relief well system located at the downstream toe of the dam. The wells require protection from slope deformation induced by liquefaction of the foundation sands during or immediately after the design seismic event. The shear walls are transverse to the axis of the dam, unreinforced, and relatively brittle members that may be exposed to relatively large shear strains, and possible cracking, during or immediately after shaking. An extensive laboratory investigation was conducted on recovered core samples to optimize the mix design and stabilization scheme. Furthermore, as is the topic of this paper, a portion of the laboratory investigation was to determine the large-strain, or post-peak, shear strength of the c-b material for use in limit-equilibrium slope stability analyses and numerical deformation modeling to assess the magnitude of permanent deformation caused by the design earthquake. These data may be beneficial to other projects that are considering the use of unreinforced c-b slurry walls for seismic retrofit purposes.

INTRODUCTION

Tuttle Creek Dam, located on the Big Blue River in the Kansas River Basin, is part of a system that provides a comprehensive plan for flood control and other functions in the Missouri River Basin. The dam was designed and constructed by the US Army Corps of Engineers, Kansas City District in the 1950's. It is located about 10 km north of the city of Manhattan in eastern Kansas, as shown in Fig. 1.

The embankment is 2,300 m (7,550 ft) long and about 43 m (140 ft) high. A typical cross-section of the dam is shown in Fig. 2, identifying the general locations of the various embankment fill zones. The crest width is 15.2 m (50 ft) and the base width varies from about 430 to 490 m (1,400 to 1,600 ft). The top of the dam is at elevation 353.3 m (1,159 ft) while the original ground surface varies in elevation from about 310 to 313 m (1,017 to 1,027 ft) across the valley. Tuttle Creek Dam is a rolled earthfill dam; details of the fill zones and construction of the dam can be found in Lane and Fehrman (1960).

The main influential seismic source zones are the Nemaha Ridge uplift zone and the Humboldt Fault zone. The maximum credible earthquake (MCE) is a magnitude 6.6 event

at 20 km (12.5 miles) with a return period of about 3000 years. The peak horizontal ground acceleration, PHGA, of the MCE is 0.30g mean and 0.56g mean plus one standard deviation. The threshold liquefaction event is a magnitude 5.7 with a return period of about 1700 years. The Kansas City District found that rehabilitation of the liquefiable foundation sands is required to prevent an uncontrolled release of the reservoir during or after the design ground motion.



[FIG. 1] General Location of Tuttle Creek Dam

As part of the required seismic rehabilitation, transverse shear walls were constructed through the embankment and underlying foundation soils in the downstream slope and toe of the dam. Some preliminary design

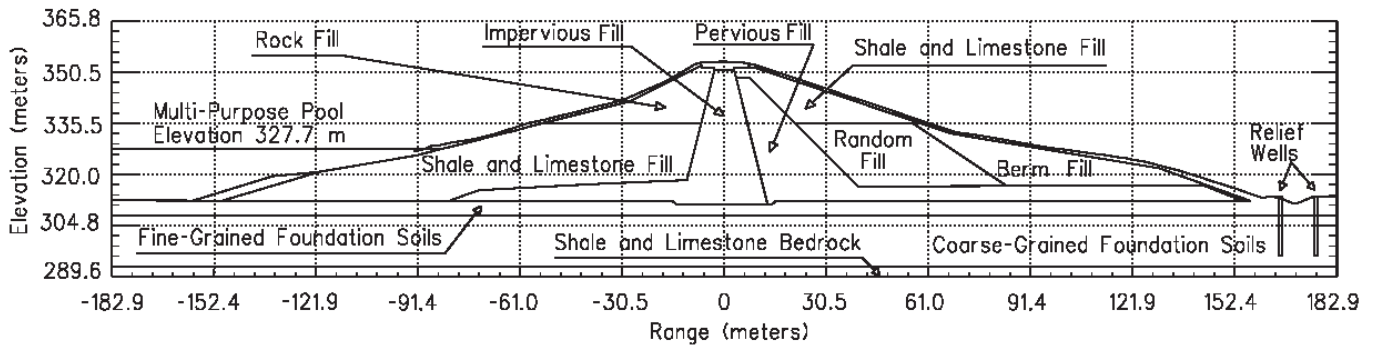


[FIG. 2] Typical cross-section of Tuttle Creek Dam

drawings depicting the plan and profile of these shear walls are shown in Figs. 3 and 4, respectively. The walls are 1.22 m (4 ft) wide, 13.72 m (45 ft) long, and generally about 21 m (69 ft) deep. A 3.05 m (10 ft) clear-space generally exists between them. Design of the clear-spacing considered requirements for unimpeded seepage between the walls in both the pervious drain and foundation sands, while also considering soil displacement between the walls using limit equilibrium methods. These transverse shear walls are self-hardening cement-bentontie (c-b) slurry walls, primarily excavated with a clam-shell. Note that slightly smaller walls were also excavated with a long-reach excavator early in the project for comparison purposes between the two construction methods. The c-b slurry walls are oriented perpendicular to the crest of the dam, unreinforced, and

relatively brittle members that will be exposed to relatively large shear strains during or immediately after the design seismic event. Such loading may crack the shear walls, after which the frictional resistance of the cracked section will govern the ability of the shear walls to resist gravitational forces induced by the slope. Large deformations at the downstream toe are not acceptable because of the presence

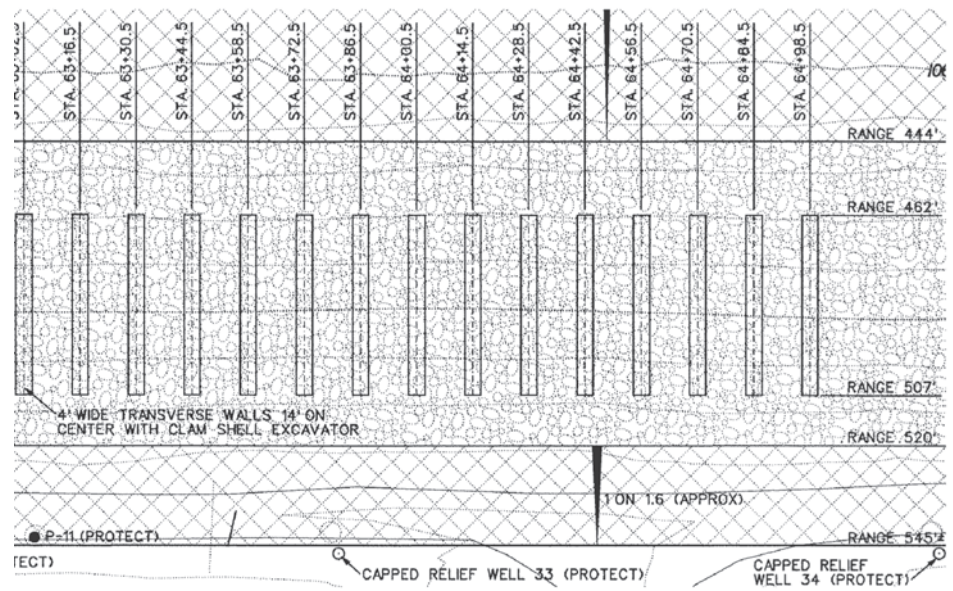


[FIG. 3] Plan View of Transverse Shear Walls (units in feet, 1 m = 3.28 ft)

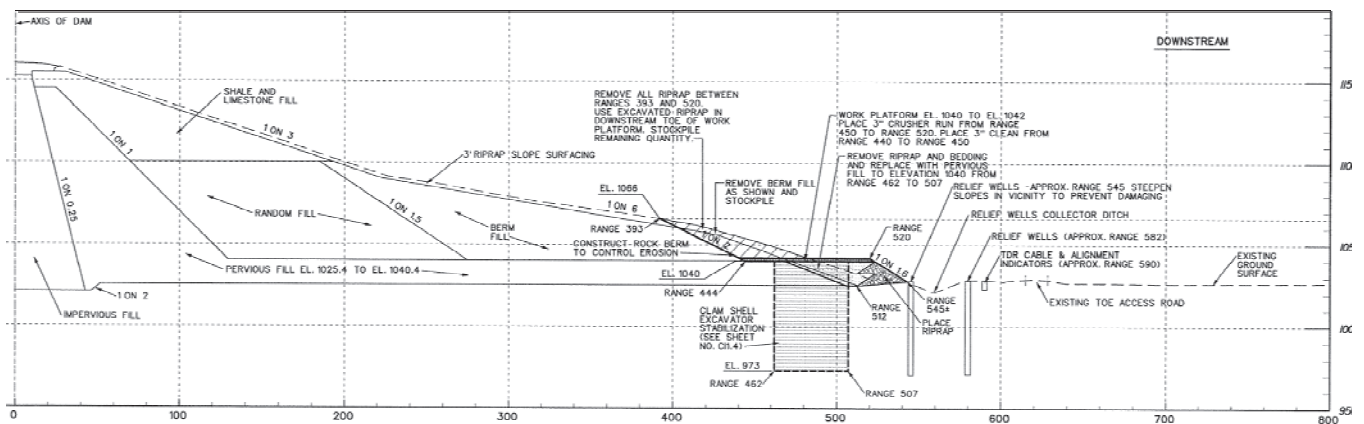


[FIG. 4] Profile View of Transverse Shear Walls (units in feet, 1 m = 3.28 ft)

of a fragile pressure relief well system. This relief well system provides vital underseepage pressure relief during operation of the reservoir and damage could lead to foundation erosion and piping.

A laboratory investigation was conducted on recovered samples obtained from production walls (initially they were test walls) to determine the large-strain, or post-peak, shear strength of the hardened cement-bentonite material. Testing included isotropically consolidated, undrained shear (R-bar) triaxial compression tests and drained direct shear tests. Testing was performed on samples that were recovered from walls constructed with cement-to-water (c/w) ratios of 0.3, 0.4 and 0.5. Both mixes include a 5 percent bentonite component. The results of the laboratory investigation were required for use in limit-equilibrium slope stability analyses used to design the shear walls and numerical deformation modeling to assess the earthquake induced permanent deformation of the dam and foundation materials. For the majority of the production work, unconfined compression tests were used to validate the design. The test results presented in this paper are for samples recovered from a test section that also serves as production shear walls. The testing presented herein was required for design.

SOIL PROFILE

A working platform was constructed on the downstream slope of the dam to facilitate construction of the shear walls. The platform was constructed by: 1) removing the existing random fill material to expose the underlying pervious drain fill; 2) importing and placing sand (SP); and 3) placing approximately 60 cm (2 ft) of road sub-base for a working surface. The only portion of the embankment that the walls are in contact with is the pervious drain material downstream of the core, which lies above the natural cohesive blanket (ML and CL). The pervious drain material is composed of dense dredged SP soil, and is approximately 4.6 m (15 ft) thick.

The soils in the alluvial foundation of the dam consist of 2.4 to 8.2 m (8 to 27 ft) of silt and clay (natural cohesive blanket) underlain by sand, silty sand, and gravelly sand to a depth of 12.2 to 24.4 m (40 to 80 ft). The silt and clay form a natural cohesive soil blanket over the more permeable sands. This natural cohesive blanket is an important component of the

seepage control system for the dam, as are the pressure relief wells at the downstream toe. The sand deposits vary in thickness from about 7.6 to 18.3 m (25 to 60 ft) and can be separated into two distinct zones. The upper zone consists of a 4.6 to 6.1 m (15 to 20 ft) thick loose fine to medium sand (SM, SP, and SW) and the lower zone consists of a 7.6 to 9.1 m (25 to 30 ft) thick dense coarse to gravelly sand that increases in grain-size with depth (SP, SW, GP, GW). Due to the alluvial nature of the foundation deposit, multiple lenses of cohesive soil exist within the coarse-grained layers. The upper sand zone was determined to be potentially liquefiable during the design ground motion. The bedrock consists of alternating layers of shale and limestone (Permian age); however, the transverse shear walls do not penetrate bedrock. The c-b walls were keyed into the dense, coarse to gravelly sand and occasionally were founded on bedrock, particularly near the left abutment.

SAMPLING AND TESTING

Wet-grab samples were cast in 7.6 cm by 15.2 cm (3 in by 6 in) cylinders and stored underwater until testing was performed. The grab sample was obtained from a shear wall shortly after construction and before the slurry hardened. After hardening, the shear walls were cored and the resulting core samples were also stored underwater until testing was performed. Wall coring was conducted with the Geobore system (double-barrel wireline) producing 10 cm (4 in) diameter samples. Coring was conducted about three weeks after construction of the walls. Testing was conducted at least 70 days after construction.

Based on an independent laboratory investigation of the proposed mixes, and verified by full-scale field measurements, relatively minor strength increases can be expected beyond 90 days for these materials. The majority of the tests occurred within the 90 day time frame. A significant unconfined compressive strength discrepancy between the wet-grab and core sample strength was observed at higher c/w ratios as described by Axtell, et al. (2009).

INTERPRETATION OF TEST RESULTS

Testing included isotropically consolidated, undrained shear (R-bar) triaxial compression tests and drained direct shear tests. The tests were performed by Kleinfelder, in Topeka,

Kansas. The post-peak or ultimate strength measured on core samples via R-bar and direct shear tests was taken into consideration during the design of these walls for the seismic retrofit because some cracking of the walls is expected during the design ground motions. Thus, the peak strength of the hardened shear walls would not be operational, i.e., would have been exceeded due to cracking of the walls. The results of the R-bar tests are provided below, along with the results from the direct shear tests.

R-BAR SHEAR RESULTS

The R-bar tests were performed on 6.6-cm (2.5 in) diameter samples with heights ranging from 11.5 to 14.5 cm (4.5 in to 5.7 in). R-bar tests were conducted on recovered core samples from walls constructed by both the clam-shell and long-reach excavation methods. Trimming of the samples was achieved by re-coring the selected specimens to the proper diameter. It is unknown if the trimming process had any effect on the results. In addition, two suites of tests were conducted on wet-grab samples from clam-shell constructed walls. Three of the samples were from walls constructed with a c/w ratio of 0.4 and one with a c/w ratio of 0.3. The remaining six samples were obtained from walls constructed with a c/w ratio of 0.5. Total stress failure envelopes for peak and post-peak strength were determined, as was the effective stress failure envelope for post-peak strength. All failure envelopes were determined by testing separate samples at confining stresses of 69,

207, and 552 kPa (10, 30 and 80 psi), which are thought to adequately encompass the expected in-situ stress range. The strain rate for all of the tests was 0.08 mm/min (.003 in/min). This rate was chosen to facilitate drainage of excess pore pressures generated during shear and was estimated based on consolidation test results. Each specimen was tested to the maximum axial strain practical, which was usually less than 20 percent in the R-bar tests. A common constraint was ripping or tearing of the specimen membrane during shear due to the sharp pieces of concrete from the specimens. Post-peak values were obtained at the maximum axial strain measured (excluding data after a membrane tear occurred). The results of the tests are summarized in Table 1. The values of dry unit weight, moisture content, and void ratio provided in Table 1 are average values for the three specimens tested at each location (three data points are used to define the failure envelope). The moisture contents reported in Table 1 are from portions of the specimen collected after the shearing phase of the test. Generally, but not always, the moisture content of the samples decreased by around 5 percent during the consolidation phase of the test. Back-pressure saturation was utilized; the mean B was 0.96, with a standard deviation of 0.05.

Deviator stress versus axial strain relationships for the 15 specimens of c/w=0.5 core samples (five suites of tests, each with three points associated with the three different confining stresses) are provided in Fig. 5. The results of tests conducted on c/w=0.4 walls are not

[TABLE 1] R-bar results (both total and effective stress).

Core Hole	Excavation method	Sample Depth (m)	c/w ratio	Dry Unit Weight (kN/m ³)	Moisture Content (%)	Void Ratio	Strain at Peak (%)	Peak		Post-Peak		Post-Peak	
								c	Φ	c	Φ	c'	Φ'
								(kPa)	(°)	(kPa)	(°)	(kPa)	(°)
VC06	Long Reach	19.8	0.3	10.36	68	1.68	1.3	276	36	255	34	0	51
VC08	Clam-Shell	9.1	0.4	9.11	69	2.03	2.4	593	0	476	0	0	46
		19.8	0.4	12.09	45	1.44	2.2	310	41	407	30	0	51
VC05	Long Reach	9.1	0.5	10.21	60	1.71	0.7	538	29	421	22	0	45
C-958		19.8	0.5	12.40	42	1.22	0.8	1151	18	731	25	0	49
VC14	Clam-Shell	9.1	0.5	10.99	48	1.52	1.6	352	37	262	39	0	46
VC17		15.2	0.5	10.21	57	1.69	0.6	931	8	434	17	0	46
		19.8	0.5	10.68	54	1.58	0.9	690	27	310	34	0	46
Wet Grab		15.2	0.4	9.11	66	2.04	0.9	986	7	207	30	0	46
		13.7	0.5	10.83	56	1.55	0.9	1655	12	807	27	0	50

shown, nor are the wet-grab results. The production walls are to have a $c/w=0.5$ so the $c/w = 0.4$ results are not relevant and data from core testing was being used for the design and acceptance criteria; hence, those were the samples used for design. The linear line super-imposed on Fig. 5 indicates the stress-strain relationship modeled in the permanent deformation analyses performed using FLAC (Itasca, 2000). The post-peak, or large-strain, strength of core samples of $c/w=0.5$ walls exceeds that required by the design. The measured initial stiffness is also somewhat greater than modeled (average initial Young's modulus equals 538 MPa (78 psi) with a standard deviation of 148 MPa (21.5 psi)) but the majority of the stress-strain relationships still indicate stronger material than modeled in the FLAC analyses. Thus, the permanent deformations estimated after wall cracking using FLAC are probably conservative and within allowable values.

The change in pore pressure during shear versus axial strain is shown in Fig. 6 for the 15 specimens of $c/w=0.5$ core samples. As expected from the relatively high void ratios measured prior to shear, all samples tended to initially generate high positive pore pressures. At higher axial strains, the excess pore pressures became negative for all 10 specimens tested at the lower confining stresses (69 and 207 kPa or 10 and 30 psi), whereas the 5 specimens at the higher confining stress (552 kPa or 80 psi) remained positive.

Note that the actual strain values are reported on the x-axis in Figs. 5 and 6 ($\Delta l/l$) whereas the corresponding values in Table 1 have been reported as a percentage.

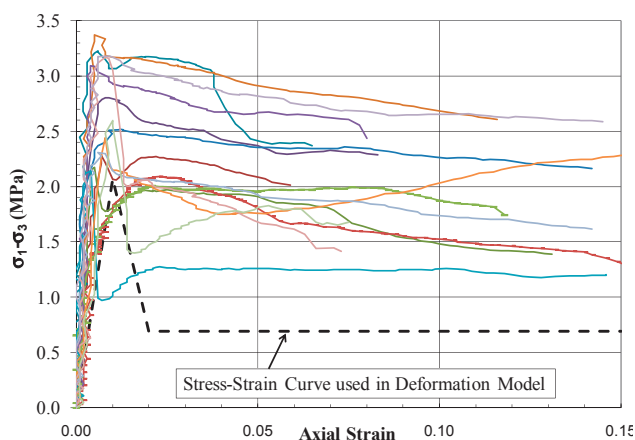


[FIG. 5] Stress-strain relationships from R-bar tests on $c/w = 0.5$ core samples (both long-reach and clam-shell excavators, at all confining stresses) and relationship used in FLAC deformation analyses.

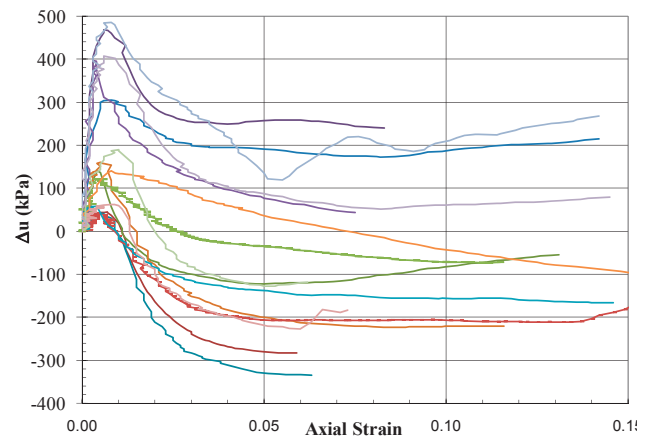


[FIG. 6] Pore pressure change versus axial strain from R-bar tests on $c/w = 0.5$ core samples (both long-reach and clam-shell excavators, at all confining stresses).

DIRECT SHEAR RESULTS

The direct shear tests were performed on 6.35-cm (2.5 in) diameter samples with a height of 2.54 cm (1 in). All direct shear tests were conducted on recovered core samples from shear walls constructed by the clam-shell excavation method. Trimming of the samples was achieved by re-coring the selected specimens to the proper diameter. It is unknown if the trimming process had any effect on the results. The tests were performed by Kleinfelder in Topeka, Kansas. Three of the samples were obtained from walls constructed with a c/w ratio of 0.4. The remaining six samples were from walls constructed with a c/w ratio of 0.5. Failure envelopes for peak and post-peak strength were normal stresses of 96, 192, 384, and 574 kPa (14, 28, 56 and 83 psi). The shear displacement rate for all of these tests is 0.005 mm/min (0.0002 in/min). This rate was chosen to facilitate drainage of excess pore pressures generated during shear based on consolidation test results. Each specimen was tested to a 0.64 cm (0.25 in) horizontal displacement. Post-peak strength values were obtained at the maximum horizontal displacement (0.64 cm) (0.25 in), whereas the peak values were generally observed at a horizontal displacement of less than 0.25 cm (0.1 in). The results of these tests are summarized in Table 2. The values of dry unit weight, moisture content, and void ratio provided in Table 2 are average values for the four specimens tested at each location (four data points defining the failure envelope).

Approximately three-quarters of the 36 specimens (9 tests, each with four normal stresses) show a slight contraction initially, after which the specimens began to dilate. Initial contraction on the order of about 0.5

[TABLE 2] Direct shear results (Clam-Shell Constructed Walls and Core Samples).

Core Hole	Sample Depth (m)	c/w ratio	Dry Unit Weight (kN/m ³)	Moisture Content (%)	Void Ratio	Peak		Post-Peak	
						c' (kPa)	Φ' (°)	c' (kPa)	Φ' (°)
VC08	9.1	0.4	8.01	76	2.5	172	44	21	41
	15.2	0.4	9.26	63	1.8	400	56	110	60
	19.2	0.4	9.73	60	1.8	296	37	41	39
VC17	3.7	0.5	8.16	79	2.4	303	33	48	36
	4.6	0.5	8.64	79	2.4	386	20	193	23
	6.1	0.5	8.64	76	2.2	276	32	14	42
	9.1	0.5	8.64	72	2.0	400	25	97	27
	12.2	0.5	8.95	71	2.1	241	41	28	37
VC14	15.5	0.5	9.89	59	1.7	352	40	62	40

percent of the original sample height was common whereas dilation on the order of 0.5 to 5 percent was observed with increasing horizontal displacement. Opposite behavior was observed for the remaining one-quarter of the specimens. Unfortunately, no discernable trend was apparent between volumetric change and c/w ratio, depth, void ratio, moisture content, or dry unit weight.

The two upper samples from core hole VC08 indicate effective friction angles that are noticeably higher than the other samples, both at peak and post-peak. The exact reason for the phenomenon is not known, but expected to be a result of the presence larger or more angular natural soil particles in the sample. The R-bar results from VC08 do not appear to validate or dispel this conclusion.

The effective cohesion and effective friction angle versus depth as determined by direct shear testing are provided in Figs. 7 and 8, respectively. These figures only present the results of tests conducted on samples with a c/w ratio equal to 0.5, because the production work is utilized for this mix. Also included in Figs. 7 and 8 are the mean, mean minus one standard deviation, and mean plus one standard deviation for each data set. Based on these figures, there does not appear to be a discernable trend between shear strength and depth in the shear wall. The presence of a post-peak cohesion value indicates that the shear displacement imposed in the direct shear tests was not sufficient to reach a residual strength condition.

Unlike soil, there also does not appear to be a distinct relationship between void ratio and

shear strength, as shown in Fig. 9. This seems apparent for the effective cohesion and friction angle at both peak and post-peak values.

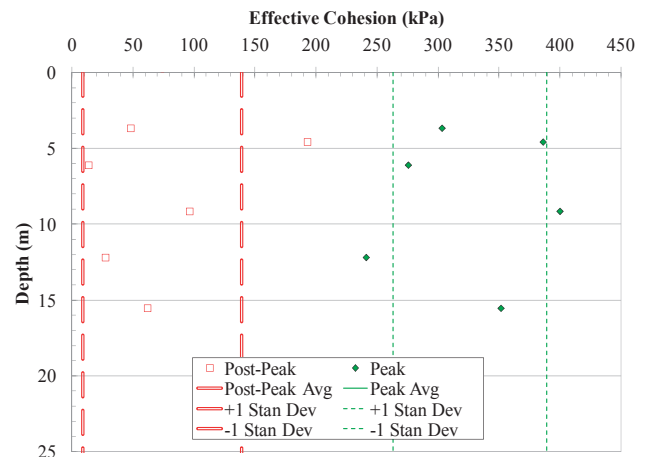


[FIG. 7] Direct shear effective cohesion versus depth in shear wall for c/w=0.5 samples.

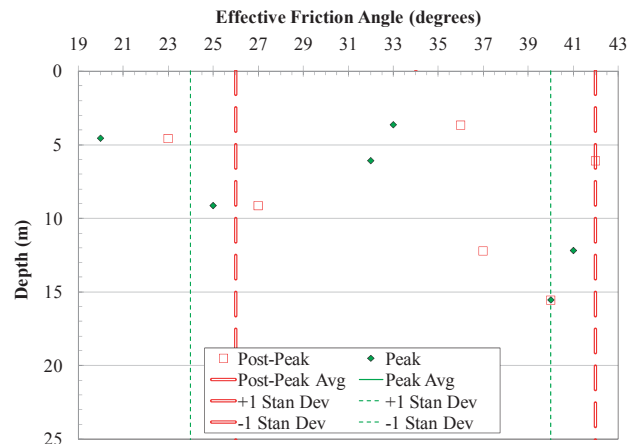


[FIG. 8] Direct shear effective friction angle versus depth in shear wall for c/w=0.5 samples.

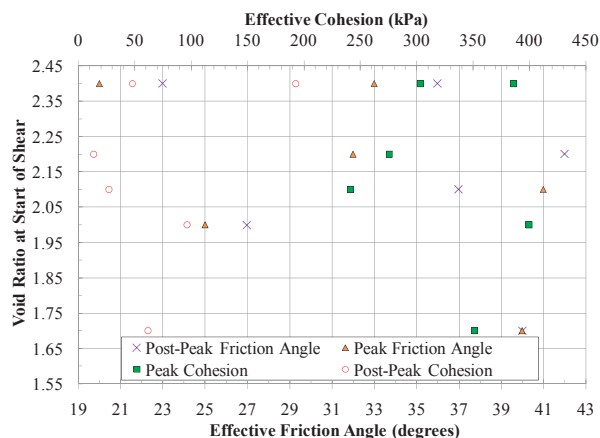


[FIG. 9] Direct shear strength parameters versus void ratio for $c/w=0.5$ samples (all cored samples, constructed with clam shell excavator).

REPRESENTATION OF TEST RESULTS IN ANALYSES

The data presented herein was used to estimate a strength and modulus profile for the depth of a transverse shear wall to model the variation in strength and stiffness with depth in the FLAC analyses. Results from both the R-bar and direct shear tests were considered in determining the strength and stiffness design values. However, results from the R-bar tests were more heavily relied upon as a result of the forced failure plane orientation in the direct shear tests, as well as questions resulting from the somewhat limited magnitude of the direct shear test displacements. Based on this data, the following average stress-strain behavior was used in the deformation analyses:

1. Peak strength (total stress): $c = 655$ kPa (95 psi) and $\phi = 24^\circ$.
2. Post-peak strength (effective stress): $\phi' = 46^\circ$.
3. Young's modulus (tangent): $E = 496$ MPa (72 ksi).
4. Peak strength attained at axial strain: $\epsilon = 0.8\%$
5. Post-peak strength begins at axial strain: $\epsilon = 1.6\%$.

This characterization may be beneficial to other projects that are trying model the seismic performance of shear walls.

CONCLUSIONS

Cement-bentonite (c-b) self-hardening slurry walls were constructed as a seismic retrofit of the downstream slope of Tuttle Creek Dam. Post-peak, or large-strain, shear strength will likely dictate the performance of these

unreinforced walls during or following the design seismic event due to cracking of the walls during shaking. Laboratory R-bar and direct shear testing of recovered core and wet-grab samples was conducted to evaluate both peak and post-peak strength for use in the wall design and estimate of post-earthquake permanent deformations. The results of the laboratory testing program are presented and indicate that a $c/w=0.5$ mix that includes a 5 percent bentonite component will meet or exceed the peak and post-peak strength requirements dictated by the design. These data may be beneficial to other projects that are considering the use of unreinforced c-b slurry walls for seismic retrofit purposes.

ACKNOWLEDGMENTS

The contents of this paper are the authors' and do not necessarily reflect those of the represented entities. The authors acknowledge the support provided by the U.S. Army Corps of Engineers - Kansas City District and Kleinfelder. The authors are particularly appreciative of the efforts by Joe Topi, Francke Walberg, Bill Empson, and David Mathews. Finally, the expertise of the contractor, Treviicos South, was essential.

REFERENCES

1. Axtell, P.J., Stark, T.D., and Dillon, J.C. (2009). "Strength Difference between Clam-Shell and Long-Reach and Excavator Constructed Cement-Bentonite Self-Hardening Slurry Walls." *Contemporary Topics in Ground Modification, Problem Soils, and Geo-Support, ASCE Geotechnical Special Publication No. 187*; Iskander, Laefer, and Hussein, editors.
2. Itasca Consulting Group, Inc. (2000). *FLAC - Fast Lagrangian Analysis of Continua*, version 4.0, Itasca Consulting Group, Inc., Minneapolis, MN.
3. Lane, K.S., and Fehrman, R.G. (1960). "Tuttle Creek Dam of Rolled Shale and Dredged Sand." *Journal Soil Mechanics and Foundation Division*, ASCE, 86(SM6). 11-34.

Underwriters: Gold



HAYWARD BAKER
Geotechnical Construction
KELLER

North America's Leading
Geotechnical Construction Contractor

- Grouting
- Ground Improvement
- Earth Retention
- Structural Support
- Additional Services
- Design-Construct Services

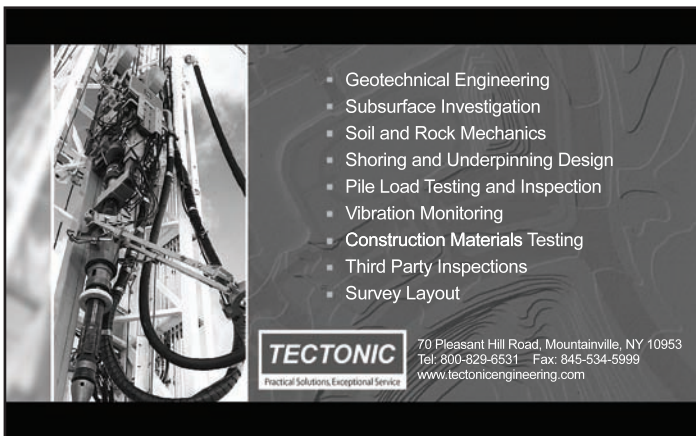
800-456-6548 ♦ www.HaywardBaker.com

Brasfond is a group of companies specialized in the most modern technologies for foundation engineering and infrastructure. With over **35 years** experience in the market, we have participated in more than **2,000 projects** with a highly specialized team and equipment, in order to exceed the expectations of the most demanding clients. For further information, any kind of assistance and career opportunities, please contact us. We will be glad to help you!

brasfond USA ^{*} | A Brasfond Group Company

www.brasfondusa.com | www.brasfond.com

Underwriters: Silver



- Geotechnical Engineering
- Subsurface Investigation
- Soil and Rock Mechanics
- Shoring and Underpinning Design
- Pile Load Testing and Inspection
- Vibration Monitoring
- Construction Materials Testing
- Third Party Inspections
- Survey Layout

TECTONIC
Practical Solutions. Exceptional Service

70 Pleasant Hill Road, Mountainville, NY 10953
Tel: 800-829-6531 Fax: 845-534-5999
www.tectonicengineering.com



Schnabel ENGINEERING

Providing specialty services with solutions for a changing world

- Geotechnical and Geostuctural Engineering
- Dam, Tunnel and Underground Engineering
- Construction and Owner Services
- Geosciences, Environmental and Sustainable Geotechnics

West Chester, Pennsylvania / 610-696-6066 / schnabel-eng.com

DFI Journal Paper Review Process

The peer review process for documents considered for publication in the DFI Journal is still evolving. The following is a description of the current process, however, the publication is still in its infancy and the review process is still in a state of flux. DFI reserves the right to alter the procedures as necessary.

Paper Submittal

Papers may be submitted at any time. Authors wishing to submit their papers for consideration of publication in the DFI Journal are invited to access www.dfi-journal.org. The website will ask for a login or, for new submitters, will ask for creation of an account. Once logged in the author must upload a full paper in MS Word format as well as any ancillary files such as figures, photos and other graphics which are included in the paper. The paper is then converted to a PDF file which the author must approve before the paper will be released to the publisher and journal editors for viewing. The journal editors preliminarily review the paper for relevancy to the Journal mission.

Paper Review

The journal editors assign those papers deemed to be worthy of consideration for Journal publication to the appropriate editorial board member, which currently consists of DFI technical committee chairmen and other industry leaders, so that appropriate reviewers for the paper topic can be obtained. Reviewers are chosen based on their knowledge, areas of expertise, and qualifications to act as a reviewer on the particular subject matter of the paper in question. At least three reviewers will be assigned to each paper.

After the reviewers are selected, they are provided with instructions and a password for entry into the website where they can view the paper PDF and submit their evaluation. The criteria on which they base their review fall under two areas: technical content and quality of paper presentation. The criteria for technical content include relevancy, originality, appropriate references to support statements, significance of results and exclusion of personal opinion and commercialism. The criteria for paper presentation include quality of figures, quality of English language, paper organization and completeness. The reviewers enter their evaluation by responding to a number of questions rating the paper as well as entry of comments to authors. They are also required to make a recommendation to the journal editors of: accept as is; accept with mandatory changes; or reject. The author is advised by automatic email of the posting of reviews and he/she can access the reviews and respond and/or modify the paper to satisfy comments by the reviewers. A second round review can then take place if necessary, ultimately leading to second round reviewer recommendations. The publisher and editors, acting as a final review committee, make the decision, based on the reviewers' recommendations, as to acceptance of the paper for publication in the next issue of the journal or in a subsequent issue.

Throughout the process, automatic emails are sent out to reviewers when papers are ready for their review and to the authors to keep them aware of the progress of their paper.

Paper Finalization

Upon acceptance, the final paper submission by the author and all graphic files are downloaded by the publisher for processing and formatting for publication. The publisher is provided with proofs by the production house and these are edited to ensure acceptable layout, the absence of typos, clarity of figures, etc. In most cases the author(s) are provided with a final PDF for their review and approval.

2010 DFI Journal Subscriptions

Electronic Subscriptions for the two-issue volume (May & November 2010) are provided to all DFI members at no cost – the electronic version is included as a benefit of annual membership dues.

DFI Members may order print versions of the *DFI Journal*. **Non-Members** can join DFI to receive the electronic version and print version at member rates OR can purchase a subscription only of either electronic, print or both.

Volume 4 (Aug. & Nov. 2010) Subscription Rates	Electronic	Print Only (USA)	Print Only (Outside USA)	Electronic & Print (USA)	Electronic & Print (Outside USA)
DFI MEMBER	Free with membership	\$125	\$175	N/A	N/A
NON-MEMBER	\$150	\$300	\$350	\$405	\$455
Join DFI	\$95 & receive electronic subscription plus other member benefits				

Build up your Journal Library! Past volumes are available for purchase while supplies last.

Past Volumes Single Issue Rates	Electronic	Print Only (USA)	Print Only (Outside USA)
Volume 1 (Nov 2007) MEMBER & NON-MEMBER	FREE online	\$45	\$70
Volume 2 (Nov 2008) MEMBER & NON-MEMBER	\$45	\$45	\$70
Volume 3 (May+Nov 2009) MEMBER & NON-MEMBER	\$90	\$90	\$150

Last: _____ First: _____	
Jr., III, etc: _____ P.E., Ph.D., Etc. _____ Mr./Ms/etc: _____	
Organization: _____ Position: _____	
Address: _____	
City: _____ State/Prov: _____ Zip/Postal Code: _____	
Country: _____ Tel: _____ Fax: _____	
E-mail Address: _____	
Circle Your Selections in Rate Charts Above	Total \$: _____
<input type="checkbox"/> Check Enclosed: *Payments from outside the US are requested to pay by credit card or Bank Draft on a USA Bank.	
<input type="checkbox"/> Visa/MasterCard/AMEX/Discover/Diner's Club (Circle One)	
Card Number: _____	
Exp. Date: ____/____/____ Signature: _____	
Order online at www.dfi.org/dfijournal.asp	

DFI Journal Call for Papers

The Deep Foundations Institute compiles and publishes a Journal of practical and technically rigorous papers each year and has plans to reduce the interval between editions, aiming ultimately to publish on a quarterly schedule. The DFI Journal content is subject to quality technical review, and must meet a standard in quality on practical subjects dealing with case studies, deep foundations history, design, construction, testing, innovations and research in the field.

Each journal consists of at least five documents collected from technical papers that are invited or selected from papers submitted by international industry members based on this call. Papers presented at the DFI Annual Conference and Specialty Seminars may be included if expanded to the Journal review and standard.

The editors are herein sending out a call for original papers for consideration of inclusion in the upcoming journals. Full draft papers up to 15 pages in length are to be submitted to: <http://www.dfi-journal.org> for review. Authors will be required to create a login account and will be notified via email on the status of their submission.

Papers are solicited on the following topics:

- Case studies involving foundation systems with technical data support
- Historical evolution of deep foundations
- Relationship between use of design, construction and equipment
- Quality control, quality assurance and non-destructive testing
- Innovation in all aspects of deep foundations and earth retention
- Practice-oriented research

The Journal Editorial Board will review submitted papers and contact authors who have been chosen for publication in one of the journals with full reviews and edits in order to complete their final paper. Authors of papers accepted for publication will be required to sign a copyright license agreement.

Deep Foundations Institute was incorporated in 1976 in the State of New Jersey as a non-profit educational activity. DFI is a technical association of firms and individuals in the field of designing and constructing deep foundations and excavations. DFI covers the gamut of deep foundation construction and earth retention systems.

Although the bulk of the membership is in North America, the Institute is worldwide.

DFI's strengths are:

- Communication of information concerning the state-of-the-art and state of the practice of deep foundation technologies
- Offering networking opportunities for our members
- Offering opportunities for members to improve the industry through publications produced by volunteer committees
- Offering educational conferences, seminars and workshops in the industry

The core strength of DFI is the broad spectrum of its membership. All disciplines participate on an equal footing, be they contractors, engineers, owners, academicians, equipment manufacturers and distributors or materials manufacturers and suppliers. All types of foundation systems are represented, whether installed by driving, drilling or other means. This diversity and openness without bias provides a forum for the free exchange of knowledge and a platform for the development of new technology and opportunity.

DFI is:

- An international network of heavy construction professionals dedicated to quality and economy in foundation design and construction
- A forum open to all construction professionals across disciplines and borders.
- A technological association devoted to gathering, storing and disseminating practical information
- A resource for identifying and locating the specialists and sources of expertise.
- An initiator and participant in research

DFI Sustaining Members

Aecom USA Inc.
AGL Manufacturing Ltd.
American Equipment & Fabricating Corp.
Anderson Drilling

APE/J&M
ASC Geosciences Inc.
Ben C. Gerwick Inc.
Berkel & Company Contractors Inc.
Brasfond Fundações Especiais S/A
Brayman Construction Corporation
Cajun Deep Foundations LLC
Case Foundation Company
Ciport S.A.
Dean Construction Co. Ltd.
Dewitt Construction Inc.
Dosdourian Enterprises Inc.
Foundation Constructors Inc.
Geokon Inc.
Hayward Baker Inc.
HJ Foundation Company
Intercoastal Foundations and Shoring
Kiewit Construction Group Inc.
Kleinfelder
L.G. Barcus & Sons Inc.
Langan Engineering and Environmental Services
Mactec Engineering & Consulting Inc.
McKinney Drilling Company
Menard
Moretrench
Mueser Rutledge Consulting Engineers
Nicholson Construction Company
North American Construction Group
North American Steel Sheet Piling Association
O.C.I. Division / Global Drilling Suppliers Inc.
Pileco Inc.
Pnd Engineers Inc.
Richard Goettle Inc.
Sas Stressteel Inc.
Schnabel Foundation Company
Tei Rock Drills Inc.
ThatCher Engineering Corporation
Urban Foundation/Engineering LLC
William F. Loftus Associates Foundation Engineers.

Deep Foundations Institute Sustaining Members Are Corporate Members Of DFI Who Have Voluntarily Granted Funding To The Institute For Expanded Support Of The Industry. The fund is managed by the DFI Educational Trust.



DFI JOURNAL

The Journal of the Deep Foundations Institute

International Standard Serial Number (ISSN): 1937-5247

Deep Foundations Institute
326 Lafayette Avenue
Hawthorne, New Jersey 07506 USA
Tel: 973-423-4030
Fax: 973-423-4031
www.dfi.org